Including gauge corrections to thermal leptogenesis

Dissertation
zur Erlangung des Doktorgrades
der Naturwissenschaften

vorgelegt beim Fachbereich 13
der Johann Wolfgang Goethe-Universität
in Frankfurt am Main

von
Janine Hütig
aus Warendorf

Frankfurt 2013
(D30)

vom Fachbereich Physik der
Johann Wolfgang Goethe-Universität als Dissertation angenommen.

Dekan: Prof. Dr. J. Stroth

Gutachter: Prof. Dr. O. Philipsen
Prof. Dr. C. Greiner

Datum der Disputation: 17.05.2013

I think physicists are the Peter Pans of the human race.
They never grow up and they keep their curiosity.

Isidor Isaac Rabi

Zusammenfassung

Die Frage nach dem Ursprung der Materie in unserem Universum stellt Kosmologen bis zum heutigen Tag vor ein ungelöstes Problem. Geht man vom weithin anerkannten Urknallmodell aus, so müsste hierbei zu gleichen Teilen Materie sowie Antimaterie entstanden sein. Aufgrund von Annihilationsprozessen sollte demnach die gesamte Materie zerstrahlt sein und ein leeres Universum zurückbleiben. Da dies aber offensichtlich nicht der Fall ist, stellt sich die Frage, wie das Ungleichgewicht zwischen Materie und Antimaterie entstehen konnte. Der Wert der Asymmetrie lässt sich durch bisherige Experimente sehr genau bestimmen. Die Messung der sogenannten Baryonen-zu-Photonen-Rate η_{B}, das bedeutet die Differenz von Baryonen und Antibaryonen geteilt durch die Anzahl an Photonen, liefert hierfür einen Wert von $\eta_{\mathrm{B}} \approx 6 \cdot 10^{-10}$, welcher sowohl durch Messungen von WMAP (Vermessung der kosmischen Hintergrundstrahlung) als auch durch Ergebnisse der primordialen Nukleosynthese (Messung der Häufigkeiten der leichten Elemente) angegeben wird.

Es gibt eine große Anzahl an Modellen, die versuchen, diesen Wert zu reproduzieren. Diese Vielzahl erklärt sich dadurch, dass selbst zwei der erfolgreichsten und anerkanntesten Theorien bisher nicht in der Lage sind, die beobachtete Asymmetrie zu erklären: das Standardmodell der Kosmologie (oder auch Urknallmodell) sowie das Standardmodell der Teilchenphysik. Obwohl ersteres die Häufigkeiten der leichten Elemente, die kosmische Hintergrundstrahlung sowie die Expansion des Universums sehr gut beschreibt, liefert es für die Asymmetrie zwischen Baryonen und Antibaryonen einen viel zu kleinen Wert der Größenordnung $\mathcal{O}(10^{-18})$.

Das Standardmodell der Kosmologie geht von einer anfänglichen *inflationären Phase* direkt nach dem Urknall aus, welche zu einer exponentiellen Ausdehnung und somit zu einem Zustand im Nichtgleichgewicht führte. Hieran schließt sich eine *Wiederaufheizungsphase*, in der die Teilchen des frühen Universums thermalisierten und so ein sehr heißes und dichtes Plasma bildeten. Dieses *Quark-Gluon-Plasma* (QGP) wird aktuell ebenfalls stark untersucht, so finden in den Beschleunigern RHIC und LHC sowie zukünftig in der Anlage FAIR in Darmstadt Schwerionenkollisionen statt, die diese Phase des frühen Universums im kleinen Maßstab reproduzieren. Daraus lassen sich insbesondere Rückschlüsse auf den Phasenübergang vom QGP, welches freie Quarks und Gluonen beinhaltet, hin zu „gewöhnlicher“ Materie, welche aus gebundenen Quarks und Gluonen besteht, ziehen. Die Natur dieses Phasenübergangs ist bislang nicht bestimmt. Für diesen Energiebereich ist das Standardmodell der Teilchenphysik die anerkannteste Theorie. Dieses Modell hat schon hervorragende Übereinstimmungen zwischen Theorie und Experiment hervorgebracht (wie z. B. die Messung des magnetischen Moments des Elektrons), ist aber ebenfalls nicht in der Lage, die Baryonenasymmetrie des Universums zu erklären. Die Suche nach der Masse des Higgs-Teilchens ist hierfür von besonderer Wichtigkeit: Der Bereich, in dem diese Masse für einen funktionierenden Baryogenesemechanismus im Standardmodell liegen müsste, wurde durch bisherige Messungen der Beschleuniger am RHIC und LHC bereits ausgeschlossen. Somit lassen sich Theorien

jenseits des Standardmodells motivieren.

Für eine systematische theoretische Beschreibung dieser Problematik legte Andrei Dmitrijewitsch Sacharow 1967 den Grundstein. Er stellte drei Bedingungen auf, die erfüllt sein müssen, um eine Baryonenasymmetrie zu generieren:

1. Verletzung der Baryonenzahl
2. Verletzung der Invarianz von Ladungskonjugation $\mathcal{C}$ sowie der Zusammensetzung von Ladungskonjugation und Parität $\mathcal{CP}$
3. Abweichung vom thermischen Gleichgewicht.

Jede Theorie, die versucht die Asymmetrie zu erklären, muss somit diese drei Bedingungen erfüllen. Die vorliegende Dissertation beschäftigt sich mit der Theorie der Leptogenese, welche statt von einer ursprünglichen Baryonenasymmetrie von einer Leptonenasymmetrie ausgeht. Zu einem späteren Zeitpunkt wird diese dann mittels sogenannter *Sphaleron*-Prozesse, welche die Baryonenzahl verletzen, in eine Baryonenasymmetrie übertragen. Da das Standardmodell der Teilchenphysik nicht in der Lage ist, die Asymmetrie zu erklären, werden im Kontext der thermischen Leptogenese neue Teilchen eingeführt: schwere Majorana-Neutrinos. Diese zerfallen im thermischen Nichtgleichgewicht dann $\mathcal{CP}$-verletzend in die bekannten Standardmodell-Leptonen und Higgs-Teilchen.

Im hierfür zugrundeliegenden Standardmodell wird die starke Farbsymmetrie und die elektroschwache Eichsymmetrie zur $\mathrm{SU(3)_c}\times\mathrm{SU(2)_w}\times\mathrm{U(1)_Y}$ vereinigt. Die hinzugefügten Teilchen sind drei elektroschwache Singulett-Fermionen, welche demnach rechtshändig transformieren. Somit erhält man mit nur drei neuen Teilchen einerseits eine Erklärung für die Baryonenasymmetrie des Universums, andererseits liefert die thermische Leptogenese gleichzeitig eine Erklärung der beobachteten leichten Neutrinomassen. Da das Majorana-Neutrino eine so hohe Masse hat (typischerweise $M \approx 10^9\,\mathrm{GeV}$), erhalten die leichten (Dirac) Neutrinos über den *See-saw*-Mechanismus (engl. „Wippe“) Massen von $m_i < 0,12\,\mathrm{eV}$ für $i = e, \mu, \tau$.

In dieser Arbeit wird eine hierarchische Anordnung $M \ll M_2, M_3$ der drei schweren Neutrinomassen betrachtet. Dies hat zur Folge, dass zwei der drei Majorana-Neutrinos ausintegriert werden können und eine effektive Theorie aufgestellt werden kann. Dieses Modell wird auch *vanilla leptogenesis* genannt und im Folgenden verwendet.

Die Dissertation ist wie folgt gegliedert. Die Details der vorangegangenen Betrachtungen sind Gegenstand der Kapitel 1 und 2. Dort werden weiterhin drei andere Modelle zur Lösung des Problems der Baryonenasymmetrie kurz vorgestellt: Große vereinheitlichte Theorien (GUT) Baryogenese, Elektroschwache Baryogenese und Affleck-Dine Baryogenese. Außerdem werden deren Vor- und Nachteile erörtert. Die thermische Leptogenese wird ausführlich eingeführt und der See-saw-Mechanismus sowie die $\mathcal{CP}$-Asymmetrie genauer beschrieben. Am Ende des Kapitels wird zusätzlich der klassische Ansatz für Leptogenese über Boltzmann Gleichungen präsentiert. Weiterhin wird das in der Arbeit verwendete effektive Model sowie eine Liste der zugehörigen Feynman-Regeln, welche auch nochmals ausführlich in Anhang A.2.1 aufgelistet werden, vorgestellt.

In Kapitel 3 werden dann die Grundlagen für Quantenfeldtheorien im Nichtgleichgewicht eingeführt. Zunächst werden die wichtigsten Definitionen im Falle des thermischen Gleichgewichts gegeben, wie zum Beispiel das erzeugende Funktional, mit dessen Hilfe sich alle n-Punkt-Funktionen ableiten lassen. Ein besonderer Schwerpunkt liegt auf den Verknüpfungen zwischen den verschiedenen Propagatoren, z. B. zwischen dem

statistischen und spektralen Propagator sowie den *Wightman*-Funktionen, die öfter benötigt werden. Anschließend findet sich die Verallgemeinerung auf Nichtgleichgewichtszustände, welche im sogenannten *real-time*-Formalismus eingeführt wird. Dessen Verwendung führt zusätzliche, nicht-physikalische Freiheitsgrade ein, was eine nichttriviale Echtzeit-Kontur in der komplexen Zeitebene zur Folge hat. Somit erhält man für diesen *Schwinger-Keldysh*-Formalismus typischerweise Propagatoren in Matrixgestalt.

Die Herleitung der Bewegungsgleichungen im Nichtgleichgewicht ist Thema des nächsten Unterkapitels. Diese *Kadanoff-Baym*-Gleichungen werden im Folgenden sowohl für skalare Teilchen als auch für Fermionen gelöst. Dabei wird das Majorana-Neutrino als Fermion verwendet, so dass die Ergebnisse im nächsten Kapitel übernommen werden können. Abschließend werden die freien Propagatoren für Skalare und Fermionen im Gleichgewicht sowie der Nichtgleichgewichtspropagator des Majorana-Neutrinos aufgeführt.

Kapitel 4 präsentiert die Hauptmotivation dieser Dissertation: Die Notwendigkeit von Eichkorrekturen im Kontext der thermischen Leptogenese. Zunächst werden die Lösungen der Boltzmann Gleichung hergeleitet um diese später mit den Lösungen der Kadanoff-Baym-Gleichungen vergleichen zu können. Weiterhin wird eine sogenannte Leptonenzahlmatrix L aus der Definition des Leptonenstroms eingeführt. Diese entspricht im Falle freier Felder im Gleichgewicht gerade der naiven Leptonenasymmetrie $L = f_l - f_{\bar{l}}$ mit der Fermi-Dirac-Verteilungsfunktion f für Leptonen l, bzw. Antileptonen $\bar{l}$. Diese Leptonenzahlmatrix lässt sich nun mit Hilfe der Ergebnisse des vorangegangenen Kapitels durch die Kadanoff-Baym Gleichung für Leptonen umschreiben, so dass sie sowohl abhängig vom Leptonpropagator als auch von der Leptonselbstenergie ist. Die zu letzterer beitragenden Diagramme werden ebenfalls beschrieben. Außerdem wird diskutiert, warum nur zwei der sechs Diagramme die Asymmetrie bedingen. Eine detaillierte Berechnung der beiden Beiträge findet sich in Anhang A.2.2.

Der Vergleich von Boltzmann und Kadanoff-Baym Gleichungen im letzten Teil dieses Kapitels zeigt Unterschiede im Zeitverhalten: Während der Boltzmann Ansatz einen einfachen exponentiellen Abfall in der Zeit zeigt, gibt es in der Kadanoff-Baym Lösung eine quadratische Abhängigkeit bezüglich dieses Faktors, was der Nichtlokalität in der Zeit im Ansatz geschuldet ist. Außerdem tritt ein zusätzlicher Faktor aus Verteilungsfunktionen auf. Um diese Diskrepanzen weiter zu untersuchen, werden im Kadanoff-Baym Ansatz thermische Standardmodell-Breiten des Higgsfeldes γ_ϕ und der Leptonen γ_l eingeführt. Diese sollten im Beisein des schweren Majorana-Neutrinos nicht zu vernachlässigen sein, da für diese Breiten gilt: $\gamma_l \sim \gamma_\phi \sim g^2 T \gg \lambda^2 M \sim \Gamma$, mit Standardmodell-Kopplung g und Yukawa-Kopplung λ für das schwere Neutrino. Thermische Massen werden für einen ersten Ansatz vernachlässigt, dennoch erhält man schon mit dieser naiven Erweiterung ein ebenfalls einfaches exponentielles Abfallen im Ausdruck für die Leptonenzahlmatrix, welches lokal in der Zeit ist, wie die Lösung der Boltzmann Gleichung.

Um das Hinzufügen der Standardmodell-Breiten der Teilchen per Hand zu umgehen, ist eine systematische Einführung von Standardmodellkorrekturen für thermische Leptogenese unumgänglich. Daher werden im Rahmen der vorliegenden Dissertation von Grund auf Eichkorrekturen der Diagramme, die zur Asymmetrie führen, berücksichtigt. Um dies auch systematisch sicherzustellen, müssen einige Resummationschemata verwendet werden, weshalb dies Gegenstand von Kapitel 5 ist.

Ein Blick auf die Skalen, die dem vorliegenden System eines Majorana-Neutrinos in einem thermischen Bad aus Higgs-Teilchen und Leptonen zu Grunde liegen, lässt vier

signifikante Bereiche erkennen:

Harte Skala: Dies ist der Bereich, in dem üblicherweise störungstheoretische Rechnungen durchgeführt werden. Er liegt vor für Impulse mit $k \sim T$, $k^2 \sim T^2$.

Weiche Skala: In diesem Bereich kommt es zu kollektiven Anregungen mit dem thermischen Bad und thermische Massen werden wichtig. In diesem Bereich für $k \sim gT$ ist ein Resummationsschema unabdingbar, das *Hard Thermal Loop* (HTL) Schema.

Ultraweiche Skala: Für den Impulsbereich $k \sim g^2T$ ist eine störungstheoretische Betrachtung des Problems nicht mehr zulässig. Nichtperturbative Methoden oder effektive Theorien sind hier notwendig, da transversale Polarisationen der Eichfelder dominieren.

Lichtkegel Skala: Für harte kollineare Impulse, also $k \sim T$ mit $k^2 \sim g^2T^2$, müssen asymptotische Massen berücksichtigt werden, da kollineare Divergenzen entstehen. Somit ist auch hier eine Resummation notwendig, das *Collinear Thermal Loop* (CTL) Schema.

In unserem Fall werden somit für Temperaturen $T \gtrsim M$ die Standardmodellteilchen aufgrund der thermischen Massen „schwerer“ als das Majorana-Neutrino und das HTL Schema muss angewendet werden. Für den Fall $T \sim M$ befindet sich das Neutrino im Bereich der harten Skala und daher wird keine Resummation benötigt. Für Higgs-Teilchen und Leptonen jedoch finden wir harte lichtartige Impulse, so dass hier das CTL Schema benötigt wird.

Bevor die beiden Resummationsschemata diskutiert werden, werden zu Beginn des Kapitels die verschiedenen Skalen diskutiert. Anschließend werden dann zunächst die Grundzüge des HTL Schemas erörtert und thermische sowie asymptotische Massen eingeführt. Explizite Rechnungen und Herleitungen dazu finden sich in Anhang A.2.3. Nach einer Einführung der Lichtkegel-Koordinatenschreibweise, welche im Folgenden verwendet wird, werden die *power counting* Regeln zusammengefasst. Die für das CTL Schema typischen Leiterdiagramme werden im nächsten Unterkapitel vorgestellt, außerdem liefert der Landau-Pomeranchuk-Migdal Effekt eine gute Anleitung, um diese Diagramme auszuwerten. An dieser Stelle wird die anfangs erwähnte Verknüpfung zu Fragestellungen des Quark-Gluon-Plasmas sehr deutlich: Die ursprünglichen Arbeiten zu diesem Thema stammen aus Betrachtungen der Photon-Produktion im QGP.

Die Auswertung der Leiterdiagramme führt schließlich zu zwei Differenzialgleichungen, deren Herleitung diskutiert wird. In einem anschließenden Kapitel 6 wird die thermische Produktionsrate des Majorana-Neutrinos numerisch weiter ausgewertet. So wird im Vergleich zwischen der Rate in führender Ordnung und derjenigen, die alle Eichkorrekturen einschließt, deutlich, wie wichtig diese Korrekturbeiträge sind. In führender Ordnung gibt es einen weiten Bereich, in dem die Rate verschwindet. Bei voller Rechnung erhält man für den gesamten betrachteten Bereich eine nichtverschwindende Majorana-Neutrino Produktionsrate. Die beiden Differenzialgleichungen beschreiben Prozesse, die einer Änderung, bzw. einer Konstanz der Helizität entsprechen. Auch für diese beiden Fälle wird die Produktionsrate jeweils für führende Ordnung sowie für die eichkorrigierte Rate ausgewertet. Abschließend wird das Impulsspektrum des Neutrinos betrachtet: Es zeigt sich, dass es sich nicht thermisch verhält, da es nicht proportional zur Fermi-Dirac Verteilung ist, unabhängig davon, ob es sich um helizitätsändernde oder -erhaltende Prozesse handelt.

In Kapitel 7 werden die einzelnen Bausteine aus den vorangegangenen Kapiteln zusammengetragen. Zunächst erfolgt noch eine naive Berechnung aller eichkorrigierter 3-Schleifen-Diagramme, die zu den beiden die Asymmetrie verursachenden Diagrammen gehören. Es ergeben sich 17 Diagramme sowie ihre spiegelbildlichen Versionen, die mit Hilfe des Programms QGRAF gefunden wurden. Da aber bereits erörtert wurde, dass eine einfache Berechnung der 3-Schleifen-Diagramme nicht ausreicht, wird an dieser Stelle ein neues, zylindrisches Diagramm eingeführt. Dieses Diagramm enthält alle wichtigen Beiträge, insbesondere die HTL- und CTL-resummierten. Zunächst wird gezeigt, dass die 34 vorher betrachteten 3-Schleifen-Diagramme im neuen Diagramm bereits enthalten sind.

Durch dieses neuartige Diagramm ist es dann möglich, die Ergebnisse des letzten Kapitels direkt in den Kontext der Leptogenese einzubauen. Nach einigen analytischen Bemühungen lässt sich die Leptonenzahlmatrix durch ein Produkt der Selbstenergien des Majorana-Neutrinos umschreiben. Diese Selbstenergie ist bereits aus dem letzten Kapitel bekannt und wird hier als Ergebnis geschlossen präsentiert. Eine analytische Behandlung des Problems ist somit nicht mehr möglich, da die Lösung der Differenzialgleichungen nur numerisch zur Verfügung stehen. Da die Selbstenergie bis hierher auch einen temperaturunabhängigen Anteil enthält, müssen zunächst noch etwaige Divergenzen beseitigt werden. Die einzige auftretende Divergenz ist jedoch auch in diesem temperaturunabhängigen Teil enthalten, so dass sie aufgrund der Renormierung der Theorie bei $T = 0$ nicht weiter zu berücksichtigen ist. Für den Fall der thermischen Leptogenese sind nur temperaturabhängige Teile interessant, da sonst die anfangs erwähnte 3. Sacharow Bedingung, nämlich die Abweichung vom thermischen Gleichgewicht, nicht mehr erfüllt ist. Am Ende des Kapitels findet sich schließlich der erste geschlossene Ausdruck für die eichkorrigierte Leptonenzahlmatrix in führender Ordnung.

Abschließend gibt es eine kurze Zusammenfassung und einen Ausblick in Kapitel 8. In dieser Dissertation findet sich zum ersten Mal ein systematischer Zugang zur Berücksichtigung aller Eichwechselwirkungen in der Theorie der thermischen Leptogenese. Ein geschlossener Ausdruck für die eichkorrigierte Leptonenasymmetrie konnte vorgestellt werden. Außerdem ist durch die Einführung des zylindrischen Diagramms eine Berechnung der Leptonenasymmetrie für den Fall nicht-hierarchisch geordneter Majoranamassen, der sogenannten *resonanten* Leptogenese, möglich.

In einem nächsten Schritt wäre eine numerische Auswertung des Ausdrucks wünschenswert, um einen exakten Wert für die Asymmetrie zu erhalten. Dieses numerische Ergebnis wäre das erste quantitative Resultat, welches Korrekturbeiträge führender Ordnung für *alle* Wechselwirkungen des Majorana-Neutrinos mit den Teilchen des Standardmodells beinhaltet. Weitere Korrekturen durch die Berücksichtigung der Hubble Expansion sowie der *washout*-Beiträge sollten dagegen hinreichend klein sein. Das numerische Ergebnis kann dann direkt mit den Ergebnissen aus dem ursprünglichen Boltzmann Ansatz als auch mit denen aus dem Kadanoff-Baym Ansatz verglichen werden. Hierbei ist es interessant zu sehen, wie gut die Näherung durch die per Hand eingefügten Breiten der Standardmodellteilchen wirklich ist. Des Weiteren lässt sich durch das zylindrische Diagramm der Fall der resonanten Leptogenese direkt auswerten: Durch die Entartung der Majoranamassen ist es nicht mehr möglich, zwei der Massen auszuintegrieren. Dadurch erhält man im zylindrischen Diagramm keinen effektiven Vertex mehr und das Diagramm kann direkt ausgewertet werden. Auch lassen sich hierdurch Beschränkungen für die Produktion des Gravitinos finden, durch welche sich sypersymmetrische Theorien

testen lassen: Falls das leichteste supersymmetrische Teilchen das Gravitino ist, welches auch Bestandteil der Dunklen Materie sein kann, so könnte in absehbarer Zukunft am LHC auch Supergravitation getestet werden.

In einem Anhang sind zunächst die verwendeten Konventionen gelistet, des Weiteren findet sich in Anhang A eine Liste der Feynmanregeln der effektiven Theorie sowie die detaillierte Berechnung der beiden Asymmetrie verursachenden Diagramme. Überdies werden Propagatoren im HTL und CTL Schema hergeleitet sowie die thermischen und asymptotischen Massen berechnet. Abschließend findet sich die Auswertung der 1-Schleifen Renormierungsgruppengleichungen für die Kopplungen des Standardmodells, welche für die numerischen Kalkulationen verwendet wurden.

In Anhang B wird zunächst die explizite Herleitung des Ausdrucks für die Produktionsrate des Majorana-Neutrinos vorgestellt. Anschließend findet sich eine detaillierte Anleitung zur Lösung der Integralgleichungen, wobei zunächst die Umwandlung der Integralgleichungen in Differenzialgleichungen aufgeführt ist. Deren Implementierung und die dazu verwendeten numerischen Hilfsmittel in Form eines Programms zur Lösung gewöhnlicher Differenzialgleichungen sowie die Monte Carlo Integrationsmethode werden vorgestellt. Abschließend finden sich Beweise von wichtigen Relationen, die innerhalb der Dissertation verwendet wurden.

Contents

1 Introduction

Der Spaß fängt erst dann an, wenn man die Regeln kennt.
Im Universum aber sind wir momentan noch dabei,
die Spielanleitung zu lesen.
Richard P. Feynman

The very fundamental question of why matter exists in our universe remains yet unsolved. This problem formerly addressed to only by metaphysicists became theoretically accessible for cosmologists half a century ago, when Andrei D. Sakharov discovered three necessary conditions for generating a baryon asymmetry. Since starting with the same amount of particles and antiparticles at the Big Bang, the current universe should remain void of matter.

Even the familiar Standard Model of Cosmology depicted in fig. 1.1 is not able to solve this issue. Though we are well able to explain the abundance of light elements, the cosmic microwave background radiation and the expansion of the universe as can be seen by the excellent current measurements of the Wilkinson Microwave Anisotropy Probe[1] as well as the earlier ones of the Cosmic Background Explorer[2]. In this model a period of *inflation* is presumed shortly after the Big Bang, which led to an exponential expansion of the universe, and thus, it remained in a nonequilibrium state. Afterwards, the phase of *reheating* took place so that the particles of the early universe thermalised to bring forth a very hot and dense plasma. This so-called quark-gluon plasma (QGP) is under current investigation, e. g. the experiments LHC (Large Hadron Collider) at CERN[3] and RHIC[4] at the Brookhaven National Laboratory study the features of the plasma. There is also another family of colliders that experimentally surveys the properties for even higher densities, namely the FAIR project at GSI[5].

Considering the current state of knowledge, one can maintain that everything in time before the Big Bang Nucleosynthesis (BBN), which corresponds to the abundance of light elements, has not been well understood yet. Nevertheless, there is much consensus about the fundamental interactions, i. e. the strong, the electroweak and the gravitational force, that describe the physics afterwards. Thus at times sufficiently far away from the Planck scale, the theoretical background for further studies via the Standard Model of particle physics provides a well accepted framework. At those times a classical description in terms of General Relativity is adequate and therefore the lack of a consistent theory of quantum gravity becomes minor. Furthermore, it becomes clear that the different processes in the QGP as well as in the early universe, especially the case of interest for this thesis namely baryon asymmetry, can make use of the same mathematical tools [2].

[1] See WMAP website `http://map.gsfc.nasa.gov/` .
[2] See COBE website `http://lambda.gsfc.nasa.gov/product/cobe/` .
[3] Conseil Européen pour la Recherche Nucléaire, see website url http://lhc.web.cern.ch/lhc/ .
[4] Relativistic Heavy Ion Collider, see website `http://www.bnl.gov/rhic/` .
[5] Facility for Antiproton and Ion Research in Europe GmbH at Gesellschaft für Schwerionenforschung, see website `http://www.fair-center.de/index.php?id=1&L=1` .

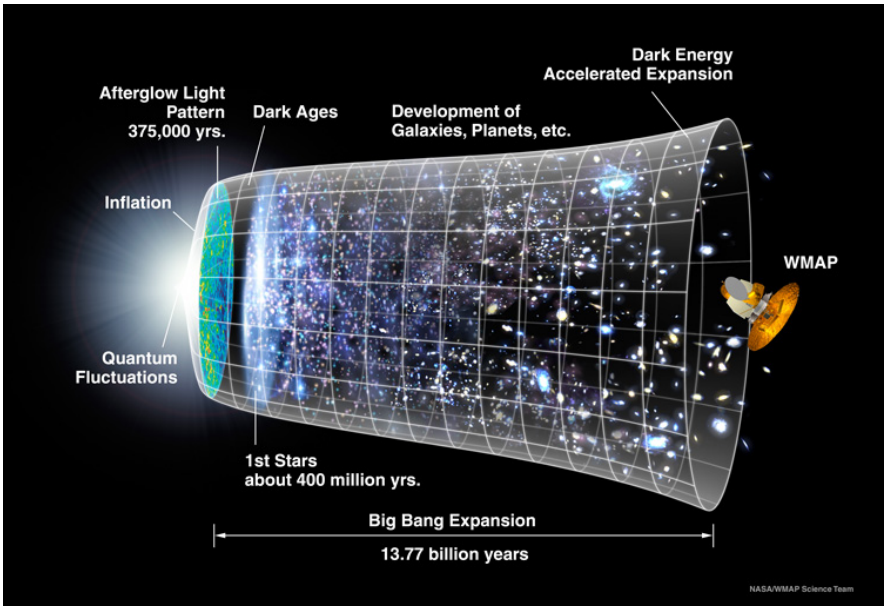

Figure 1.1: Evolution of the universe: The Big Bang is depicted in the far left with a subsequent inflationary phase and the relic radiation, which was emitted at the time of photon decoupling. Later on, the expansion of the universe slowed down due to gravity, while recently, it started accelerating again as the repulsive effect of dark energy became dominating. Taken from [1].

In addition, the results are often even applicable to the other issue and vice versa as shown in this thesis using the examples of Kadanoff-Baym equations and the Landau-Pomeranchuk-Migdal effect.

Up to date, there are several approaches that deal with the baryon asymmetry of the universe, yet none of them has been tested successfully. In this thesis our model of choice is the ansatz of leptogenesis, in which a former lepton asymmetry is converted into a baryon asymmetry via sphaleron processes in the early universe. The out of equilibrium decay of heavy Majorana neutrinos generates the former asymmetry, so they have to be added to the ordinary Standard Model particles. A convenient side effect is the prediction of very light ordinary neutrino masses, thus two problems can be explained by adding only three new particles.

There is much effort in progress as can be seen by the different groups operating on the topic of leptogenesis, e. g. the Heidelberg group [3–6] as well as the Aachen group [7–9] and several others [10–14]. This work is mainly based on the Hamburg and Bielefeld results [15–18].

The thesis is structured as follows. The next chapter contains an introduction to the baryon asymmetry of the universe including its evidence and magnitude. Several promising approaches for solving this problem are presented in the following and their advantages and disadvantages are discussed. Furthermore, the topic of thermal leptogenesis is adopted and a classical ansatz is shown, giving also measurable constraints on this model. We also present an effective model and its Feynman rules.

Chapter 3 is devoted to nonequilibrium dynamics and its theoretical description. After the main definitions given in equilibrium thermal field theory, we introduce the dynamics

for out of equilibrium systems via the Schwinger-Keldysh formalism. Throughout this thesis, real-time observables are used and therefore the Kadanoff-Baym equations are presented. We discuss results for scalars as well as for fermions, the latter using the example of heavy Majorana neutrinos. Based on this, we continue in chapter 4 with comparing the solutions of the Kadanoff-Baym equations to those derived from using Boltzmann equations. The lepton number matrix is introduced with which we calculate the lepton asymmetry. We further present the two asymmetry-causing diagrams and discuss the necessity of systematically including gauge interactions to this setup.

In order to deal with this task, two resummation schemes are needed that are discussed in chapter 5, namely the hard thermal loop (HTL) resummation scheme and the collinear thermal loop (CTL) resummation scheme. Therefore we discuss the different scales of our system and its power counting. Furthermore, the Landau-Pomeranchuk-Migdal effect is presented for finding integral equations that lead to the Majorana neutrino production rate. Our numerical results for the tree-level as well as for the full expression including gauge corrections are shown in chapter 6.

In the last but one chapter we present the systematic inclusion of gauge interactions to the context of leptogenesis. After discussing several gauge corrected three-loop Feynman diagrams, we construct a new type of diagram that includes all necessary contributions due to the former discussed resummation schemes. A complete expression for the lepton asymmetry including gauge corrections up to one-loop order is given. Finally, conclusions and further research perspectives are discussed in chapter 8.

Attached are two appendices: The first one encloses used conventions and the Feynman rules of the effective theory. Furthermore, the calculation of the asymmetry-causing diagrams and of the HTL and CTL propagators are given, including thermal and asymptotic masses. Also the solutions of the Standard Model couplings from one-loop renormalisation group equations are presented. Appendix B is devoted to the numerical procedure used within this thesis. At first, the explicit derivation of the Majorana neutrino production rate is given, afterwards a detailed description of how to solve the integral equations is shown. As a last point, some important relations used within this thesis are proven.

2 Leptogenesis

There is something fascinating about science.
One gets such wholesale returns of conjecture
out of such a trifling investment of fact.
Mark Twain

This chapter introduces the issue of baryon asymmetry in the universe (BAU) [19]. Evidence and magnitude are discussed as well as the essential conditions for obtaining an asymmetry. Additionally, we argue why the Standard Model (SM) is not able to explain the BAU. Therefore different approaches are presented that try to solve this problem, namely Grand Unified Theory (GUT) baryogenesis, electroweak baryogenesis and the Affleck-Dine mechanism. Their advantages and disadvantages are described, too. For an overview see [20–23].

The last part of this chapter inaugurates the model of our choice for dealing with this problem, namely thermal leptogenesis. A classical ansatz is presented via Bolzmann equations and an effective model is introduced.

2.1 Baryon asymmetry of the universe

Antimatter seems to be very rare in the universe except for small amounts at the large particle accelerators at CERN or GSI as well as in cosmic rays. Because of the annihilation process of a baryon with an antibaryon $b + \bar{b} \to \gamma\gamma$ there would be no matter left nowadays if one started with symmetric initial conditions at the Big Bang. Furthermore, if there are regions of larger amounts of antimatter, there will be an interface in the outer space where the annihilation reaction takes place. Since this is not observed in any experiment one can even state that the asymmetry is maximal in the meaning of nearly no antibaryons but mere baryons.

Current measurements of the acoustic peaks of the WMAP seven-year observation [24] found values of

$$\eta_{\mathrm{B}}^{\mathrm{WMAP}} = \frac{n_b - n_{\bar{b}}}{n_\gamma} = (6.19 \pm 0.15) \cdot 10^{-10} \tag{2.1}$$

for the baryon to photon ratio. This is in good agreement with the values determined via Big-Bang-Nucleosynthesis (BBN) [25] by measuring the cosmological abundances of all light elements:

$$\eta_{\mathrm{B}}^{\mathrm{BBN}} = (5.1 - 6.5) \cdot 10^{-10}. \tag{2.2}$$

Thinking of the asymmetry occurring because of asymmetric initial conditions one has to mention the concept of cosmic inflation [26] at the beginning of the universe. In this model justified by WMAP and its precise measurement of the fluctuations of

the cosmic microwave background the baryons are heavily diluted so that the initial asymmetry should have been of order 10^{69} [27]. That is why a dynamical explanation immediately suggests itself.

2.1.1 Sakharov conditions

In 1967 Andrei Dmitrijewitsch Sakharov found three necessary conditions named after him that always have to be fulfilled to gain a baryon asymmetry [28]:

1. Baryon number violation
2. $\mathcal{C}$- (charge conjugation) and $\mathcal{CP}$- (charge parity) violation
3. Deviation from thermal equilibrium.

The first condition should be clear if one starts with a baryon symmetric universe with $\eta_\mathrm{B} = 0$. If the baryon number B is not broken, one will never receive a net baryon number $B \neq 0$. For the second condition one has to consider the baryon number operator $\mathcal{B}$. Its thermal average yields zero, since $\mathcal{B}$ is odd under $\mathcal{C}$- and $\mathcal{CP}$-symmetry. There are at least two possibilities for breaking $\mathcal{CP}$: It is spontaneously broken if a Higgs scalar field acquires a vacuum expectation value (vev) that is not real while it gets explicitly broken for complex phases within the Lagrangian that can not be reabsorbed by field redefinitions.

Since in thermal equilibrium the phase space densities for baryons and antibaryons are necessarily identical, it follows that $n_b = n_{\bar{b}}$. That is why deviation from thermal equilibrium is needed as well.

2.1.2 Baryogenesis in the Standard Model

The Standard Model of particle physics (for a review see [29–31]) supplies reliable predictions (e. g. the measurement of the magnetic moment of the electron), yet, it is not able to explain the BAU as can be seen in the following, considering the three Sakharov conditions.

Baryon number violation

Under extreme conditions such as in the primordial universe at very high temperatures, 't Hooft found that baryon number can be broken within the Standard Model by non-perturbative effects [32, 33]. These *instantons* violate the sum of baryon and lepton number $B + L$, but conserve its difference $B - L$. They are a solution of the field equations for a non-Abelian gauge theory, since the so-called θ-vacuum has a non-trivial periodic structure as depicted in fig. 2.1. This is why these instantons are able to tunnel between the different minima, but it is highly suppressed by a factor $\mathrm{e}^{-4\pi/\alpha_\mathrm{w}}$ with the weak coupling constant $\alpha_\mathrm{w} = g^2/4\pi$.

There is also a second solution for the field equations, the saddle point solution, which is referred to as the *sphaleron* (Greek: $\sigma\varphi\alpha\lambda\varepsilon\rho\acute{o}\varsigma$ "ready to fall") first described by Klinkhamer and Manton in 1984 [34, 35]. For large temperatures $T \gtrsim 100\,\mathrm{GeV}$ where the electroweak symmetry becomes restored, they represent a transition surmounting the barrier to the neighbouring minimum while changing baryon number [19]. If we

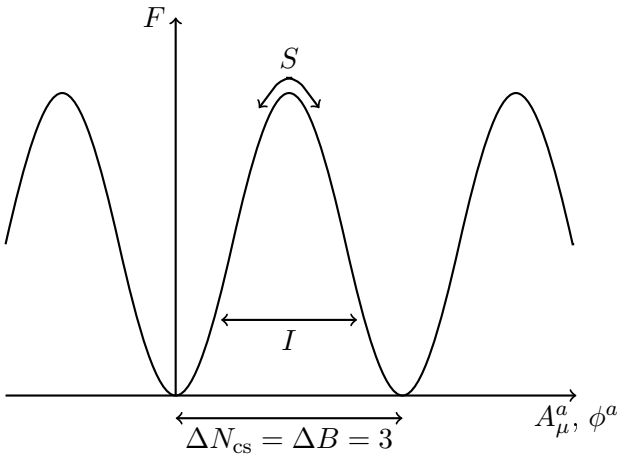

Figure 2.1: Schematic structure of the θ-vacuum for free energy F as a function of gauge and Higgs field configurations A^a_μ and ϕ^a with instanton I and sphaleron S transitions.

consider the baryon number violation between times $t = 0$ and $t = t_f$, we can express it using the Chern-Simons number, which is defined as

$$N_{\rm cs} = \frac{g^2}{32\pi^2} \int \mathrm{d}^3x\, \varepsilon^{ijk}\, \mathrm{Tr}\left(A_i \partial_j A_k + \frac{2}{3} \mathrm{i} A_i A_j A_k \right). \tag{2.3}$$

This number is not a gauge invariant quantity whereas its change is:

$$\Delta N_{\rm cs} = n_f [N_{\rm cs}(t_f) - N_{\rm cs}(0)] \equiv \Delta B\,. \tag{2.4}$$

That is why gauge transformations that connect two degenerate vacua change the baryon number ΔB by the integer winding number n in general. For neighbouring degenerate vacua this remains in $\Delta B = \Delta L = n_f$ with now $n = n_f$ number of fermion flavours. This is strictly connected to the Adler-Bell-Jackiw triangle-anomaly [36,37] which means a breaking of baryon and lepton symmetry, i. e. the derivative of their currents is proportional to n_f:

$$\partial_\mu j^\mu_{\rm B} = \partial_\mu j^\mu_{\rm L} = \frac{n_f}{64\pi^2} \left(g^2 W^a_{\mu\nu} \epsilon^{\mu\nu\alpha\beta} W^a_{\alpha\beta} - g'^2 F_{\mu\nu} \epsilon^{\mu\nu\alpha\beta} F_{\alpha\beta} \right). \tag{2.5}$$

The gauge couplings g and g' of $\mathrm{SU(2)_w}$ and $\mathrm{U(1)_Y}$ are used as well as the appropriate field strength tensors $W^a_{\mu\nu}$ and $F_{\mu\nu}$, respectively. The totally antisymmetric tensor is denoted by $\epsilon^{\mu\nu\alpha\beta}$.

Thus each sphaleron transition creates nine left-handed quarks (three states for each generation due to colour) and three left-handed leptons. For the sphaleron rate per unit volume one finds $\Gamma_{\rm sp}(T) = c\,(\alpha_{\rm w} T)^4$ which is dominated by the magnetic screening length $\xi = (\alpha_{\rm w} T)^{-1}$ and c is a dimensionless constant (for further discussion see [38–42]).

$\mathcal{C}$- and $\mathcal{CP}$- violation

The underlying gauge symmetry of the Standard Model is $\mathrm{SU(3)_c \times SU(2)_w \times U(1)_Y}$ which corresponds to quantum chromodynamics (QCD) and to the electroweak Weinberg-Salam model, respectively. The latter one does not exactly hold $\mathcal{CP}$ what is experimentally seen in the neutral Kaon decay that leads to mixed states of K_0 and $\overline{K_0}$ [43].

The violation occurs due to a phase in the Kobayashi-Maskawa matrix [29,30], however, this violation is much too small for explaining baryogenesis by missing at least eight orders of magnitude [44]. Thus for a successful theory of baryogenesis one has to add a $\mathcal{CP}$-violating factor.

Deviation from thermal equilibrium

At electroweak temperatures the equilibrium description of particle phenomena performs very well since the expansion rate of the universe is small compared to the rate of B-violating processes. That is why a deviation from thermal equilibrium can only be derived via a phase transition (PT) at those low scales and therefore, the order of such a transition becomes quite important. Solely a first order PT is able to gain a relevant baryon number, a second order PT or a continuous cross-over do not lead to a number $B \neq 0$.

In the electroweak theory one has to investigate the Higgs field ϕ. A necessary condition for a first order PT is the existence of a non-zero minimum of the effective potential at the critical temperature T_c. Whereas the minimum is strongly dependent on the Higgs particle mass m_H it was already found that this mass has to be small, $m_\mathrm{H} < 100\,\mathrm{GeV}$ [1] [45, 46], in particular lattice results state a critical Higgs mass of $m_\mathrm{H}^\mathrm{crit} = 66.5 \pm 1.4\,\mathrm{GeV}$ [47]. Latest measurements of the ATLAS and CMS Collaboration at LHC discovered an alleged Higgs particle at $m_\mathrm{H} \simeq 125\,\mathrm{GeV}$ [48,49] so that there should not be a first order PT but a smooth cross-over. Thus the Standard Model is not able to explain the observed asymmetry.

2.1.3 Further approaches

There have been many theories invented that try to solve the problem of the BAU, yet none of them has been experimentally confirmed. In the following the most successful ones are presented. For more exotic theories like baryogenesis produced by primordial black holes see [50]. Thermal leptogenesis, the model that is used within this thesis, is presented in the next section 2.2 in more detail.

GUT baryogenesis

Grand unified theories [51] try to unify the strong and the electroweak interaction within a framework of a non-Abelian symmetry group, e. g. SU(5) or SO(10). In these models, quarks and leptons are naturally members of the same gauge group representation. The energy scale of GUTs is of order $10^{14}\,\mathrm{GeV}$ or even greater, thus baryogenesis is obtained by decays of super-heavy bosons with masses according to this energy scale. The Sakharov conditions get fulfilled by the baryon number violating out-of-equilibrium decay of these bosons. Furthermore $\mathcal{CP}$-violation is given automatically by the interference of tree-level and loop graphs, which results in the use of complex Yukawa couplings.

The main problem of the simplest GUTs are the Standard Model sphalerons described earlier. Since they are acting after the GUT baryogenesis at a temperature $T \sim 10^{12}\,\mathrm{GeV}$ the sphalerons are able to destroy the asymmetry again. Further problems of GUTs are

[1] We are using natural units throughout this thesis, cf. app. A.

unwanted relics like magnetic monopoles as well as the predicted but not observed proton decay.

Electroweak baryogenesis

This class of models tries to receive the departure from thermal equilibrium via the electroweak phase transition [52–55]. As we have seen earlier, the Standard Model in general belongs to this class, but since its PT is not strongly first order and its $\mathcal{CP}$-violation is too small, some extentions are needed. One example is the insertion of two Higgs doublets that break $\mathcal{CP}$, another is the extension to supersymmetry within the framework of the MSSM (Minimal Supersymmetric Standard Model) [56]. One disadvantage of this kind of theories is the large number of new parameters. However they might soon be tested experimentially at the LHC.

Affleck-Dine baryogenesis

In 1984, Affleck and Dine [57] introduced a mechanism naturally implemented in supersymmetric models. It is defined on a SU(5) GUT with a many-parameter set of vacuum expectation values for scalar quarks and leptons. One then starts with very large vev's so that after the supersymmetry breaking and an inflationary phase, the quarks and leptons can have a large non-zero expectation value and thus a substantial baryon number is generated. Furthermore, it provides a candidate for dark matter: Soliton solutions of the scalar field of the Affleck-Dine baryogenesis, called Q-balls. This mechanism is a prominent example of non-thermal baryogenesis. Its main problems are the non-existence of a "standard model" for this kind of baryogenesis as well as the difficulty of falsifying the theory.

2.2 Thermal Leptogenesis

An elegant way of solving two problems at once, namely the BAU and the question of why the ordinary neutrinos are that light, is supplied by thermal leptogenesis [58]. All one has to do is to add only one type of new particles to the Standard Model which are heavy right-handed neutrinos N with masses $M \gtrsim 10^8\,\mathrm{GeV}$. At temperatures $T \sim M$ the $\mathcal{CP}$-violating out-of-equilibrium decay of these heavy neutrinos generates a lepton asymmetry which is later converted into a baryon asymmetry via the SM sphalerons. Therefore, the three Sakharov conditions are fulfilled and moreover the see-saw mechanism [59–61] can explain the observed small neutrino masses [62,63]. Current overviews are given in [64–66].

2.2.1 Underlying theory

Three additional electroweak singlet fermions ν_{Ri}, $i = 1, 2, 3$, namely the right-handed neutrinos, are added to the Standard Model. They couple via Yukawa couplings λ to the Standard Model lepton doublets[2] l_{Li} and Higgs doublet ϕ as described by the following

[2] Throughout this thesis the subscript L denotes left-handed particles and R right-handed ones, defined via $P_{R,L}\psi \equiv \psi_{R,L}$, with $P_{R,L} \equiv \frac{1}{2}(1 \pm \gamma_5)$.

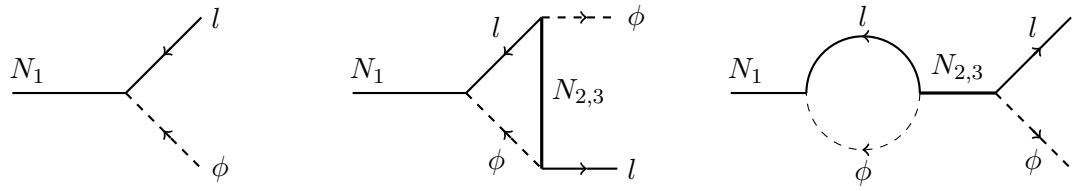

Figure 2.2: Tree-level and one-loop contributions to $\mathcal{CP}$-violating decay of a heavy Majorana neutrino N_1.

Lagrangian

$$\mathscr{L} = \mathscr{L}_{\mathrm{SM}} + \overline{\nu}_{Ri}\mathrm{i}\partial\!\!\!/\nu_{Rj} + \bar{l}_{Li}\widetilde{\phi}\lambda^*_{ij}\nu_{Rj} + \overline{\nu}_{Rj}\lambda_{ij}l_{Li}\phi - \frac{1}{2}M_{ij}(\overline{\nu^c}_{Ri}\nu_{Rj} + \overline{\nu}_{Rj}\nu^c_{Ri}), \quad (2.6)$$

with sum over i, j and $\nu^c_R = C\overline{\nu}^T_R$, where $C = \mathrm{i}\gamma_2\gamma_0$ denotes the charge conjugation matrix and $\widetilde{\phi} = \mathrm{i}\sigma_2\phi$. SU(2) isospin indices have been neglected. In the following, we have a closer look at the ingredients that are needed to produce the lepton asymmetry within the theory of thermal leptogenesis, namely the see-saw mechanism and the creation of $\mathcal{CP}$-asymmetry. Furthermore, we discuss the possibilities of verifying this ansatz.

See-saw mechanism

The advantage of the additional Majorana neutrinos [67] is both, the explanation for the BAU and for the smallness of the ordinary neutrino masses within the see-saw mechanism [59–61]. Since these heavy right-handed neutrinos are invariant under $\mathrm{SU(2)_w}\times\mathrm{U(1)_Y}$, i. e. electroweak singlets, one can add a Majorana mass term to the Lagrangian that does not affect chirality and other gauge properties of the SM (cf. eq. (2.6)). That is also why the Majorana mass M_R can be chosen very large in the following. One then obtains the 2×2 mass matrix $\mathscr{M}$

$$\mathscr{M} = \begin{pmatrix} 0 & M_{\mathrm{D}} \\ M_{\mathrm{D}} & M_{\mathrm{R}} \end{pmatrix}, \quad (2.7)$$

where M_{D} denotes the Dirac mass term typically of the order of the charged fermion mass of the same generation, e. g. $(M_{\mathrm{D}})_{\nu_e} \simeq m_e$. If one then calculates the eigenvalues $m_\pm$ of this matrix, one finds

$$m_\pm = \frac{1}{2}\left(M_{\mathrm{R}} \pm \sqrt{M^2_{\mathrm{R}} + 4M^2_{\mathrm{D}}}\right), \quad (2.8)$$

so that one obtains $m_\nu \simeq \frac{M^2_{\mathrm{D}}}{M_{\mathrm{R}}}$ for a neutrino mass which turns out to be very small, since $M_{\mathrm{R}} \gg M_{\mathrm{weak}} \gg M_{\mathrm{D}}$.

$\mathcal{CP}$-asymmetry

Normally $\mathcal{CP}$-violation occurs due to the interference of tree-level and loop diagrams as shown in fig. 2.2. For zero temperature $T = 0$ one can define

$$\varepsilon_i = \frac{\Gamma(N_i \to \phi l) - \Gamma(N_i \to \overline{\phi}\,\bar{l})}{\Gamma(N_i \to \phi l) + \Gamma(N_i \to \overline{\phi}\,\bar{l})}, \quad i = 1, 2, 3\,, \quad (2.9)$$

where Γ is the decay width of the heavy neutrino into Higgs boson and lepton doublet and their conjugated particles, respectively. In the following we denote the lightest Majorana neutrino $N_1 = \nu_{\mathrm{R}1} + \nu_{\mathrm{R}1}^c \equiv N$.

For hierarchical heavy neutrino masses ($M_1 \ll M_2, M_3$) one finds [68] a value of

$$\varepsilon_1 \simeq -\frac{3}{16\pi} \sum_{k=2}^{3} \frac{\mathrm{Im}\left[(\lambda^\dagger\lambda)^2_{k1}\right]}{(\lambda^\dagger\lambda)_{11}} \frac{M_1}{M_k} + \mathcal{O}\Big(\Big(\frac{M_1}{M_k}\Big)^{\frac{3}{2}}\Big) \tag{2.10}$$

for the $\mathcal{CP}$-asymmetry. Due to the interference of tree-level and loop graphs, the Yukawa coupling λ is a complex number. This result is obtained for zero temperature by using the Cutkosky cutting rules [69] for computing the imaginary part of vertices and self-energy loop contributions that are needed. At finite temperature, things become more costly so that one has to calculate the integrated decay rates for $\varepsilon(T)$. A hard thermal loop (HTL) corrected result can be found in [6, 70, 71]. The result of eq. (2.10) becomes modified there by a factor including the momentum integrations of Majorana neutrino and leptons. Results including the effect of thermal masses can be found in [72, 73], where one finds explicit contributions arising from the $T = 0$ propagators and from the thermal corrections to the fermion and boson propagators as well as a contribution due to their mixing:

$$\varepsilon_1^T = \varepsilon_1 \left(1 - n_{\mathrm{F}}(m) + n_{\mathrm{B}}(m) - 2n_{\mathrm{F}}(m)n_{\mathrm{B}}(m)\right) , \tag{2.11}$$

with $m = M_1/2$ and $n_{\mathrm{F,B}}(x) = (\exp(|x|/T) \pm 1)^{-1}$. Hence one can see that thermal effects are very important for leptogenesis. Later on these effects are naturally taken into account when a pure quantum treatment is used. Therefore resummation schemes (HTL, CTL, cf. chap. 5) for finite temperature scenarios are used within the calculation of the asymmetry-causing two-loop lepton self-energy so that the thermal effects are included.

Falsifying leptogenesis?

Postulating additional particles like the right-handed Majorana neutrinos and implementing new mechanisms like see-saw and thermal leptogenesis to explain the BAU is much easier than testing them. Since Majorana neutrinos are both, too heavy and too weakly coupled for a direct detection in current accelerators, one has to think about indirect tests. If there are heavy Majorana neutrinos, the neutrinoless double beta decay [74] will become a possible scenario and thus shall be measurable. There are current experiments trying to find evidence for it (for a review see [75]). Another possibility is the measuring of lepton flavour violating processes which allows measuring off-diagonal entries of $(\lambda^\dagger\lambda)$ that might be a circumstantial evidence for the see-saw mechanism and thermal leptogenesis. However, at the end one can say that "Archaeology is not an exact science" [76].

Nevertheless, there are even some constraints from leptogenesis concerning the ordinary neutrino mass [62, 63, 77, 78]. Since the $\mathcal{CP}$-asymmetry connects the baryon-to-photon rate with the atmospheric neutrino masses due to the Davidson-Ibarra bound [79] one can find limits for both, the heavy neutrino as well as for the ordinary ones. The lower bound on M_1 becomes

$$M_1 > M_1^{\min} \simeq 10^9\,\mathrm{GeV}\,\frac{m_{\nu_1} + m_{\nu_3}}{0.1\,\mathrm{eV}\,\kappa_f^{\max}} \tag{2.12}$$

with an efficiency factor κ_f maximized with respect to the decay parameter K. The efficiency factor depends on the effective neutrino mass $\widetilde{m}_1$ (cf. sec. 2.2.2) and is defined according to

$$\kappa_f \equiv (2 \pm 1) \times 10^{-2} \left(\frac{0.01\,\mathrm{eV}}{\widetilde{m}_1} \right)^{1.1 \pm 0.1} . \tag{2.13}$$

Therefore it is possible to find regions, in which condition (2.12) is fulfilled so that for the ordinary neutrinos one can find upper bounds

$$m_i < 0.12\,\mathrm{eV}, \qquad i = e,\, \mu,\, \tau\,. \tag{2.14}$$

These results are obtained using the simplest model of the see-saw mechanism with hierarchical heavy Majorana neutrinos and without taking into account e. g. 'spectator processes' [80]. The bounds imply that the Majorana neutrinos must be produced at $T \gtrsim 10^9$ GeV so that the reheating temperature after inflation also has to be of the same order.

2.2.2 Classical ansatz

Describing the evolution of phase space distribution functions classically the Boltzmann equations provide an appropriate ansatz. The general form is given by

$$L[f_\psi] = -\frac{1}{2} C[f_\psi]\,, \tag{2.15}$$

with the Liouville operator L for the phase-space density f of a particle species ψ in a Robertson-Walker metric [20]

$$L[f_\psi] \equiv E_\psi \frac{\partial f_\psi}{\partial t} - H\,|\mathbf{p}_\psi|^2 \frac{\partial f_\psi}{\partial E_\psi}. \tag{2.16}$$

The Hubble expansion rate is denoted by H and the energy of the particle with momentum $\mathbf{p}_\psi$ is E_ψ. The collision term C is defined according to

$$\begin{aligned} C[f_\psi] \equiv \sum_{\psi X \leftrightarrow Y} \int \mathrm{d}\Phi_{XY} (2\pi)^4 \delta^4(p_\psi + p_X - p_Y) \\ \times \left(f_\psi f_X |\mathcal{M}(\psi X \to Y)|^2 - f_Y |\mathcal{M}(Y \to \psi X)|^2 \right) , \end{aligned} \tag{2.17}$$

with the sum including all allowed processes $\psi X \leftrightarrow Y$ and X, Y multiparticle states. The transition amplitude is denoted by $\mathcal{M}$ and $\mathrm{d}\Phi_{XY}$ is the phase space integration:

$$\mathrm{d}\Phi_{XY} \equiv \mathrm{d}\Pi_X \mathrm{d}\Pi_Y \quad \text{with} \quad \mathrm{d}\Pi_X \equiv \prod_{\chi \in X} \mathrm{d}\Pi_\chi, \quad \mathrm{d}\Pi_\chi \equiv g_\chi \frac{\mathrm{d}^3 p_\chi}{(2\pi)^2} \frac{1}{2E(\mathbf{p}_\chi)}\,. \tag{2.18}$$

We used $p_X \equiv \sum_{\chi \in X} p_\chi$ and $f_X \equiv \prod_{\chi \in X} f_\chi$. The number of internal degrees of freedom is denoted by g_χ. Integrating the Boltzmann equation (2.15) with respect to $\mathrm{d}\Pi_\psi$ we obtain

$$\frac{\mathrm{d}n_\psi}{\mathrm{d}t} + 3Hn_\psi = -\sum_{\psi X \leftrightarrow Y} \left(\frac{n_\psi n_X}{n_\psi^{\mathrm{eq}} n_X^{\mathrm{eq}}} \gamma(\psi X \to Y) - \frac{n_Y}{n_Y^{\mathrm{eq}}} \gamma(Y \to \psi X) \right) , \tag{2.19}$$

where we assume kinetic equilibrium as well as Maxwell-Boltzmann statistics. The number density of the particle is defined according to

$$n_\psi \equiv g_\psi \int \frac{\mathrm{d}^3 p}{(2\pi)^3} f_\psi(\mathbf{p})\,. \tag{2.20}$$

Its equilibrium analogue is denoted by n_ψ^{eq} and

$$\gamma(\psi X \to Y) \equiv \int \mathrm{d}\Pi_\psi \mathrm{d}\Phi_{XY} (2\pi)^4 \delta^4(p_\psi + p_X - p_Y) f_\psi^{\mathrm{eq}} f_X^{\mathrm{eq}} |\mathcal{M}(\psi X \to Y)|^2\,. \tag{2.21}$$

Applying this result to the case of thermal leptogenesis we obtain for the lightest Majorana neutrino N_1 and the $B-L$ asymmetry the Boltzman equations [81]

$$\frac{\mathrm{d}n_{N_1}}{\mathrm{d}t} + 3Hn_{N_1} = \left(\frac{n_{N_1}}{n_{N_1}^{\mathrm{eq}}} - 1\right)(\gamma_D + \gamma_S)\,, \tag{2.22a}$$

$$\frac{\mathrm{d}n_{B-L}}{\mathrm{d}t} + 3Hn_{B-L} = \varepsilon_1 \left(\frac{n_{N_1}}{n_{N_1}^{\mathrm{eq}}} - 1\right)\gamma_D - \frac{n_{B-L}}{n_l^{\mathrm{eq}}}\gamma_W\,. \tag{2.22b}$$

The number densities for a left-handed doublet is n_l, D denotes decay and inverse decay processes, S scattering and W washout processes. Scaling out the expansion of the universe leads to

$$N_{N_1} \equiv \frac{n_{N_1}}{s}\,, \tag{2.23}$$

with the entropy density s. Hence we can rewrite the equations according to [78, 82]

$$\frac{\mathrm{d}N_{N_1}}{\mathrm{d}z} = -(D+S)(N_{N_1} - N_{N_1}^{\mathrm{eq}})\,, \tag{2.24a}$$

$$\frac{\mathrm{d}N_{B-L}}{\mathrm{d}z} = -\varepsilon_1 D(N_{N_1} - N_{N_1}^{\mathrm{eq}}) - W N_{B-L}\,, \tag{2.24b}$$

where $z = M_1/T$ as well as N_{N_1} and N_{B-L} being number density and amount of the asymmetry. The scattering term $S = \gamma_S/(Hz)$ represents the $\Delta L = 1$ scatterings while $D = \gamma_D/(Hz)$ takes into account decays and inverse decays. The Hubble expansion rate is given by

$$H \simeq \sqrt{\frac{8\pi^3 g_*}{90}}\,\frac{M_1^2}{M_{\mathrm{Pl}}}\,\frac{1}{z^2} \simeq 1.66 g_* \frac{M_1^2}{M_{\mathrm{Pl}}}\,\frac{1}{z^2}\,. \tag{2.25}$$

The total number of degrees of freedom for our purposes is $g_* = g_{\mathrm{SM}} = 106.75$ and the Planck mass $M_{\mathrm{Pl}} = 1.22 \cdot 10^{19}\,\mathrm{GeV}$. The $\mathcal{CP}$-violation is denoted by ε_1 and $W = \gamma_W/(Hz)$ is the washout term [78].

The decay and scattering terms D and S depend on the effective neutrino mass $\widetilde{m}_1$ that is defined via the ratio of Dirac and Majorana neutrino masses as

$$\widetilde{m}_1 = \frac{(m_{\mathrm{D}}^\dagger m_{\mathrm{D}})_{11}}{M_1}\,, \tag{2.26}$$

which is connected to the equilibrium neutrino mass

$$m_* = \frac{16\pi^{\frac{5}{2}}\sqrt{g_*}}{3\sqrt{5}}\,\frac{v^2}{M_{\mathrm{Pl}}} \simeq 1.08 \cdot 10^{-3}\,\mathrm{eV} \tag{2.27}$$

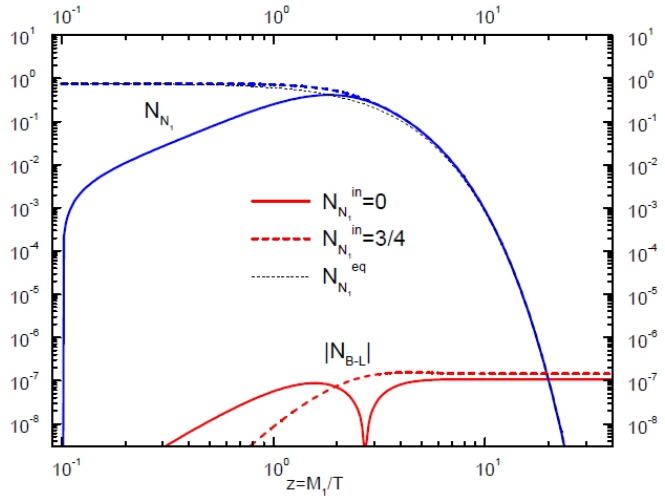

Figure 2.3: Dependence on zero and thermal initial abundance for Majorana neutrino production rate and $B-L$-asymmetry, from [77].

with the Higgs vev v via the decay parameter

$$K = \frac{\Gamma_D(z=\infty)}{H(z=1)} = \frac{\widetilde{m}_1}{m_*}\,. \tag{2.28}$$

This parameter is introduced for GUT baryogenesis and controls whether or not N_1 decays are in equilibrium. For example if $K \ll 1$, the Majorana neutrino does not decrease in number and thus equilibrium will not be preserved. This corresponds to the weak washout regime, where scattering processes with the thermal bath are less important. In contrast to this for $K \gg 1$, i. e. for the strong washout regime, no baryon asymmetry is generated since there is no departure from equilibrium.

The solution of eq. (2.24) for N_{B-L} certainly depends on the initial conditions $N^{\rm i}_{B-L}$ and $z_{\rm i}$ via

$$N_{B-L}(z) = N^{\rm i}_{B-L}{\rm e}^{-\int_{z_{\rm i}}^{z}{\rm d}z'\,W(z')} - \frac{3}{4}\varepsilon_1\kappa(z;\widetilde{m}_1, M_1\overline{m}^2)\,, \tag{2.29}$$

with an expression for the efficiency factor

$$\kappa_f(z) = \frac{4}{3}\int_{z_{\rm i}}^{z}{\rm d}z'\,D(N_{N_1} - N^{\rm eq}_{N_1}){\rm e}^{-\int_{z'}^{z}{\rm d}z''\,W(z'')}\,. \tag{2.30}$$

The sum of the light neutrino masses squared is denoted by $\overline{m}^2 = m_1^2 + m_2^2 + m_3^2$.

The dependence on zero and thermal initial abundance of the Majorana neutrino production rate and the $B-L$-asymmetry is depicted in fig. 2.3. As can be seen, also for zero initial abundance, the generated asymmetry is of the order of the one including an initial abundance. Thus it is sufficient to consider a zero initial asymmetry, i. e. $N^{\rm i}_{B-L} = 0$, so that now we can compare the predicted baryon to photon number ratio with the value of $\eta_{\rm B}$. Using the fraction $a_{\rm sph} = 28/79$ of $B-L$ asymmetry converted to a baryon asymmetry by sphalerons [83] and the dilution factor $f = N^{\rm rec}_\gamma/N^\star_\gamma = 2387/86$ one obtains using eq. (2.30)

$$\eta_{\rm B} = \frac{3}{4}\frac{a_{\rm sph}}{f}\varepsilon_1\kappa_f \simeq 0.96\cdot 10^{-2}\varepsilon_1\kappa_f\,. \tag{2.31}$$

This shows that these calculations are consistent with current observations, but since it is not possible to present a reasonable theoretical error one has to improve these methods. Since Boltzmann equations are valid only for classical non-equilibrium processes in dilute, weakly coupled systems, one should better deal with a quantum mechanical treatment using Kadanoff-Baym equations which are well-defined by means of Green's functions instead of number densities. Their validity is not questionable in a strongly interacting plasma like the one emerging in the considered non-Abelian gauge theory and could provide a better understanding of the underlying size of uncertainties that have to be made.

2.2.3 Effective model

The so-called *vanilla leptogenesis* is the model we deal within this thesis. Starting from eq. (2.6)) we can integrate out the two heavier neutrinos M_2, $M_3 \gg M_1 \equiv M$ which leads to an effective theory with Lagrangian (cf. [21])

$$\begin{aligned}\mathscr{L} = \mathscr{L}_{\text{SM}} + \bar{l}_{Li}\,\tilde{\phi}\,\lambda^*_{i1} N + N^T \lambda_{i1}\, C\, l_{Li}\,\phi - \frac{1}{2} M N^T C N \\ + \frac{1}{2}\eta_{ij}\, l^T_{Li}\,\phi\, C\, l_{Lj}\,\phi + \frac{1}{2}\eta^*_{ij}\,\bar{l}_{Li}\,\tilde{\phi}\, C\, \bar{l}^T_{Lj}\,\tilde{\phi}\,.\end{aligned} \tag{2.32}$$

Here the lightest Majorana neutrino is again denoted as $N \equiv N_1 = \nu_{R1} + \nu^c_{R1}$ and we consider only small Yukawa couplings $\lambda_{i1} \ll 1$ so that the decays and inverse decays of N dominate. The effective coupling η_{ij} is defined as

$$\eta_{ij} = \sum_{k=2}^{3} \lambda_{ik} \frac{1}{M_k} \lambda^T_{kj}\,. \tag{2.33}$$

In the Boltzmann approach one then has to consider phase space distribution functions for all contributing particles. Since the generation of lepton asymmetry is a process close to equilibrium, one can even linearise the Boltzmann equations in the deviations from equilibrium distribution functions. Assuming small number densities for simplicity, this leads to [21, 80]

$$\begin{aligned} g_N \frac{\partial}{\partial t}\,\delta f_N(t,p) = &- g_N \frac{\partial}{\partial t} f_N(p) \\ &- \frac{1}{2E}\int \mathrm{d}\Phi(p)\,\delta f_N(t,p)\left(|\mathcal{M}(N \to l\,\phi)|^2 + |\mathcal{M}(N \to \bar{l}\,\bar{\phi})|^2\right)\end{aligned} \tag{2.34}$$

for a Majorana neutrino with deviation of the phase space distribution function from equilibrium δf_N, the phase space integration $\mathrm{d}\Phi$ and $g_N = 2$ number of initial degrees of freedom. The matrix elements $\mathcal{M}(\ldots)$ indicate the in eq. (2.32) considered processes. For the lepton doublets one obtains a similar equation (for details see [21]) but including more matrix elements due to the higher amount of possibilities of interactions (cf. eq (2.32)).

For further investigations later on we also need the Feynman rules for the calculation of contributing diagrams. From eq. (2.32) we can derive the following Feynman rules for propagators and vertices [16]:[3]

[3] A list of the explicit form of the propagators can be found in app. A.2.1.

- Majorana neutrino propagator:

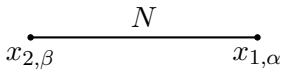

$\mathrm{i}\, G_{\alpha\beta}(x_1, x_2)$

- Lepton propagator:

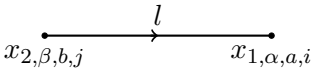

$\mathrm{i}\, \delta_{ij}\, \delta_{ab}\, S_{\alpha\beta}(x_1, x_2)$

- Scalar propagator:

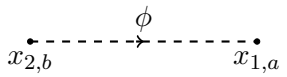

$\mathrm{i}\, \delta_{ab}\, \Delta(x_1, x_2)$

- Majorana-lepton-scalar-vertices:

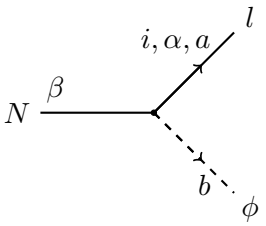

$\mathrm{i}\, \lambda^*_{i1} \epsilon_{ab} (P_R)_{\alpha\beta}$

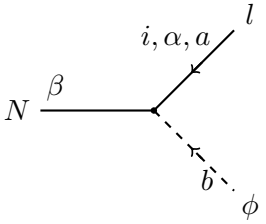

$\mathrm{i}\, \lambda_{i1} \epsilon_{ab} (C P_L)_{\beta\alpha}$

- Lepton-lepton-scalar-scalar-vertices:

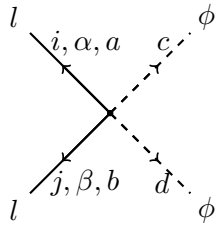

$\mathrm{i}\, \eta^*_{ij} (\epsilon_{ac}\epsilon_{bd} + \epsilon_{ad}\epsilon_{bc}) (P_R C)_{\alpha\beta}$

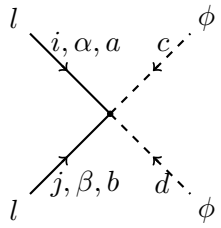

$\mathrm{i}\, \eta_{ij} (\epsilon_{ac}\epsilon_{bd} + \epsilon_{ad}\epsilon_{bc}) (C P_L)_{\alpha\beta}$

We used the projectors $P_L = \frac{1}{2}(1 - \gamma_5)$ and $P_R = \frac{1}{2}(1 + \gamma_5)$ with the Dirac matrix $\gamma_5 = \mathrm{i}\gamma_0\gamma_1\gamma_2\gamma_3$. The Levi-Civita tensor in 2 dimensions is denoted by ϵ_{ab}.

3 Nonequilibrium quantum field theory

Wer hohe Türme bauen will,
muss lange am Fundament verweilen.
Anton Bruckner

In this chapter, the basis for describing nonequilibrium dynamics of quantum systems is presented. At first a brief introduction of how to treat systems in thermal field theory in equilibrium is given according to [84–88]. Afterwards nonequilibrium systems are considered (cf. [89–92]) and the Schwinger-Keldysh formalism is introduced. The equations of motion are presented in the third section which deals with the Kadanoff-Baym equations [93–96] and their solutions. Therefore, the equilibrium propagators for lepton and Higgs are calculated as well as the out-of-equilibrium propagators for the Majorana neutrino.

3.1 Thermal field theory

In the early universe similar to e. g. heavy ion collisions one has to consider large temperatures that can not be neglected. That is why one has to use the framework of thermal field theory. In natural units[1] one can then start from the definition of the canonical partition function

$$Z[\beta] = \operatorname{Tr} \mathrm{e}^{-\beta H} = \sum_n \mathrm{e}^{-\beta E_n} \tag{3.1}$$

where a complete set of eigenvectors of the Hamilton operator

$$H|n\rangle = E_n|n\rangle \tag{3.2}$$

is used for taking the trace. The inverse temperature is denoted by $\beta = 1/T$. If one also rewrites the trace in terms of this set of eigenvectors, one can derive the generating functional for the path integral formalism including a time-dependent source $j(\tau)$, which is defined for a path $\phi(\tau)$ as

$$Z[\beta; j] = \int \mathcal{D}\phi(\tau)\, \exp\left\{ - S_\mathrm{E}(\beta) + \int_0^\beta \mathrm{d}\tau\, j(\tau)\phi(\tau) \right\}. \tag{3.3}$$

Here the Euclidean action S_E is used as well as periodic boundary conditions $\phi(\beta) = \phi(0)$. For these issues, it is standard to use imaginary times, which means an analytical continuation from Minkowski to Euclidean space time $t \to \mathrm{i}\tau$. Via functional differentiation one can now derive the n-point functions, for example the propagator in imaginary time:

$$\frac{1}{Z[\beta]} \frac{\delta^2 Z[\beta; j]}{\delta j(\tau_1) \delta j(\tau_2)}\Big|_{j=0} = \frac{1}{Z[\beta]} \int \mathcal{D}\phi(\tau)\phi(\tau_1)\phi(\tau_2)\mathrm{e}^{-S_\mathrm{E}(\beta)}\,. \tag{3.4}$$

[1] They are used throughout this thesis with $k_\mathrm{B} = \hbar = c = 1$. For conventions consult app. A.

If one compares this to the thermal average $\langle\mathcal{O}\rangle$ of an operator $\mathcal{O}$ that is defined by

$$\langle\mathcal{O}\rangle_\beta = \frac{1}{Z[\beta]}\,\mathrm{Tr}\left(\mathcal{O}\,\mathrm{e}^{-\beta H}\right)\,, \tag{3.5}$$

one can define the two-point functions $D^{\gtrless}(t,t')$, the so-called *Wightman functions*:

$$D^{>}(t,t') = \langle\phi(t)\,\phi(t')\rangle_\beta \tag{3.6a}$$
$$D^{<}(t,t') = \langle\phi(t')\,\phi(t)\rangle_\beta = D^{>}(t',t)\,, \tag{3.6b}$$

which are now valid for all times t, especially real values. Using the *Kubo-Martin-Schwinger (KMS) relation* (cf. [86])

$$D^{>}(t,t') = D^{<}(t+\mathrm{i}\beta,t')\,, \tag{3.7}$$

one can define the time-ordered propagator for real values of t and t':

$$\begin{aligned} D(t,t') &= \langle T(\phi(t)\,\phi(t'))\rangle \\ &= \theta(t-t')D^{>}(t,t') + \theta(t'-t)D^{<}(t,t')\,. \end{aligned} \tag{3.8}$$

For later purposes as well as for completeness it is quite useful to define the *spectral propagator* $D^{-}(x,y)$ and the *statistical propagator* $D^{+}(x,y)$:

$$D^{-}(x,y) = \mathrm{i}\,\langle[\phi(x),\phi(y)]\rangle = \mathrm{i}\,(D^{>}(x,y) - D^{<}(x,y)) \tag{3.9a}$$
$$D^{+}(x,y) = \frac{1}{2}\langle\{\phi(x),\phi(y)\}\rangle = \frac{1}{2}(D^{>}(x,y) + D^{<}(x,y))\,, \tag{3.9b}$$

with $\phi(x)$ denoting a scalar field depending on the four-vector x. These propagators form the connection between all kinds of propagators, i. e. imaginary time, real time, retarded and advanced ones. The physical interpretation of the first one becomes more obvious by considering its Fourier transform[2], which is the spectral function

$$\rho(k_0) = D^{>}(k_0) - D^{<}(k_0)\,. \tag{3.10}$$

It characterises the spectrum of the theory, whereas the statistical propagator gives information about the occupation numbers.

With $D(k_0)$, the Fourier transform of $D(t) \equiv D(t,0)$, one can rewrite the two-point functions in terms of the spectral function

$$D^{>}(k_0) = (1 + f_\mathrm{B}(k_0))\,\rho(k_0) \tag{3.11a}$$
$$D^{<}(k_0) = f_\mathrm{B}(k_0)\,\rho(k_0)\,, \tag{3.11b}$$

using the Bose-Einstein distribution $f_\mathrm{B}(k_0) = (\mathrm{e}^{\beta k_0} - 1)^{-1}$.

For defining the *retarded* and the *advanced propagators*, one has to do an analytic continuation of the imaginary-time propagator $\Delta(\tau)$. The latter one is also called Matsubara propagator, since its Fourier transform

$$\Delta(\mathrm{i}\omega_n) = \int_0^\beta \mathrm{d}\tau \mathrm{e}^{\mathrm{i}\omega_n\tau}\Delta(\tau) \tag{3.12}$$

[2] Note that for easier notation we use the same symbol for functions in coordinate space as well as in momentum space.

as well as its inverse transform

$$\Delta(\tau) = T \sum_n \mathrm{e}^{\mathrm{i}\omega_n \tau} \Delta(\mathrm{i}\omega_n) \tag{3.13}$$

depend on the discrete *Matsubara frequencies* $\omega_n = 2\pi n/\beta$. Therefore, we get

$$D^{\mathrm{R}}(k_0) = -\mathrm{i}\Delta(k_0 + \mathrm{i}\eta) \tag{3.14a}$$
$$D^{\mathrm{A}}(k_0) = \quad \mathrm{i}\Delta(k_0 - \mathrm{i}\eta)\,, \tag{3.14b}$$

for the retarded and advanced propagators, which simplifies to $k_0 = \pm\omega$ in the free case.

3.2 Schwinger-Keldysh formalism

For systems out of equilibrium the specification of an initial state is needed[3], for example a density matrix $\rho_D(t_0 = 0)$ with normalisation $\mathrm{Tr}\,\rho = 1$. Then one can define the *nonequilibrium effective action*, i. e. the generating functional that contains all information:

$$Z[J, R; \rho_D] = \mathrm{Tr}\left[\rho_D(0)\, T_{\mathcal{C}}\, \exp\left\{\mathrm{i}\int_x J(x)\Phi(x) + \frac{\mathrm{i}}{2}\int_{xy} R(x,y)\Phi(x)\Phi(y)\right\}\right]. \tag{3.15}$$

Here we introduce two source terms J and R instead of one (cf. eq. (3.3)) for an easier derivation of the equations of motion later on. Furthermore we use $T_{\mathcal{C}}$ for time-ordering along a time path $\mathcal{C}$ and $\int_x \equiv \int_{\mathcal{C}} \mathrm{d}x^0 \int \mathrm{d}^3x$. In analogy to eq. (3.4) we can then derive all n-point functions from eq. (3.15) with respect to the time-ordering $T_{\mathcal{C}}$. This path is defined on the *real-time contour* as depicted in fig. 3.1 with usual time ordering along the forward piece $\mathcal{C}^+$ and anti-temporal ordering along the backward one $\mathcal{C}^-$. This implies that every time on $\mathcal{C}^-$ is considered later than all times on $\mathcal{C}^+$. A consequence of this formalism is the doubling of fields Φ, i. e. the degrees of freedom. Thus one inserts additionally so-called *ghost* fields Φ_2 that live on $\mathcal{C}^-$ to the physical fields Φ_1 so that even the propagator of a neutral boson without spin becomes a 2×2 matrix. With a symmetric choice the diagonalized Feynman propagator D_F for example then looks like

$$\begin{aligned} D_F \equiv \begin{pmatrix} D^{11} & D^{12} \\ D^{21} & D^{22} \end{pmatrix} &= \begin{pmatrix} \mathrm{i}\mathbb{P}\frac{1}{k^2 - m^2} & 0 \\ 0 & -\mathrm{i}\mathbb{P}\frac{1}{k^2 - m^2} \end{pmatrix} \\ &\quad + 2\pi\delta(k^2 - m^2) \begin{pmatrix} \frac{1}{2} + f_{\mathrm{B}}(|k_0|) & \mathrm{e}^{\beta|k_0|/2} f_{\mathrm{B}}(|k_0|) \\ \mathrm{e}^{\beta|k_0|/2} f_{\mathrm{B}}(|k_0|) & \frac{1}{2} + f_{\mathrm{B}}(|k_0|) \end{pmatrix} \end{aligned} \tag{3.16}$$

as decomposed into a real and imaginary part, where we can find

$$D^{12}(x,y) \equiv D^{<}(x,y) \qquad \text{and} \qquad D^{21}(x,y) \equiv D^{>}(x,y) \tag{3.17a}$$
$$D^{11}(x,y) = D^{+}(x,y) - \frac{\mathrm{i}}{2}\,\mathrm{sign}(x^0 - y^0) D^{-}(x,y)\,. \tag{3.17b}$$
$$D^{22}(x,y) = D^{+}(x,y) + \frac{\mathrm{i}}{2}\,\mathrm{sign}(x^0 - y^0) D^{-}(x,y)\,. \tag{3.17c}$$

The principal value is denoted by $\mathbb{P}$.

[3] Its state at later times is unknown, that is why this formalism is referred to as the 'in-in' formalism.

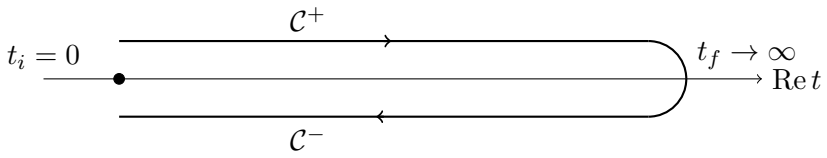

Figure 3.1: Real-time contour $\mathcal{C}$ in the complex time plane for nonequilibrium Green's functions.

This approach helps avoiding singularities that emerge from the delta function in eq. (3.16), which needs to be squared while calculating a self-energy [97]. Considering for example the vertices one finds that since ghost and physical fields do not mix, one is left with two different types of vertices. These two components exactly cancel the arising singularities due to the square of the delta function.

A better way for calculating real-time observables is the use of self-energies which will be applied throughout this thesis. Starting from Dyson's equation [86] the self-energy[4] $\Pi(k)$ in matrix form is defined in terms of the full propagator $D(k)$

$$D(k) = D^F(k) + D^F(k)\,(-\mathrm{i}\Pi(k))\,D(k)\,. \tag{3.18}$$

3.3 Kadanoff-Baym equations (KBEs)

3.3.1 KBEs for scalars

For describing the dynamics of a nonequilibrium system the equations of motion are needed. Starting from eq. (3.15) one again can derive all n-point functions via functional derivative analogously to eq. (3.4). Furthermore, the *2PI effective action* $\Gamma_2[\Phi, \Delta]$, i. e. the action including only contributions from two-particle irreducible[5] (2PI) diagrams, is obtained after performing a Legendre transform [30] with respect to the two sources J and R. It is given by

$$\Gamma_2[\Phi, \Delta] \equiv \Gamma_1[\Phi] - \frac{1}{2}\int_{x,y} R(x,y)\Phi(x)\Phi(y) - \frac{1}{2}\,\mathrm{Tr}\, R\Delta\,, \tag{3.19}$$

where $\Gamma_1[\Phi]$ denotes the 1PI effective action, which is defined according to

$$\Gamma_1[\Phi] \equiv -\mathrm{i}\ln Z[J,R] - \int_x \Phi(x)J(x)\,. \tag{3.20}$$

Thus, only 1PI diagrams contribute to the following self-energy (cf. [91])

$$\Pi(x,y;\Phi,\Delta) \equiv 2\,\mathrm{i}\,\frac{\delta\Gamma_2[\Phi,\Delta]}{\delta\Delta(x,y)}\,, \tag{3.21}$$

with the full effective propagator for a scalar

$$\Delta^{-1}(x,y) = \mathrm{i}\,\left(\Delta_0^{-1}(x,y) - \mathrm{i}R(x,y) - \Pi(x,y)\right)\,. \tag{3.22}$$

[4] Unless stated otherwise, bosonic self-energies are denoted by $\Pi(p)$ and fermionic ones by $\Sigma(p)$.
[5] This means that only diagrams are considered that are still connected after cutting two internal lines.

From the Legendre transform, one directly obtains the *stationarity condition* for the propagator

$$\frac{\delta\Gamma_2[\Phi,\Delta]}{\delta\Delta(x,y)} = -\frac{1}{2}\,R(x,y)\,, \tag{3.23}$$

which yields the equation of motion in the absence of the sources, meaning $R = 0$. Using eq. (3.22) and the solution of the classical propagator in scalar theory, which is $\Delta_0^{-1}(x-y) = \mathrm{i}(\Box_x + m^2)\delta^4(x-y)$, we obtain the evolution equation of the time-ordered propagator

$$(\Box_x + m^2)\Delta(x,y) + \mathrm{i}\int_z \Big(\Pi(x,z;\Delta) - \mathrm{i}R(x,y)\Big)\Delta(z,y) = -\mathrm{i}\delta^4(x-y)\,. \tag{3.24}$$

In the absence of the source $R = 0$, this becomes the well-known *Schwinger-Dyson equation* (cf. [30]). For notation is used $\delta^4(x-y) \equiv \delta_{\mathcal{C}}(x^0-y^0)\delta^3(\mathbf{x}-\mathbf{y})$ and $\Box_x = \partial_{x,\mu}\partial_x^\mu$.

Deriving the *Kadanoff-Baym equations* for the correlation functions $\Delta^{\lessgtr}$, which means the explicit decomposition in terms of the time coordinate being on the upper or lower branch on the contour $\mathcal{C}$, one has to use the relations of eq. (3.9) that also hold for self-energies $\Pi^{\lessgtr}$ and $\Pi^{\pm}$. The latter ones are connected to the retarded and advanced self-energies via

$$\Pi^R(x,y) = \theta(x^0-y^0)\Pi^-(x,y) \tag{3.25a}$$

$$\Pi^A(x,y) = -\theta(x^0-y^0)\Pi^-(x,y)\,. \tag{3.25b}$$

Thus the Kadanoff-Baym equations for the spectral function and the statistical propagator are given by

$$(\Box_x + m^2)\Delta^-(x,y) = -\,\mathrm{i}\int \mathrm{d}^3\mathbf{z}\int_{t_2}^{t_1}\mathrm{d}z^0\,\Pi^-(x,z)\Delta^-(z,y) \tag{3.26a}$$

$$\begin{aligned}(\Box_x + m^2)\Delta^+(x,y) = &-\,\mathrm{i}\int \mathrm{d}^3\mathbf{z}\int_{t_i}^{t_1}\mathrm{d}z^0\,\Pi^-(x,z)\Delta^+(z,y)\\ &+\,\mathrm{i}\int \mathrm{d}^3\mathbf{z}\int_{t_i}^{t_2}\mathrm{d}z^0\,\Pi^+(x,z)\Delta^-(z,y)\end{aligned} \tag{3.26b}$$

with $t_1 \equiv x^0$, $t_2 \equiv y^0$ and an initial time t_i. The space integrations without explicitly given boundaries are evaluated in $\mathbb{R}^3$. For a detailed derivation, consult [98].

In the following, only systems with spatial translational invariance are considered, i. e. all two-point functions depend on the difference of spatial coordinates so that it is obvious to perform a Fourier transform of the Kadanoff-Baym equations (3.26). If also backreactions of the field Φ can be neglected due to the use of a very large medium, one can further simplify the equations. For the medium being in thermal equilibrium one can achieve time-translational invariance for the self-energy and the spectral function as well [98]. Altogether, the Kadanoff-Baym equations reduce to

$$(\partial_{t_1}^2 + \omega_{\mathbf{q}}^2)\Delta_{\mathbf{q}}^-(t_1-t_2) = -\int_{t_2}^{t_1}\mathrm{d}t'\,\Pi_{\mathbf{q}}^-(t_1-t')\Delta_{\mathbf{q}}^-(t'-t_2) \tag{3.27a}$$

$$\begin{aligned}(\partial_{t_1}^2 + \omega_{\mathbf{q}}^2)\Delta_{\mathbf{q}}^+(t_1,t_2) = &\int_{t_i}^{t_2}\mathrm{d}t'\,\Pi_{\mathbf{q}}^+(t_1-t')\Delta_{\mathbf{q}}^-(t'-t_2)\\ &-\int_{t_i}^{t_1}\mathrm{d}t'\,\Pi_{\mathbf{q}}^-(t_1-t')\Delta_{\mathbf{q}}^+(t',t_2)\,,\end{aligned} \tag{3.27b}$$

with $\Delta_{\mathbf{q}}(t_1, t_2)$, $\Pi_{\mathbf{q}}(t_1, t_2)$ the Fourier transforms of $\Delta(x, y)$, $\Pi(x, y)$ in momentum space and $\omega_{\mathbf{q}}^2 = \mathbf{q}^2 + m^2$.

3.3.2 KBEs for fermions

As we are interested in heavy Majorana neutrinos, i. e. fermionic particles, we now derive the KBE's for fermions. Let $S(x, y)$ be the propagator of a fermion, then for massless left-handed leptons in the Weyl representation l_i (as also used in the Lagrangian (2.6)) spectral and statistical propagator are defined as

$$(S^-_{Lij})_{\alpha\beta}(x, y) = \mathrm{i}\,\langle\{l_{i\alpha}(x), \bar{l}_{j\beta}(y)\}\rangle \tag{3.28a}$$

$$(S^+_{Lij})_{\alpha\beta}(x, y) = \frac{1}{2}\langle[l_{i\alpha}(x), \bar{l}_{j\beta}(y)]\rangle\,, \tag{3.28b}$$

with α, β spinor indices and subscript L denoting projection on left-handed fields $S^\pm_L = P_L S^\pm$ with $P_L = (1 - \gamma_5)/2$. $S^\pm$ are lepton propagators in Dirac basis, indices corresponding to SU(2) were omitted.

In analogy to the scalar case, one can define the functions $S^\lessgtr$ (cf. eq. (3.29)), which obey the same relations to spectral and statistical propagators as in the bosonic case (right-hand side of eq. (3.9)). So one finds for the Majorana neutrino propagator $G(x, y)$ with Majorana field N

$$G^>_{\alpha\beta}(x, y) = \quad\langle N_\alpha(x), N_\beta(y)\rangle\,, \tag{3.29a}$$

$$G^<_{\alpha\beta}(x, y) = -\langle N_\beta(y), N_\alpha(x)\rangle \tag{3.29b}$$

and for the spectral and statistical propagator

$$G^-_{\alpha\beta}(x, y) = \mathrm{i}\,\langle\{N_\alpha(x), N_\beta(y)\}\rangle\,, \tag{3.30a}$$

$$G^+_{\alpha\beta}(x, y) = \frac{1}{2}\langle[N_\alpha(x), N_\beta(y)]\rangle\,. \tag{3.30b}$$

For later purposes, i. e. the calculation of the matter-antimatter asymmetry caused by the out-of-equilibrium decay of the Majorana neutrinos, we can define the Green's function for the Majorana as well as the self-energy $\Sigma_{\mathcal{C}}(x, y)$ on the Keldysh contour $\mathcal{C}$ (cf. fig. 3.1). Altogether one is left with the relations (3.17) for the Majorana propagator $G_{\mathcal{C}}(x, y)$. After a straight forward calculation starting from the Schwinger-Dyson equation for the Majorana propagator[6] with Majorana mass M

$$C(\mathrm{i}\not{\partial}_x - M)G(x, y) - \int_z C\Sigma(x, z)G(z, y) = -\mathrm{i}\delta^4(x - y) \tag{3.31}$$

using the conventions of eq. (3.24) and multiplying with the charge conjugation matrix C for later purposes, one again can derive the two coupled Kadanoff-Baym equations

[6] We omit the subscript for the Keldysh contour $\mathcal{C}$ from now on for the propagators and self-energies.

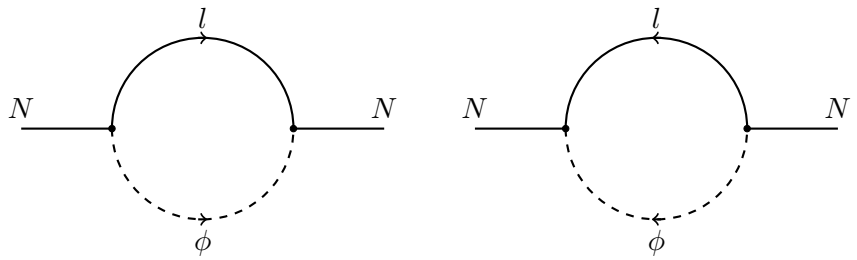

Figure 3.2: One-loop contributions to the Majorana neutrino self-energies $\Sigma^{\pm}_{\mathbf{p}}$.

for the spectral and statistical propagator [16]:

$$C(\mathrm{i}\gamma^0\partial_{t_1} - \mathbf{p}\boldsymbol{\gamma} - M)G^{-}_{\mathbf{p}}(t_1,t_2) = -\int_{t_1}^{t_2} \mathrm{d}t'\, C\Sigma^{-}_{\mathbf{p}}(t_1,t')G^{-}_{\mathbf{p}}(t',t_2) \tag{3.32a}$$

$$\begin{aligned} C(\mathrm{i}\gamma^0\partial_{t_1} - \mathbf{p}\boldsymbol{\gamma} - M)G^{+}_{\mathbf{p}}(t_1,t_2) = &-\int_{t_i}^{t_2} \mathrm{d}t'\, C\Sigma^{+}_{\mathbf{p}}(t_1,t')G^{-}_{\mathbf{p}}(t',t_2) \\ &+\int_{t_i}^{t_1} \mathrm{d}t'\, C\Sigma^{-}_{\mathbf{p}}(t_1,t')G^{+}_{\mathbf{p}}(t',t_2)\,. \end{aligned} \tag{3.32b}$$

Again a Fourier transform into momentum space was implemented. The one-loop contributions to the Majorana self-energies are depicted in fig. 3.2.

For the lepton propagators $S^{\pm}_{L,\mathbf{k}}$ one obtains exactly the same KBE's by replacing $C\Sigma^{\pm}_{\mathbf{p}}$ by the lepton self-energies $\Sigma^{\pm}_{L,\mathbf{k}}$ and omitting the factor C in the kinetic term. The contributing diagrams up to two loop order are presented in fig. 4.1. In contrast to the Majorana KBE's, also two-loop contributions become important for leptons as will be discussed in the next chapter.

3.3.3 Solutions for the propagators

In case of the Standard Model particles remaining in thermal equilibrium one can simplify the above discussed KBE's so that the self-energies and the spectral propagator only depend on the difference in times. Applying a Laplace transform on them, these equations both become exactly solvable (cf. [98, 99]).

This procedure leads to results for the lepton and Higgs propagators, since the Standard Model interactions keep the system in thermal equilibrium, ensuring the validity of the ansatz. This becomes apparent by comparing the corresponding time scale $\tau_{\mathrm{sm}} \approx 1/(g^2 T)$ at temperatures $T \approx M$ to the much larger equilibration time $\tau_N \approx 1/(\lambda^2 M)$ of the heavy neutrino.

The propagators then fulfil the KMS relation (cf. [86])

$$\Delta^{<}_{\mathbf{q}}(w) = \mathrm{e}^{-\beta\omega}\Delta^{>}_{\mathbf{q}}(w) \tag{3.33a}$$

$$S^{<}_{\mathbf{k}}(w) = -\mathrm{e}^{-\beta\omega}S^{>}_{\mathbf{k}}(w)\,, \tag{3.33b}$$

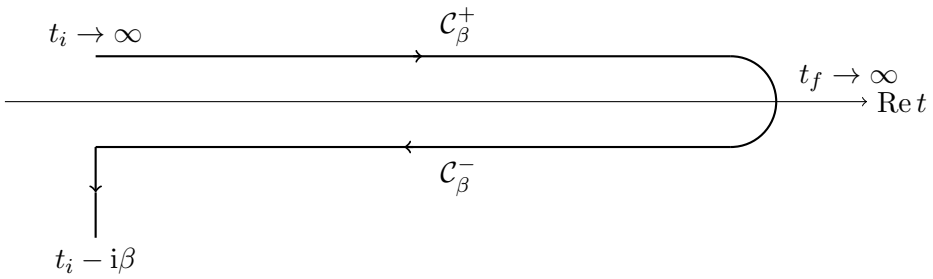

Figure 3.3: Real-time contour $\mathcal{C}_\beta$ in the complex time plane for equilibrium Green's functions.

which implies

$$\Delta_{\mathbf{q}}^+(\omega) = -\frac{\mathrm{i}}{2}\coth\left(\frac{\beta\omega}{2}\right)\Delta_{\mathbf{q}}^-(\omega)\,, \tag{3.34a}$$

$$S_{\mathbf{k}}^+(\omega) = -\frac{\mathrm{i}}{2}\tanh\left(\frac{\beta\omega}{2}\right)S_{\mathbf{q}}^-(\omega)\,. \tag{3.34b}$$

Note that the energy ω is not on-shell. The free equilibrium propagators can be evaluated on the contour $\mathcal{C}_\beta$, depicted in fig. 3.3. One obtains

$$\Delta_{\mathbf{q}}^-(y) = \frac{1}{\omega_{\mathbf{q}}}\sin(\omega_{\mathbf{q}}y)\,, \tag{3.35a}$$

$$\Delta_{\mathbf{q}}^+(y) = \frac{1}{2\omega_{\mathbf{q}}}\coth\left(\frac{\beta\omega_{\mathbf{q}}}{2}\right)\cos(\omega_{\mathbf{q}}y)\,, \tag{3.35b}$$

$$S_{\mathbf{k}}^-(y) = \mathrm{i}\,\gamma_0\cos(\omega_{\mathbf{k}}y) + \frac{M-\mathbf{k}\boldsymbol{\gamma}}{\omega_{\mathbf{k}}}\sin(\omega_{\mathbf{k}}y)\,, \tag{3.35c}$$

$$S_{\mathbf{k}}^+(y) = -\frac{1}{2}\tanh\left(\frac{\beta\omega_{\mathbf{k}}}{2}\right)\left(\mathrm{i}\gamma_0\sin(\omega_{\mathbf{k}}y) - \frac{M-\mathbf{k}\boldsymbol{\gamma}}{\omega_{\mathbf{k}}}\cos(\omega_{\mathbf{k}}y)\right)\,. \tag{3.35d}$$

The other propagators can be evaluated via the relations (3.17).

For deriving the Majorana neutrino propagator in equilibrium, one can use time-translational invariance again. Since the leading order contributions to the self-energies are given by the two diagrams in fig. 3.2 and all its propagators are time-translational invariant, the spectral propagator itself only depends on the time difference $G_{\mathbf{p}}^-(t_1,t_2) \to G_{\mathbf{p}}^-(y)$ with $y = t_1 - t_2$. Hence one can find the general solution of eq. (3.32a) for small couplings $\lambda \ll 1$ and thus small width $\Gamma \ll M$ in the Breit-Wigner approximation (cf. [16]):

$$G_{\mathbf{p}}^-(y) = \left(\mathrm{i}\gamma_0\cos(\omega_{\mathbf{p}}y) - \frac{M-\mathbf{p}\boldsymbol{\gamma}}{\omega_{\mathbf{p}}}\sin(\omega_{\mathbf{p}}y)\right)\mathrm{e}^{-\Gamma_{\mathbf{p}}|y|/2}C^{-1}\,, \tag{3.36a}$$

$$\begin{aligned} G_{\mathbf{p}}^+(y) = &-\left(\mathrm{i}\gamma_0\sin(\omega_{\mathbf{p}}y) - \frac{M-\mathbf{p}\boldsymbol{\gamma}}{\omega_{\mathbf{p}}}\cos(\omega_{\mathbf{p}}y)\right) \\ &\times\left[\frac{1}{2}\tanh\left(\frac{\beta\omega_{\mathbf{p}}}{2}\right)\mathrm{e}^{-\Gamma_{\mathbf{p}}|y|/2} + f_N^{\mathrm{eq}}(\omega_{\mathbf{p}})\mathrm{e}^{-\Gamma_{\mathbf{p}}t}\right]C^{-1}\,. \end{aligned} \tag{3.36b}$$

For obtaining the second equation, the KMS relation was used and for the initial time

$t_i = 0$ was chosen. It is $t = (t_1 + t_2)/2$ and

$$\Gamma_{\mathbf{p}} \equiv \Gamma_{\mathbf{p}}(\omega_{\mathbf{p}}) = (\lambda^\dagger \lambda)_{11} \frac{2}{\omega_{\mathbf{p}}} \int_{\mathbf{q},\mathbf{k}} p \cdot k \, f_{l\phi}(k,q)(2\pi)^4 \delta^4(p-k-q) \tag{3.37}$$

is the sum of decay and inverse decay widths for the Majorana neutrino with momentum integration denoted by $\int_{\mathbf{p}} = \int \mathrm{d}^3 p/((2\pi)^3 \, 2\,\omega_{\mathbf{p}})$. The equilibrium distribution functions are enclosed in the function $f_{l\phi}(k,q) \equiv 1 - f_l(k) + f_\phi(q)$.[7]

[7] According to eq. (3.11) the distribution function for bosons is $f_\phi(q) = f_{\mathrm{B}}(q) = (\mathrm{e}^{\beta q} - 1)^{-1}$, while $f_l(k) = f_{\mathrm{F}}(k) = (\mathrm{e}^{\beta q} + 1)^{-1}$ describes the Fermi-Dirac distribution for fermions.

4 Lepton asymmetry

Symmetry, as wide or as narrow as you may define its meaning,
is one idea by which man through the ages has tried to
comprehend and create order, beauty and perfection.
Hermann Weyl

In order to derive a complete 'theory of leptogenesis' from first principles, the use of Kadanoff-Baym equations becomes apparent after the discussion in the last section. As already introduced there, we can calculate the lepton number following [15, 16, 98, 100]. The first part of this chapter reviews the solution of the Boltzmann equations for leptogenesis [21, 101]. Hereafter the lepton number matrix is introduced and the important steps of the calculation of the lepton asymmetry using the KBEs is shown. The comparison of the two solutions is the content of the last part of this chapter. This prepares us for the inclusion of gauge interactions in the Kadanoff-Baym ansatz, which is dealt with in the next chapters and what is the main task of this thesis.

4.1 Solutions of the Boltzmann equations

For comparing the Boltzmann ansatz with the Kadanoff-Baym one, we first have to present the solution of the former. Starting from the Boltzmann equation for the heavy Majorana neutrino (2.34) we can further simplify it by inserting the averaged decay matrix element $|\mathcal{M}(N(p) \to l(k)\phi(q))|^2 = 2(\lambda^\dagger\lambda)_{11}\, p\cdot k$ [21][1] and find

$$\frac{\partial}{\partial t} f_N(t,\omega_{\mathbf{p}}) = -\frac{2}{\omega_{\mathbf{p}}} \int_{\mathbf{k},\mathbf{q}} (2\pi)^4 \delta^4(k+q-p)(\lambda^\dagger\lambda)_{11}\, p\cdot k \times \Big\{ f_N(t,\omega_{\mathbf{p}})(1-f_l(k))(1+f_\phi(q)) - f_l(k) f_\phi(q)(1-f_N(t,\omega_{\mathbf{p}})) \Big\} . \tag{4.1}$$

Using vacuum initial conditions, $f_N(0,\omega_{\mathbf{p}}) = 0$, the solution of the Boltzmann equations yields

$$f_N(t,\omega_{\mathbf{p}}) = f_N^{\mathrm{eq}}(\omega_{\mathbf{p}})(1-\mathrm{e}^{-\Gamma_{\mathbf{p}} t}) , \tag{4.2}$$

with $f_N^{\mathrm{eq}}(\omega_{\mathbf{p}}) = f_{\mathrm{F}}(\omega_{\mathbf{p}})$.

For the lepton distribution function one now has to take into account $\mathcal{O}(\lambda^4)$ corrections for the matrix elements. The Boltzmann equation is derived analogously to eq. (4.1) and ends up in

$$\frac{\partial}{\partial t} f_l(t,k) = -\frac{1}{2k} \int_{\mathbf{q},\mathbf{p}} (2\pi)^4 \delta^4(k+q-p) \Big\{ |\mathcal{M}(l\phi \to N)|^2 f_l(k) f_\phi(q)(1-f_N(t,\omega_{\mathbf{p}})) - |\mathcal{M}(N\to l\phi)|^2 f_N(t,\omega_{\mathbf{p}})(1-f_l(k))(1+f_\phi(q)) \Big\} . \tag{4.3}$$

[1] Following [16, 98, 100], we use the same symbol for the modulus of 3-momentum and 4-momentum, i. e. $k = |\mathbf{k}|$ and $k = (k_0, k)$, respectively. Thus the 4-scalar product is denoted by $k\cdot p$, while the product of moduli is denoted by kp.

Now we can define the lepton asymmetry

$$f_{Li} = f_{li} - f_{\bar{l}i} \tag{4.4}$$

which leads to the result

$$f_{Li}(t,k) = -\epsilon_{ii}\frac{1}{k}\int_{\mathbf{q},\mathbf{p}} (2\pi)^4\delta^4(k+q-p)\, p\cdot k\, f_{l\phi}(k,q)\, f_N^{\mathrm{eq}}(\omega_{\mathbf{p}})\frac{(1-\mathrm{e}^{-\Gamma_{\mathbf{p}}t})}{\Gamma_{\mathbf{p}}}\,, \tag{4.5}$$

for initial condition $f_{Li}(0,k)=0$ with the familiar $\mathcal{CP}$-asymmetry

$$\epsilon \equiv -\epsilon_1 = \sum_i \frac{\epsilon_{ii}}{(\lambda^\dagger\lambda)_{11}} = \frac{3}{16\pi}\,\frac{\mathrm{Im}(\lambda^\dagger\eta\lambda^*)_{11}}{(\lambda^\dagger\lambda)_{11}}\,M\,. \tag{4.6}$$

For better comparison with the Kadanoff-Baym solution, we can rewrite eq. (4.5) by inserting another δ-function to obtain a 4-fold integral

$$\begin{aligned} f_{Li}(t,k) = -\epsilon_{ii}\frac{16\pi}{k}\int_{\mathbf{q},\mathbf{p},\mathbf{q}',\mathbf{k}'} & k\cdot k'\,(2\pi)^4\delta^4(k+q-p)(2\pi)^4\delta^4(k'+q'-p) \\ & \times f_{l\phi}(k,q)\, f_N^{\mathrm{eq}}(\omega_{\mathbf{p}})\frac{(1-\mathrm{e}^{-\Gamma_{\mathbf{p}}t})}{\Gamma_{\mathbf{p}}}\,, \end{aligned} \tag{4.7}$$

This shows the strong suppression of the generated lepton asymmetry for low temperatures $T \ll M$ where the integrand falls off like $\mathrm{e}^{-\beta\omega_{\mathbf{p}}} < \mathrm{e}^{-\beta M}$.

4.2 Lepton number matrix

Starting from the definition of the flavour non-diagonal lepton current,

$$j^\mu_{ij}(x) = -\,\mathrm{Tr}\left[\gamma^\mu S^+_{ij}(x,y)\right]_{y\to x}\,, \tag{4.8}$$

with flavour index i,j, that can be calculated using the results for the statistical propagator from the last chapter in sec. 3.3.2, we now can derive the so-called *lepton number matrix* as the zeroth component of the current in order to calculate the lepton asymmetry. For spatially homogeneous systems as used before, the statistical propagator only depends on the difference of two space coordinates $\mathbf{x}-\mathbf{y}$. Therefore a Fourier transform yields

$$L_{\mathbf{k},ij}(t,t') = -\,\mathrm{Tr}\left[\gamma^0 S^+_{\mathbf{k},ij}(t,t')\right]\,. \tag{4.9}$$

For free fields in equilibrium one obtains

$$L_{\mathbf{k},ii}(t,t) = f_{li}(k) - f_{\bar{l}i}(k)\,, \tag{4.10}$$

which is the definition of the asymmetry, cf. eq. (4.4).

Using the Kadanoff-Baym equations for leptons (cf. eq. (3.32) with $M=0$ and replacing $C\Sigma^\pm_{\mathbf{p}}$ by $\Sigma^\pm_{L,\mathbf{k}}$)[2] with initial condition $t_i = 0$ one can derive[3] for the lepton

[2] From now on, we only deal with Majorana self-energies and lepton self-energies instead of scalar ones, thus we denote $\Sigma^\pm_{L,\mathbf{k}} \equiv \Pi^\pm_{\mathbf{k}}$.

[3] A detailed calculation can be found in [16].

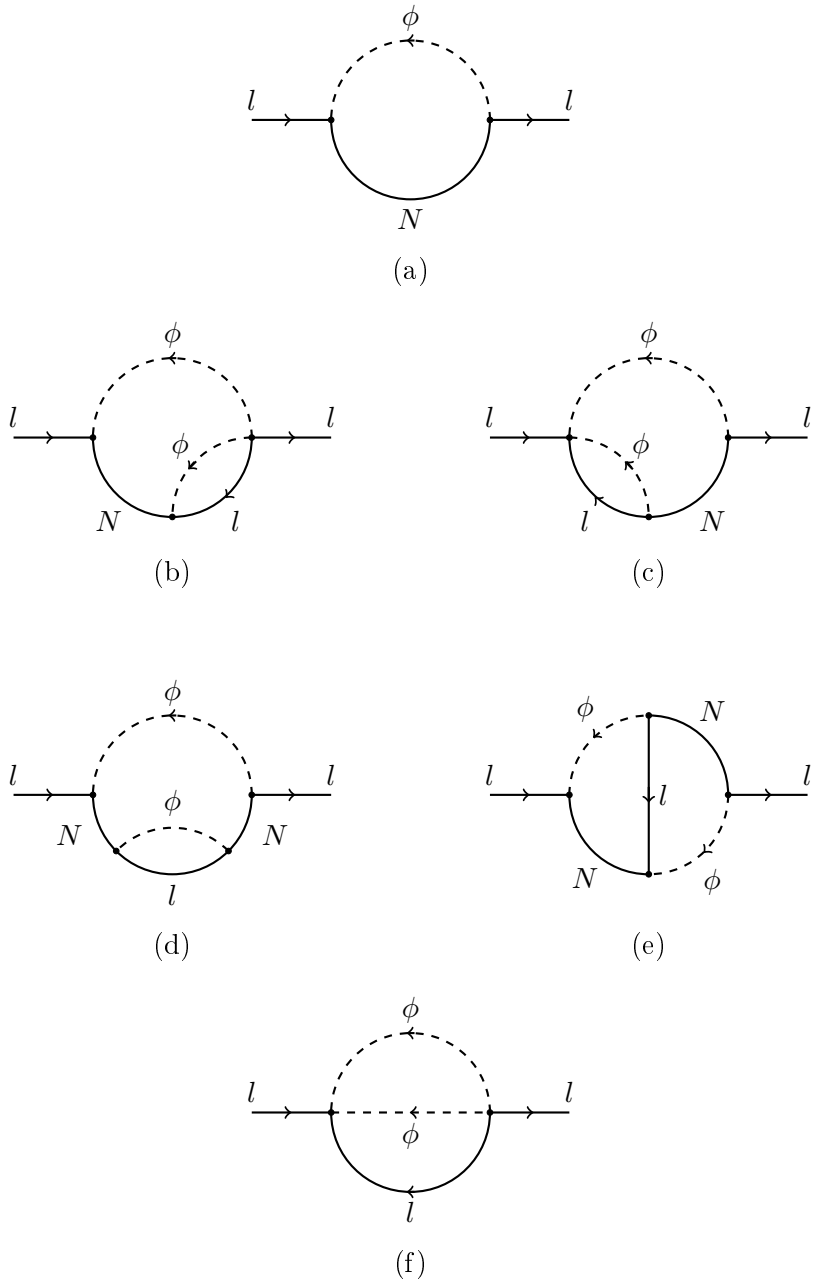

Figure 4.1: One- and two-loop contributions to the lepton doublet self-energy $\Pi^{\pm}_{\mathbf{k}}$.

number matrix

$$L_{\mathbf{k},ii}(t,t) = \int_0^t \mathrm{d}t_1 \int_0^t \mathrm{d}t_2 \,\mathrm{Tr}\left[\Pi^{>}_{\mathbf{k},ii}(t_1,t_2)S^{<}_{\mathbf{k}}(t_2,t_1) - \Pi^{<}_{\mathbf{k},ii}(t_1,t_2)S^{>}_{\mathbf{k}}(t_2,t_1)\right] . \quad (4.11)$$

The relations between the propagators (3.9) were used as well as properties of the trace and an identity for connected integrations. The contributing diagrams for the lepton self-energies up to two-loop order are depicted in fig. 4.1.

Starting with a thermal abundance of the heavy neutrino, the Hubble expansion leads

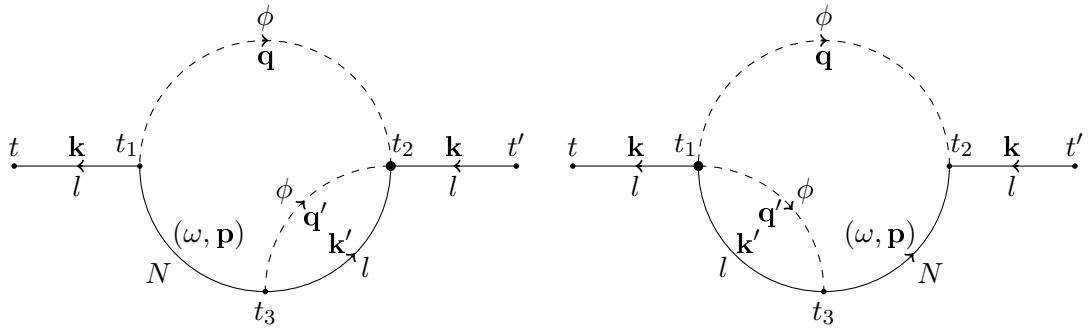

Figure 4.2: Two-loop contributions to the lepton self-energies $\Pi^{\pm}_{\mathbf{k}}$ that cause the lepton asymmetry.

to an increase of the neutrino abundance and shortly afterwards, the lepton asymmetry is *frozen in* due to washout processes not being in equilibrium any longer. However, as already seen in fig. 2.3, the final lepton asymmetry is about the same size, starting with a zero heavy neutrino abundance. This simplifies the calculations since we can neglect the change of temperatur due to Hubble expansion. Furthermore, washout terms, i. e. scattering processes with the thermal bath, will be neglected. The only contributing diagrams that generate a lepton asymmetry are those two depicted in fig. 4.2 more detailed. The reason for this becomes obvious by considering their $\mathcal{CP}$-violation: These two diagrams are the only ones that lead to the combination of Yukawa couplings which occurs in the $\mathcal{CP}$-asymmetry of the Majorana neutrino decay in eq. 2.10 and which is needed to gain a lepton asymmetry [21].

Decomposing the Majorana neutrino propagator into an equilibrium and a non-equilibrium part according to

$$G_{\mathbf{p}}(t_1, t_2) = G^{\mathrm{eq}}_{\mathbf{p}}(t_1 - t_2) + \widetilde{G}_{\mathbf{p}}(t_1, t_2)\,, \tag{4.12}$$

we can now derive the lepton asymmetry to leading order in the small Yukawa coupling λ. It can be shown [16] that only the out-of-equilibrium part of the neutrino propagator is important for the calculation of the diagrams in fig. 4.2 (cf. A.2.2). If one also takes chiral properties, e. g. the projections at the vertices, into account, only the scalar parts remain so that

$$\begin{aligned}\widetilde{G}_{\mathbf{p}}(t_1, t_2) &= \widetilde{G}^{>}_{\mathbf{p}}(t_1, t_2) = (\widetilde{G}^{>}_{\mathbf{p}}(t_1, t_2))^* = \widetilde{G}^{<}_{\mathbf{p}}(t_1, t_2) = \widetilde{G}^{11}_{\mathbf{p}}(t_1, t_2) = \widetilde{G}^{22}_{\mathbf{p}}(t_1, t_2) \\ &= \frac{M}{\omega_{\mathbf{p}}} \cos(\omega_{\mathbf{p}}(t_1 - t_2)) f^{\mathrm{eq}}_N(\omega_{\mathbf{p}}) \mathrm{e}^{-\Gamma_{\mathbf{p}} \frac{t_1 + t_2}{2}}\,.\end{aligned} \tag{4.13}$$

For lepton and Higgs propagators only the equilibrium contributions are considered as discussed earlier since corrections are of order $\mathcal{O}(\lambda^2)$. Using only the free part of them (cf. eq. (3.35)), leads for the two contributions to the lepton self-energy (cf. 4.2)

$$\Pi^{(1)}_{\mathbf{k},ij}(t_1, t_2) = -3\,\mathrm{i}\,\lambda^*_{i1}(\eta\lambda^*)_{j1}\Pi^{(1)}_{\mathbf{k}}(t_1, t_2)\,, \tag{4.14a}$$

$$\Pi^{(2)}_{\mathbf{k},ij}(t_1, t_2) = \quad 3\,\mathrm{i}\,(\eta^*\lambda)_{i1}\lambda_{j1}\Pi^{(2)}_{\mathbf{k}}(t_1, t_2)\,, \tag{4.14b}$$

with the superscripts (1) for the first and (2) for the second diagram, respectively. A detailed calculation of the contributions is presented in app. A.2.2.

Using symmetry properties like $S^{>*} = CS^{<}C^{-1}$ for the propagators[4] and relations between the contributions of (1) and (2) the lepton asymmetry simplifies to

$$L_{\mathbf{k},ii}(t,t) = 12\,\lambda_{ii}\int_0^t \mathrm{d}t_1 \int_0^t \mathrm{d}t_2\,\mathrm{Re}\left(\mathrm{Tr}\left[\Pi^{(1)>}_{\mathbf{k}}(t_1,t_2)S^{<}_{\mathbf{k}}(t_2-t_1)\right]\right), \tag{4.15}$$

with $\lambda_{ii} \equiv \mathrm{Im}\,(\lambda^*_{i1}(\eta\lambda^*)_{i1})$ and the lepton self-energy

$$\begin{aligned}\Pi^{(1)>}_{\mathbf{k}}(t_1,t_2) = \int_0^\infty \mathrm{d}t_3 \int_{\mathbf{q},\mathbf{q}',\mathbf{k}',\mathbf{p}} \Big\{ &\widetilde{G}^{>}_{\mathbf{p}}(t_1,t_3)S^{11}_{\mathbf{k}'}(t_2-t_3)\Delta^{11}_{\mathbf{q}'}(t_2-t_3)\Delta^{<}_{\mathbf{q}}(t_2-t_1) \\ &- \widetilde{G}^{22}_{\mathbf{p}}(t_1,t_3)S^{<}_{\mathbf{k}'}(t_2-t_3)\Delta^{<}_{\mathbf{q}'}(t_2-t_3)\Delta^{<}_{\mathbf{q}}(t_2-t_1)\Big\} \\ &\times (2\pi)^3\delta^3(\mathbf{p}-\mathbf{k}-\mathbf{q})(2\pi)^3\delta^3(\mathbf{p}-\mathbf{k}'-\mathbf{q}')P_L\,.\end{aligned} \tag{4.16}$$

In contrast to the Boltzmann solution, this expression contains off-shell and memory effects as shown in [16]. In the next section, we will have a closer look at the differences and similarities of the two solutions.

4.3 Boltzmann vs. Kadanoff-Baym equations

In order to compare the Kandanoff-Baym ansatz with the Boltzmann approach, some approximations are needed: Off-shell effects have to be neglected in the Kadanoff-Baym ansatz, i. e. applying $\omega_{\mathbf{p}} = k + q = k' + q'$, and the zero-width approximation $\Gamma_{\mathbf{p}} \to 0$ (while $\Gamma_{\mathbf{p}}t$ stays fixed) has to be used. Thus the 'on-shell' lepton asymmetry becomes

$$\begin{aligned}L^{\mathrm{os}}_{\mathbf{k},ii}(t,t) = -\,\epsilon_{ii}\frac{16\pi}{k}\int_{\mathbf{q},\mathbf{p},\mathbf{q}',\mathbf{k}'} &k\cdot k'\,f_{l\phi}(k,p)f_{l\phi}(k',q')f^{\mathrm{eq}}_N(\omega_{\mathbf{p}}) \\ &\times (2\pi)^4\delta^4(k+q-p)(2\pi)^4\delta^4(k'+q'-p) \\ &\times \frac{\left(1-\mathrm{e}^{-\Gamma_{\mathbf{p}}t/2}\right)^2}{\Gamma_{\mathbf{p}}}\,.\end{aligned} \tag{4.17}$$

Comparing this to the Boltzmann solution for the lepton asymmetry eq. (4.7), the only differences are the additional factor $f_{l\phi}(k',q')$ and the time dependence in the exponential fall-off. This is due to nonlocality in time (cf. fig. 4.2 and eq. (4.11)) in the quantum approach, while in the Boltzmann ansatz the lepton asymmetry is generated locally leading to a simple exponential behaviour. For cosmologically relevant times $t_{\mathrm{L}} \sim \Gamma^{-1}$ this difference can become important.

Up to now, thermal damping widths of lepton and Higgs fields have been neglected. However, gauge corrections play a crucial role in non-Abelian gauge theories since the interactions in the thermal plasma are strong. This becomes clear by comparing the Standard Model thermal widths of lepton and Higgs fields with the one of the heavy Majorana neutrino, i. e. $\gamma_l \sim \gamma_\phi \sim g^2T \gg \lambda^2 M \sim \Gamma$ for $M \lesssim T$. For simplicity, thermal masses are neglected in the first considerations following and a naive ansatz is performed by replacing the free equilibrium propagators by

$$\Delta^{\mathrm{eq}}_{\mathbf{k}}(y) = \Delta_{\mathbf{k}}(y)\mathrm{e}^{-\gamma_\phi|y|}\,, \quad S^{\mathrm{eq}}_{\mathbf{k}}(y) = S_{\mathbf{k}}(y)\mathrm{e}^{-\gamma_l|y|}\,. \tag{4.18}$$

[4] A full list of the properties and the detailed calculation can be found in [16].

This yields up to leading order in the Standard Model width ($\gamma \equiv \gamma_l + \gamma_\phi$) to

$$\begin{aligned} L^{\mathrm{th}}_{\mathbf{k},ii}(t,t) = &- \epsilon_{ii} 16\pi \int_{\mathbf{q},\mathbf{q}'} \frac{k\cdot k'}{kk'\omega_{\mathbf{p}}} f_{l\phi}(k,p) f_{l\phi}(k',q') f^{\mathrm{eq}}_N(\omega_{\mathbf{p}}) \\ &\times \frac{\gamma\gamma'}{((\omega_{\mathbf{p}}-k-q)^2+\gamma^2)((\omega_{\mathbf{p}}-k'-q')^2+\gamma'^2)} \\ &\times \frac{\left(1-\mathrm{e}^{-\Gamma_{\mathbf{p}}t}\right)}{\Gamma_{\mathbf{p}}}\,, \end{aligned} \tag{4.19}$$

with $\gamma = \gamma(k,q)$ and $\gamma' = \gamma(k',q')$. The inclusion of thermal damping widths therefore leads to a result local in time similar to the result of the Boltzmann ansatz. This shows that the neglect of the widths is not justified and thus one has to systematically include gauge interactions in order to see the resulting effect. For a numerical analysis of the comparison of the two approaches, see again [16] as well as [102].

5 Thermal particle production

In physics, you don't have to go around
making trouble for yourself —
nature does it for you.
Frank A. Wilczek

If a particle transmigrates a thermal plasma, many effects play a crucial role. Especially for very weakly coupled ones like the Majorana neutrino in a bath of SM particles, we have to take care of the underlying momentum scales and thus we need new tools for the calculation of self-energies for example. This chapter provides an overview of the contributing scales in the beginning. Afterwards a general introduction to the Hard Thermal Loop (HTL) resummation scheme is presented as well as its modifications for light-like particles. With the description of the Collinear Thermal Loop (CTL) ansatz, we present another resummation scheme needed for our purposes as well as the power counting rules needed for our aims. This chapter follows the textbooks [86, 87] as well as the important articles [103–106] for the HTL and [17,107,108] for the CTL approach. We close this chapter with the calculation of the Majorana neutrino production rate that is based on the Landau-Pomeranchuk-Migdal effect [109,110].

5.1 Scales of the system

Perturbation theory usually requires an expansion in the underlying couplings of the theory (cf. sec. 3.1). For the propagator this is equivalent to an expansion in loops of the corresponding Feynman diagrams and should ideally lead to (asymtotically) convergent series. However, this ansatz is not valid for all kinematical regimes due to the existence of new *infrared (IR)* and *collinear divergences* that occur at finite temperature[1]. Therefore, naive perturbation theory breaks down, e. g. in a hot and dense plasma, and resummation schemes are needed. One has to distinguish the following momentum scales[2] that need a different treatment:

- **Hard scale:** It is $k \sim T$, $k^2 \sim T^2$. This is the only region where ordinary perturbation theory is valid. It is the typical momentum scale of a particle inside a plasma where due to its hard momentum it is only weakly affected by the thermal bath and thus can move as a free particle.
- **Soft scale:** It is $k \sim gT$, $g \ll 1$. In this region, interactions with the thermal bath modify the propagation of particles extremely. They are of order $\mathcal{O}(1)$ and thus *collective excitations* arise. Furthermore, *thermal masses* $m \sim gT$ become important, e. g. for the dispersion relation of a scalar $\omega^2 = \mathbf{k}^2 + m^2$. The corresponding

[1] There are no new *ultraviolet (UV) divergences* appearing, only the ones occuring for zero temperature remain.
[2] In the following it is always $k = (k_0, \mathbf{k})$ the four-momentum and g the relevant coupling constant.

resummation scheme for this momentum scale is the *Hard Thermal Loop (HTL) resummation scheme* [103–106] which is dealt with in the next section.

- **Ultrasoft scale:** It is $k \sim g^2 T$. For this momentum scale, perturbation theory completely breaks down. *Magnetic screening*, i. e. transverse polarizations of the gauge fields, becomes quite important. Only effective theories [111] or theories using a nonperturbative approach such as lattice simulations (for a review see [112]) can deal with this regime.
- **Lightcone scale:** It is $k \sim T$, $k^2 \sim g^2 T^2$. For hard momenta one has to be careful again in this regime since *collinear divergences* arise and thus the so-called *asymptotic mass* m_∞ becomes important. For scalars they coincide with the thermal mass but that is not true for gauge bosons or fermions. The corresponding resummation scheme is also treated in the next section and is called *Collinear Thermal Loop (CTL) resummation scheme* [17, 107, 108].

Transferring these scales to our scenario of thermal leptogenesis we see that for temperatures T sufficiently above M the SM particles become 'heavier' than the Majorana neutrino since their generated thermal masses are much bigger than the one of the Majorana neutrino. Thus, the Higgs boson can decay into a Majorana neutrino and a SM lepton. However, thermal masses are parametrically small compared to the typical particle momentum and that is why all momenta are nearly collinear. Hence, an HTL resummation with light-like momenta is needed.

For $T \sim M$ the Majorana acts according to the hard scale and no resummation needs to be taken into account. For the scalar and lepton fields we obtain a hard and light-like behaviour so that the CTL resummation is needed.

5.2 Hard Thermal Loops (HTL)

The basic ideas of the HTL resummation scheme will be given in the following. Concerning soft momenta $k \sim gT$ ordinary perturbation theory fails to include all contributions up to a given order, since corrections are of order $\mathcal{O}(1)$ [104]. As depicted in fig. 5.1, we can consider a resummed scalar propagator with soft external and hard internal momentum, consisting of one-loop self-energy insertions. Its calculation up to one-loop order is described in detail in appendix A.2.3.

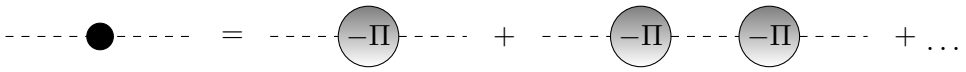

Figure 5.1: Resummed scalar propagator with one-loop scalar insertions.

According to the recursion relation in eq. (3.18) the resummed propagator is of the form

$$\Delta(k)(-\Pi(k))\Delta(k)\ldots \sim \frac{1}{(gT)^2}(gT)^2\frac{1}{(gT)^2}\ldots \sim \frac{1}{(gT)^2}\,, \tag{5.1}$$

where we assumed a hard loop momentum $k \sim T$ and a self-interaction of $g^2/4!\,\phi^4$ with the g^2 term in analogy to the gauge theories considered later. Therefore one finds for

the inserted self-energies (cf. app. A.2.3)

$$-\Pi(k) \sim g^2 \sum_{k_0} \int \mathrm{d}^3k\, \Delta(k) \sim g^2 T^2 \,. \tag{5.2}$$

Obviously this resummed propagator is of the same order as the bare propagator, thus a resummation is urgently needed. A general power counting is not easy to present since many different cases have to be distinguished. The main rules for soft external momentum p and hard loop momentum k are [104]:

- The loop integral gives a contribution of T^3.
- The first propagator (times the sum over k_0) leads to $1/T$.
- All additional propagators contribute $1/pT$.
- For three-gluon vertices or quark propagators a factor T needs to be included, powers of external momenta require p.
- If two or more propagators are either all bosonic or fermionic, an extra factor of p/T needs to be included.

These rules have to be converted in powers of the coupling g, which turns out to be different for several cases, e. g. transverse and static modes. However, we do not need a general framework for we are only interested in the HTL resummation scheme regarding gauge theories. Thus, we present the needed results in the next chapter, their explicit calculation can be found in app. A.2.3.

The main tool of the HTL resummation scheme is the introduction of a thermal mass and a thermal width. The resummed scalar propagator can then be rewritten in terms of these two parameters as described in the next chapter. For a more detailed analysis consult [86,87].

5.3 Perturbation theory close to the lightcone

5.3.1 Thermal width and asymptotic mass

In the last section the general procedure of HTL resummation has been summarised briefly. Nevertheless, it is not necessary that all components of k_μ are of order gT, but the condition $k^2 \sim g^2T^2$ is strictly needed. Consequently, this leads to an analogous resummation for momenta in the lightcone scale $k \sim T$, $k^2 \sim g^2T^2$ obtaining slightly different results than in the HTL approach.

For example we can parametrize the resummed scalar propagator in terms of thermal width $\Gamma(k)$ and thermal mass m. For $\Gamma^2 \ll m^2$ this results in

$$\mathrm{Re}\,\Pi(k) = m^2 \,, \quad \mathrm{Im}\,\Pi(k) = -2\mathrm{i}k_0\Gamma(k) \,. \tag{5.3}$$

Here m^2 as well as $k_0\Gamma$ are of order g^2T^2 since also Π is of this order. In our case, it is sufficient to limit considerations to hard loop momenta as discussed earlier, so that we obtain a purely real self-energy and thus we only need the asymptotic thermal masses. Another positive ancillary effect is that the thermal width is an IR divergent quantity whereas the asymptotic thermal mass is a well defined quantity, thus working with the ladder is much easier. Summarising we find the following results (for an explicit calculation see app. A.2.4):

- Scalar propagator:

$$\Delta(k) = \frac{-1}{k^2 - m^2}\,, \tag{5.4}$$

  with thermal mass $m^2 = g^2T^2/4$ similar to the HTL thermal mass.

- Fermion propagator:

$$S(p) = -\frac{\not{p} - \frac{m_\infty^2}{2p_0}\gamma^0}{p^2 - m_\infty^2}\,, \tag{5.5}$$

  with asymptotic thermal mass

$$m_\infty^2 = \frac{g_r^2 C_2(r) T^2}{4}\,, \tag{5.6}$$

  and Casimir operator $C_2(r)$ of the gauge group r.

The result for the gauge boson propagator is not needed thus it is not listed here. For the complete asymptotic mass of the lepton we thus have to sum the different contributions due to the gauge groups SU(2) and U(1), represented by their couplings $g \equiv g_\mathrm{w}$ and $g' \equiv g_\mathrm{Y}$, respectively. For the asymptotic mass of the Higgs, contributions of the top quark with Yukawa coupling λ_t are also taken into account[3]. This leads to the values

$$m_{l,\infty}^2 = \frac{1}{16}(3g^2 + g'^2)T^2 \tag{5.7a}$$

$$m_{\phi,\infty}^2 = \frac{1}{16}(3g^2 + g'^2 + 4\lambda_\mathrm{t}^2 + 8\Lambda)T^2\,, \tag{5.7b}$$

with Λ being the Higgs self-coupling. In the following we only use these asymptotic masses and thus drop the subscript ∞ for simplicity. The detailed calculation of the values can be found in app. A.2.4.

5.3.2 Power counting

As mentioned in the last sections, we mostly deal with hard light-like momenta. To simplify notation we introduce *lightcone coordinates*. Therefore, we define a light-like four-vector $v \equiv (1, \mathbf{v})$, $\mathbf{v}^2 = 1$. It is $k_\parallel \equiv \mathbf{k}\cdot\mathbf{v}$ and the 2-momentum perpendicular to $\mathbf{v}$ is denoted by $\mathbf{k}_\perp$. Thus we can rewrite the four-vector according to

$$k = k_\mu = (k_+, k_-, \mathbf{k}_\perp)\,, \quad k_+ = k_0 + k_\parallel\,, \quad k_- = k_0 - k_\parallel\,. \tag{5.8}$$

Therefore the scale hierarchy is given by

$$k_+ \sim T \qquad \mathbf{k}_\perp \sim gT \qquad k_- \sim g^2T\,, \tag{5.9}$$

since one can rewrite $k^2 = (k_0 + k_\parallel)(k_0 - k_\parallel) - \mathbf{k}_\perp^2 \sim g^2T^2$. For the measure one obtains $\mathrm{d}^4k \sim \mathrm{d}k_+\,\mathrm{d}k_-\,\mathrm{d}^2k_\perp$.

Considering only spin-1/2-fermions and spin-1-gauge bosons as external particles, which is everything needed for our purposes, we can find the following power counting rules in the gauge boson coupling g of our system:

[3] Fermionic contributions for lighter quarks are neglected due to the smallness of the corresponding Yukawa couplings.

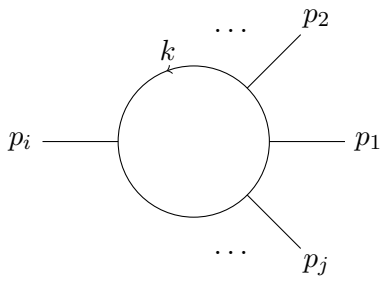

Figure 5.2: General one-loop contribution to a CTL n-point function.

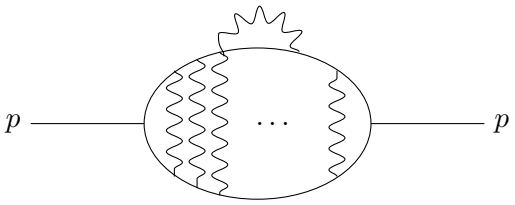

Figure 5.3: Ladder diagram including gauge lines for consistent leading-order treatment.

- For each loop integral a factor g^4 needs to be included.
- Every propagator leads to a factor g^{-2}.
- Yukawa vertices are suppressed by a factor g.
- Vertices involving gauge bosons give a factor g.

These rules are true for external as well as for internal particles. A proof of the rules is given in [107].

5.3.3 Collinear Thermal Loops (CTL)

In contrast to the HTL ansatz we now do not consider the external momenta as soft but also at the lightcone scale. Considering one-loop diagrams as depicted in fig. 5.2 the loop momentum there is of the same kind so that the resummed propagators defined in the last section are needed. Furthermore, the external momenta are collinear to the internal one according to $k \cdot p_i \sim g^2T^2$. This is the reason for being forced to sum up higher contributions to a given order in the coupling constant than the one-loop contributions of fig. 5.2 with its additional soft momenta. Using the lightcone notation this means that longitudinal components, e. g. $k_\parallel$, are of order $\mathcal{O}(T)$ while perpendicular ones of $\mathcal{O}(gT)$. Thus the angle between the vectors becomes $\vartheta \sim \mathcal{O}(g)$.

Using the power counting rules from sec. 5.3.2, we find for a CTL n-point function with j vertices including gauge bosons and $m = n - j$ additional vertices:

$$\Pi^{(n)}_{\mathrm{CTL}} \sim g^4 \left(\frac{1}{g^2}\right)^n g^j g^n \sim g^{4-m}\,. \tag{5.10}$$

This shows the self-energy without gauge corrections in the loop being of the same order $\mathcal{O}(g^2)$ as for example the one including gauge corrections. Hence one has to sum up all contributions, the so-called *ladder diagrams* as depicted in fig. 5.3.

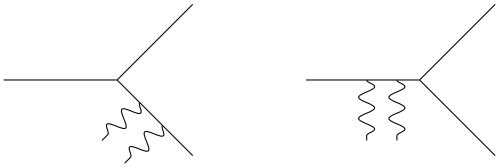

Figure 5.4: Two interfering processes obtained by cutting the ladder diagram fig. 5.3.

Crossed ladder rungs are of higher order since the time scale between two interactions is much larger than the Debye screening length, i. e. the possible interaction area, and thus, need not to be taken into account [113]. This becomes clear by cutting the ladder diagram in fig. 5.3[4]: This corresponds to interference processes, for example the ones depicted in 5.4 and shows the connection to the *Landau-Pomeranchuk-Migdal (LPM) effect* that is well-known from considering particles migrating through a medium. We will focus on this topic in more detail in the next section.

5.4 Thermal particle production

Renowned from heavy ion collisions the thermal particle production rate plays an important role for example in generating a quark-gluon plasma (QGP) [115, 116]. The same also holds for particles in the early universe, especially for thermal leptogenesis, since the heavy Majorana neutrino is so weakly coupled to the thermal bath that it does not stay in equilibrium. Hence it can be produced via decays as well as scatterings of the standard model particles and thus escape without effecting the medium analogously to the photon in the QGP.

5.4.1 The Landau-Pomeranchuk-Migdal effect

A plausible ansatz is the earlier mentioned LPM effect [109, 110], named after the persons who were the first to discover the effect in electromagnetic showers in high-energy cosmic rays. There are many proceedings to the photon production in QGP based on the LPM effect [117, 118]. Well-known are also the 'AMY'-publications [113, 119, 120], named after the authors Arnold, Moore and Yaffe. Normally, one again starts with the Boltzmann ansatz for dealing with the production rate, but as discussed earlier, this is not reasonable in our case: Due to interference effects, the Boltzmann ansatz breaks down in this quantum mechanical scenario and thus one obtains, e. g. for photons, a suppression of the production rate based on the LPM effect.

In the following we derive integral equations for the production rate of the Majorana neutrino. Therefore, the resummation of a ladder diagram, now explicitly with the particles of our interest as depicted in fig. 5.5 is needed. The basic ideas are:

- Integrate out the hard scale: This is the part where the HTL resummation scheme is used. It generates asymptotic masses for hard particles at the lightcone scale. Thermal width and hard-hard interactions are of higher order and thus can be neglected here.

[4] For cutting rules and the optical theorem see [114].

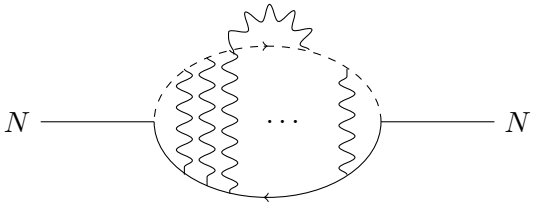

Figure 5.5: Ladder diagram for the heavy Majorana self-energy including gauge lines for consistent leading-order treatment.

- Use a recursion relation and the definition of a *current*: Start from one-loop diagrams with two external Majorana neutrinos and with an arbitrary number of soft external gauge bosons while the loop momentum and the external hard momenta are nearly collinear (cf. 5.2). Set up a recursion relation between n-point functions and $(n-1)$-point functions by using approximations for this kinematic regime. This is formulated more easily in terms of a current, that is induced by the gauge field background and defined as the integral over all external momenta contracted with the external fields (cf. [108]). Thus one only needs to calculate the 2-point function for the Majorana neutrino without additional soft gauge bosons.
- Integrate out the soft modes: This leads to thermal widths for the lepton and the Higgs. The gauge bosons then only appear in the ladder-diagram according to fig. 5.5. We can then find an integral equation for the CTL self-energy by using the new current and taking a functional derivative with respect to the external field.

In the next section we describe the single steps for deriving the integral equations in more detail to obtain the differential production rate of the Majorana neutrino.

5.4.2 Integral equations for the production rate

For calculating the production rate of Majorana neutrinos, we can start considering the differential rate per unit of time and volume that only depends on the imaginary part of the self-energy

$$\frac{\mathrm{d}\Gamma}{\mathrm{d}^3k} = \frac{1}{(2\pi)^3 k^0} f_\mathrm{F}(k^0)\,\mathrm{Tr}\left[\not{k}\,\mathrm{Im}\,\Sigma_\mathrm{ret}(k)\right] , \tag{5.11}$$

with $\Sigma_\mathrm{ret}(k)$ being the retarded self-energy of the Majorana neutrino according to eq. (3.14a).[5] In case of neglecting the SM $\mathcal{CP}$-violation and applying Weyl representation, we can simplify eq. (5.11) by using only a 2×2 matrix for the self-energy, denoted by Σ_R. This is possible since only fermions of one chirality participate at a time. We then have to multiply by 2 taking into account both contributing diagrams with different orientation of the internal fermion line (cf. fig. 3.2). This leads to

$$\frac{\mathrm{d}\Gamma}{\mathrm{d}^3k} = \frac{2}{(2\pi)^3 k^0} f_\mathrm{F}(k^0)\,\mathrm{Tr}\left[\overline{\sigma}\cdot k\,\mathrm{Im}\,\Sigma_\mathrm{R,ret}(k)\right] . \tag{5.12}$$

[5] In contrast to e. g. [86], we define the self-energy as (-1) times the corresponding Feynman diagrams and thus follow the notation of [108].

It is $\overline{\sigma}^0 = \mathbb{1}$, $\overline{\boldsymbol{\sigma}} = -\boldsymbol{\sigma}$.

Following the procedure outlined in the last section, we first have to calculate the 2-point function. For the scalar propagator we take only leading order g^2T^2 terms in the denominator into account, what is corresponding to the approximation $p_+ \simeq 2p_\parallel$. With mass m_φ we thus obtain

$$\Delta(p) \equiv \frac{-1}{p^2 - m_\varphi^2} \simeq \frac{D_\varphi(p)}{2p_\parallel}\,, \tag{5.13}$$

with the propagator in terms of the light-like 4-vector v (cf. 5.3.2) being

$$D_x(p) \equiv \frac{-1}{v\cdot p - (\mathbf{p}_\perp^2 + m_x^2)/(2p_\parallel)}\,. \tag{5.14}$$

For only considering left-handed fermions in the loop, we can again use the Weyl representation and the approximation $p_0 \simeq p_\parallel$ for spin-1/2-propagators

$$S(p) \simeq \frac{D_l(p)}{2p_\parallel}\,\sigma\cdot\tilde{p}\,, \quad \text{with} \quad \tilde{p} \equiv p - \frac{m_l^2}{2p_\parallel}\,u\,, \tag{5.15}$$

and $u \equiv (1,\mathbf{0})$ the 4-velocity of the plasma. For on-shell fermion momentum, we then can rewrite

$$S(p) = \eta(\tilde{p})\eta^\dagger(\tilde{p})D_l(p)\,, \tag{5.16}$$

with the Weyl-spinor $\eta(\tilde{p})$ that can be expanded in g by the appropriate choice of the coordinates like (cf. app. B)

$$\eta = \left(1 - \frac{\boldsymbol{\sigma}\cdot\mathbf{p}_\perp}{2p_\parallel}\right)\begin{pmatrix}0\\1\end{pmatrix} + \mathcal{O}(g^2) = \begin{pmatrix}-\frac{p_1 - \mathrm{i}p_2}{2p_\parallel}\\ 1\end{pmatrix} + \mathcal{O}(g^2)\,. \tag{5.17}$$

From now on we write $\eta(p)$ instead of $\eta(\tilde{p})$ since the difference is of order g^2T and thus not relevant here.

For later purposes it is useful to introduce the difference of the energy poles

$$\epsilon(k,\mathbf{p}) \equiv v\cdot k + \frac{(\mathbf{p}_\perp - \mathbf{k}_\perp)^2 + m_\phi^2}{2(p_\parallel - k_\parallel)} - \frac{\mathbf{p}_\perp^2 + m_l^2}{2p_\parallel} \tag{5.18}$$

of lepton and Higgs propagator that is obtained by applying partial fraction decomposition

$$D_l(p)D_\phi(p-k) = \frac{1}{\epsilon(k,\mathbf{p})}\left[D_l(p) - D_\phi(p-k)\right]\,. \tag{5.19}$$

A proof can be found in app. B.3.1. Furthermore, it appears to be useful to separate the loop momentum integration and one of the spinors and thus rewrite the self-energy in terms of a 'reduced self-energy' $\widetilde{\Sigma}(k,\mathbf{p})$ that is defined via

$$\widetilde{\Sigma}(k,\mathbf{p}) \equiv -\frac{d(r)\mathcal{F}(k_\parallel,p_\parallel)}{2\epsilon(k,\mathbf{p})}\,\frac{\eta^\dagger(p)}{p_\parallel - k_\parallel}\,, \tag{5.20}$$

with the dimension of the gauge group representation $d(r)$ and the function

$$\mathcal{F}(k_\parallel, p_\parallel) \equiv f_{\rm F}(p_\parallel) + f_{\rm B}(p_\parallel - k_\parallel)\,. \tag{5.21}$$

The reduced self-energy is connected to the 2×2 self-energy via

$$\Sigma_{\rm R}(k) = |\lambda|^2 \int \frac{{\rm d}^3p}{(2\pi)^3}\eta(p)\widetilde{\Sigma}(k,\mathbf{p})\,, \tag{5.22}$$

with the Yukawa couplings $|\lambda|^2 = \sum_i (\lambda^\dagger\lambda)_{1i}$.

Hereafter we can continue with the second step mentioned in the recipe and derive a recursion relation for the n-point function via the current J^a_μ, defined as the background of the external Majorana neutrino N and of the gauge fields A^a_μ, $a = 1,2,3$:

$$J^a_\mu(p) = \int \frac{{\rm d}^3k}{(2\pi)^3} V_\mu(k, k-p)\,{\rm Tr}\left[t^a \hat{J}(p,\mathbf{k})\right]\,, \tag{5.23}$$

with the vertex factor $V^\mu(k,k-p) \equiv \frac{1}{2k_\parallel}(2k-p)^\mu$ and the generators of the corresponding gauge group t^a. The 'unintegrated' current $\hat{J}$ is defined via

$$\hat{J}(p,\mathbf{k}) = \sum_{n=2}^{\infty}\prod_{i=1}^{n-1}\int_{p_i} A^{\mu_i}(p_i)(2\pi)^4\delta\Big(p - \sum_{j=1}^{n-1} p_j\Big)\widetilde{\Sigma}^{(n)a_1\cdots a_{n-1}}_{\mu_1\ldots\mu_{n-1}}(p_1,\cdots p_{n-1},\mathbf{k})\,, \tag{5.24}$$

with $A^{\mu_i} \equiv t_{a_i}A^{\mu_i}_{a_i}$ and the reduced self-energy $\widetilde{\Sigma}$. Thus, we can write

$${\rm Tr}\,J(k,\mathbf{p}) \equiv \widetilde{\Sigma}(k,\mathbf{p})N(k)\,, \tag{5.25}$$

where the trace concerns SU(2) indices. Using now the partial fraction decomposition of the propagators (5.19) and the reduced self-energy (5.20), we obtain a recursion relation since if we replace $\mathbf{p}\to\mathbf{p}-\mathbf{q}$ and $p^0\to p^0+q^0$ (cf. fig. 5.2 with redefining $p_i \equiv q_i, i\neq 1$) the remaining propagators are the same as in the $(n-1)$-point function and thus,

$$\begin{aligned}\epsilon(k,\mathbf{p})J(k,\mathbf{p}) = &-\frac{1}{2}\mathcal{F}(k_\parallel,p_\parallel)\frac{\eta^\dagger(p)}{p_\parallel - k_\parallel}N(k)\\ &+\int_q\left[J(k-q,\mathbf{p})V\cdot A(q) - V\cdot A(q)J(k-q,\mathbf{p}-\mathbf{q})\right]\,.\end{aligned} \tag{5.26}$$

For an explicit derivation consult [108]. Now we are ready to integrate out the soft gauge bosons: In principle, one can schematically rewrite eq. (5.26) according to $J = N + AJ$. This can be used as a recursion relation and it iterates like $J = N + A(N+AJ)$ and so forth. One now can integrate over the gauge fields, where terms linear in A vanish while for terms like $\langle AAJ\rangle = \langle AA\rangle\langle J\rangle$ one can make use of the gauge propagator for SU(2)×SU(3)

$$\left\langle A_\mu(q)A_\nu(q')\right\rangle = \tilde{\delta}(q+q')\left(C_2(r)g^2\Delta_{\mu\nu}(q) + y_l^2 g'^2\Delta'_{\mu\nu}(q)\right)\,, \tag{5.27}$$

with the thermal δ-function

$$\tilde{\delta}(q) \equiv \frac{1}{T}\delta_{q_0,0}(2\pi)^3\delta^3(\mathbf{q}) \tag{5.28}$$

in the imaginary-time formalism and the HTL resummed propagators Δ and Δ' for SU(2) and U(1), respectively. The Casimir operator $C_2(r)$ for SU(2) equals 3/4 in the fundamental representation and the lepton hypercharge is $y_l = -1/2$.

Since we are interested in the retarded self-energy $\Sigma_{\mathrm{ret}}(k) \equiv \Sigma_{\mathrm{ret}}(k^0 + \mathrm{i}0^+, \mathbf{k})$ we have to use the corresponding solutions of the occurring integrals for the HTL resummed propagators:

$$\begin{aligned} I(k^0 \pm \mathrm{i}0^+, \mathbf{k}, \mathbf{q}_\perp) &\equiv T \sum_{q_0 = \mathrm{i}\omega} \int \frac{\mathrm{d}q_\parallel}{2\pi} \frac{v^\mu v^\nu \Delta_{\mu\nu}(q)}{v \cdot (k - q)} \\ &\simeq \mp \frac{\mathrm{i}}{2} T \left(\frac{1}{\mathbf{q}_\perp^2} - \frac{1}{\mathbf{q}_\perp^2 + m_{\mathrm{D}}^2} \right) , \end{aligned} \tag{5.29}$$

with m_{D} the appropriate Debye mass. After getting rid of the background field N (cf. eq. (5.25)) we then obtain

$$\begin{aligned} \mathrm{i}\epsilon(k, \mathbf{p}) \widetilde{\Sigma}(k, \mathbf{p}) = &- \frac{\mathrm{i}}{2} d(r) \mathcal{F}(k_\parallel, p_\parallel) \frac{\eta^\dagger(p)}{p_\parallel - k_\parallel} \\ &+ \int \frac{\mathrm{d}^2 q_\perp}{(2\pi)^2} \mathcal{C}(\mathbf{q}_\perp) \left[\widetilde{\Sigma}(k, \mathbf{p}) - \widetilde{\Sigma}(k, p_\parallel, \mathbf{p}_\perp - \mathbf{q}_\perp) \right] , \end{aligned} \tag{5.30}$$

with the kernel $\mathcal{C}$ being defined as

$$\mathcal{C}(\mathbf{q}_\perp) \equiv T \left[C_2(r) g^2 \left(\frac{1}{\mathbf{q}_\perp^2} - \frac{1}{\mathbf{q}_\perp^2 + m_{\mathrm{D}}^2} \right) + y_l^2 g'^2 \left(\frac{1}{\mathbf{q}_\perp^2} - \frac{1}{\mathbf{q}_\perp^2 + m_{\mathrm{D}}'^2} \right) \right] , \tag{5.31}$$

due to the HTL resummed propagators of SU(2) and U(1) gauge fields. The associated Debye masses, m_{D} and m'_{D}, are given by [121,122]

$$m_{\mathrm{D}}^2 = \frac{11}{6} g^2 T^2 \qquad m_{\mathrm{D}}^2 = \frac{11}{6} g'^2 T^2 . \tag{5.32}$$

Thus, if one parametrises the reduced self-energy $\widetilde{\Sigma}(k, \mathbf{p})$ using a vector function $\mathbf{f}$ and a scalar function ψ according to

$$\widetilde{\Sigma}(k, \mathbf{p}) \sim \eta^\dagger = \left(-\frac{p_1 + \mathrm{i}p_2}{2p_\parallel}, 1 \right) \sim (\mathbf{w} \cdot \mathbf{f}, \psi) , \tag{5.33}$$

with the auxiliary vector $\mathbf{w} = (1, \mathrm{i})$, these two functions are the solutions of the integral equations

$$\mathrm{i}\epsilon(k, \mathbf{p}) \, \mathbf{f}(\mathbf{p}_\perp) - \int \frac{\mathrm{d}^2 q_\perp}{(2\pi)^2} \, \mathcal{C}(\mathbf{q}_\perp) \, [\mathbf{f}(\mathbf{q}_\perp) - \mathbf{f}(\mathbf{p}_\perp - \mathbf{q}_\perp)] = 2\mathbf{p}_\perp , \tag{5.34a}$$

$$\mathrm{i}\epsilon(k, \mathbf{p}) \psi(\mathbf{p}_\perp) - \int \frac{\mathrm{d}^2 q_\perp}{(2\pi)^2} \, \mathcal{C}(\mathbf{q}_\perp) \, [\psi(\mathbf{q}_\perp) - \psi(\mathbf{p}_\perp - \mathbf{q}_\perp)] = 1 . \tag{5.34b}$$

It follows that the wanted expression for the reduced self-energy becomes[6]

$$\widetilde{\Sigma}(k, \mathbf{p}) = -\frac{\mathrm{i}}{2} \, \frac{d(r) \mathcal{F}(k_\parallel, p_\parallel)}{p_\parallel - k_\parallel} \left(-\frac{f_1 + \mathrm{i}f_2}{4p_\parallel}, \psi \right) . \tag{5.35}$$

[6] Note the missing factor $\frac{1}{4}$ in the first component of $\widehat{\Sigma}$ in [108].

The two integral equations (5.34) can be solved numerically by the procedure described in app. B. Therefore, one first transforms them into differential equations that can be treated as initial condition problems. The numerical solution yields a coefficient $c_2 \equiv c_2(k, p_\parallel)$ for each of the differential equations.

Physically, the two functions are sensitive to helicity changing and conserving processes. This means ψ vanishes for $M \to 0$, whereas $\mathbf{f}$ disappears in the collinear limit $\mathbf{p}_\perp \to 0$. This explicitly becomes clear by considering the differential production rate for the Majorana neutrino: Choosing $\mathbf{v}$ in the direction of $\mathbf{k}$, we obtain $\mathbf{k}_\perp = 0$ as well as $k_\parallel = |\mathbf{k}| \equiv k$. Thus, we can indicate the rate as

$$\frac{\mathrm{d}\Gamma}{\mathrm{d}^3k} = -\frac{d(r)|\lambda|^2}{(2\pi)^3 2k} \int \frac{\mathrm{d}^3p}{(2\pi)^3} \frac{f_\mathrm{F}(p_\parallel) f_\mathrm{B}(k - p_\parallel)}{k - p_\parallel} \,\mathrm{Re}\left[\frac{k}{2p_\parallel^2}\mathbf{p}_\perp \cdot \mathbf{f} + \frac{M^2}{k}\psi\right] . \tag{5.36}$$

The detailed calculation of the Majorana neutrino production rate is presented in app. B.1. The analytic results for the leading order will be presented in the next chapter. For calculating the whole rate numerically, one also needs to integrate the total production rate, which is performed using the multidimensional *Monte Carlo* integration technique (for details consult app. B). Since the coefficients c_2 are available only numerically, they have to be evaluated for each point where the Monte Carlo integration routine analyses the integral over $p_\parallel$ and k. The results are also presented in the next chapter.

6 The Majorana neutrino production rate

Thunder is good, thunder is impressive;
but it is lightning that does the work.
Mark Twain

In order to explicitly observe the influence of soft gauge contributions to the Majorana neutrino production rate, we first calculate the leading order result according to fig. 6.1. Afterwards we present numerical investigations of the solution, which includes gauge interactions, and a discussion of the obtained results. For more detailed calculations, consult app. B.1.

6.1 Tree-level result

The tree-level result can be obtained from eq. (5.36) by neglecting the integral terms in eq. (5.34) leading to

$$\mathbf{f}(\mathbf{p}_\perp) = \frac{2\mathbf{p}_\perp}{\mathrm{i}\epsilon(k,\mathbf{p})} \quad \text{and} \quad \psi(\mathbf{p}_\perp) = \frac{1}{\mathrm{i}\epsilon(k,\mathbf{p})}\,. \tag{6.1}$$

Then an analytic solution is accessible and is given by

$$\frac{\mathrm{d}\Gamma^{\mathrm{tree}}}{\mathrm{d}^3k} = \frac{d(r)|\lambda|^2}{(2\pi)^3 4k_\parallel^2}\int_{p_-}^{p_+}\frac{\mathrm{d}p_\parallel}{2\pi}\frac{f_{\mathrm{F}}(p_\parallel)f_{\mathrm{B}}(k_\parallel - p_\parallel)}{|p_\parallel|}\left[(p_\parallel - k_\parallel)m_l^2 + p_\parallel(M^2 - m_\phi^2)\right]\,. \tag{6.2}$$

The integration over $\mathbf{p}_\perp$ is already performed in terms of an occurring δ-function in $\epsilon(k,\mathbf{p})$ (cf. eq. (5.18)). The boundaries $p_\pm$ are constituted by the particles' on-shell condition resulting in the condition that $\epsilon(k,\mathbf{p}) = 0$ has a real solution for $|\mathbf{p}_\perp|$. The calculation of the limits[1] is proven in app. B.1.2 and yields

$$p_\pm = \frac{X \pm \sqrt{Y}}{2M^2}k_\parallel\,, \tag{6.3}$$

with

$$\begin{aligned} X &\equiv M^2 + m_l^2 - m_\phi^2 \\ Y &\equiv (m_\phi + m_l + M)(m_\phi - m_l + M)(m_\phi + m_l - M)(m_\phi - m_l - M)\,. \end{aligned}$$

The term $\sqrt{Y}$ leads to the restrictions $m_\phi \geq M + m_l$ (decay of Higgs) or $M \geq m_\phi + m_l$ (inverse decay of Majorana neutrino), cf. fig. 6.1, otherwise the rate becomes zero as can be seen in fig. 6.3 in the next section.

[1] Note the missing $k_\parallel$ in the result for the boundaries in [108].

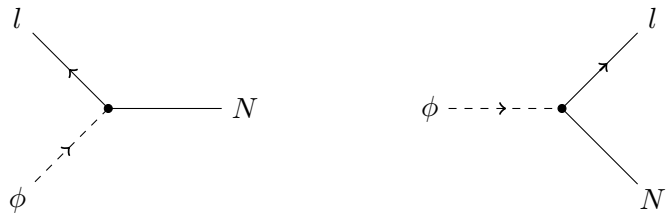

Figure 6.1: Tree-level contributions to the Majorana neutrino production rate: decay (left) and inverse decay (right).

6.2 Results including soft gauge interactions

In case of including soft gauge interactions we have to calculate the full Majorana neutrino production rate from eq. (5.36):

$$\frac{\mathrm{d}\Gamma}{\mathrm{d}^3k} = -\frac{d(r)|\lambda|^2}{(2\pi)^3 2k}\int \frac{\mathrm{d}^3p}{(2\pi)^3}\,\frac{f_\mathrm{F}(p_\parallel)f_\mathrm{B}(k-p_\parallel)}{k-p_\parallel}\,\mathrm{Re}\left[\frac{k}{2p_\parallel^2}\mathbf{p}_\perp\cdot\mathbf{f}+\frac{M^2}{k}\psi\right].$$

The results for the two functions $\mathbf{f}$ and ψ are no longer accessible analytically any more, cf. their definition eq. (5.34). The detailed description of how to solve the integral equations as well as further technical details like performing the perpendicular momentum integration can be found in app. B.

We also have to specify some parameters for the numerical treatment. For a better comparability to [108] we have chosen their values for the Majorana mass $M = 10^7\,\mathrm{GeV}$ and the Higgs mass[2] $m_\mathrm{H} = 150\,\mathrm{GeV}$ for the numerical analysis.

Due to the running of the Standard Model couplings we have to use renormalization group equations (RGE). In our case we used the following ones up to one-loop order, cf. [123,124]:

$$\frac{\mathrm{d}g_1^2}{\mathrm{d}t} = \frac{g_1^4}{8\pi^2}\,\frac{41}{10} + \mathcal{O}(g^6) \tag{6.4a}$$

$$\frac{\mathrm{d}g_2^2}{\mathrm{d}t} = \frac{g_2^4}{8\pi^2}\left(-\frac{19}{6}\right) + \mathcal{O}(g^6) \tag{6.4b}$$

$$\frac{\mathrm{d}g_3^2}{\mathrm{d}t} = \frac{g_3^4}{8\pi^2}(-7) + \mathcal{O}(g^6) \tag{6.4c}$$

$$\frac{\mathrm{d}\lambda_\mathrm{t}^2}{\mathrm{d}t} = \frac{\lambda_\mathrm{t}^2}{8\pi^2}\left(\frac{9}{2}\lambda_\mathrm{t}^2 - \frac{17}{20}g_1^2 - \frac{9}{4}g_2^2 - 8g_3^2\right) + \mathcal{O}(g^6) \tag{6.4d}$$

$$\begin{aligned}\frac{\mathrm{d}\Lambda}{\mathrm{d}t} = \frac{1}{16\pi^2}\Big(&\frac{27}{200}g_1^4 + \frac{9}{20}g_1^2g_2^2 + \frac{9}{8}g_2^4 - \frac{9}{5}g_1^2\Lambda - 9g_2^2\Lambda \\ &- 6\lambda_\mathrm{t}^4 + 12\lambda_\mathrm{t}^2\Lambda + 24\Lambda^2\Big) + \mathcal{O}(g^6)\,,\end{aligned} \tag{6.4e}$$

where $t \equiv \ln\frac{\mu}{\mu_0}$ and $\mathcal{O}(g^6)$ meaning any combination of the different coupling constants.[3]

[2] Note that current measurements of CMS and ATLAS supply a value of $m_\mathrm{H} \simeq 126\,\mathrm{GeV}$.
[3] Note that $\Lambda \equiv g^2$ in the counting here.

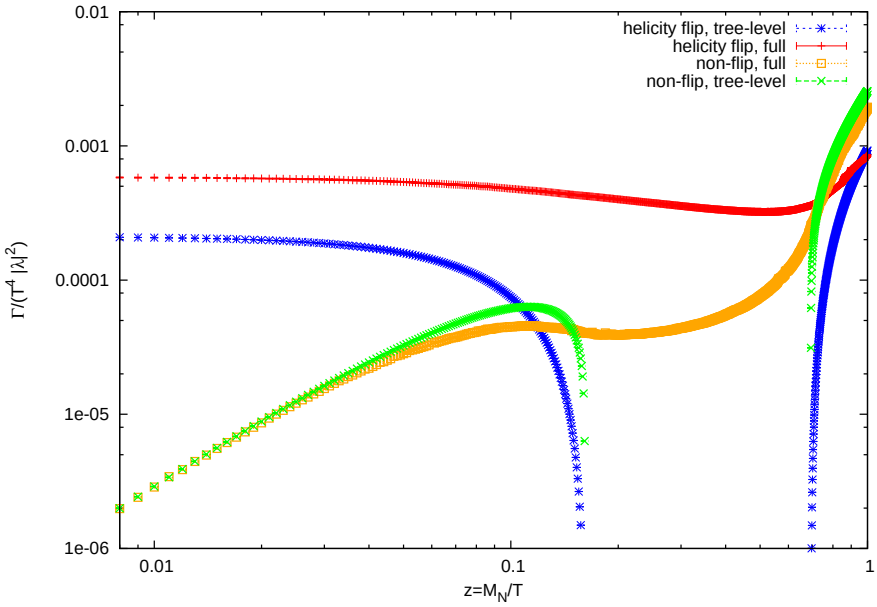

Figure 6.2: Majorana neutrino production rate as a function of z in terms of helicity changing/conserving processes for the tree-level and the full result.

We also used the relations for the Standard Model couplings

$$\alpha_1(\mu) \equiv \frac{g_1^2(\mu)}{4\pi} = \frac{\alpha_{\mathrm{em}}(\mu)}{\cos^2\theta_{\mathrm{W}}(\mu)} \tag{6.5a}$$

$$\alpha_2(\mu) \equiv \frac{g_2^2(\mu)}{4\pi} = \frac{\alpha_{\mathrm{em}}(\mu)}{\sin^2\theta_{\mathrm{W}}(\mu)} \tag{6.5b}$$

$$\alpha_3(\mu) \equiv \frac{g_3^2(\mu)}{4\pi} \equiv \alpha_{\mathrm{s}}(\mu) \tag{6.5c}$$

$$\lambda_{\mathrm{t}}^2 \equiv g_{\mathrm{t}}^2(\mu) = \frac{2m_{\mathrm{t}}^2}{v^2} \tag{6.5d}$$

$$\Lambda(\mu) \equiv g_\Lambda^2(\mu) = \frac{m_{\mathrm{H}}}{2v^2}\,, \tag{6.5e}$$

for implementing the initial condition $\mu = m_{\mathrm{Z}} = 91.1876\,\mathrm{GeV}$. Therefore, we took the values [25]:

$$\alpha_{\mathrm{em}}(m_{\mathrm{Z}}) = \frac{1}{128}, \qquad \alpha_{\mathrm{s}}(m_{\mathrm{Z}}) = 0.1184, \qquad \sin^2\theta_{\mathrm{W}}(m_{\mathrm{Z}}) = 0.23116$$
$$m_{\mathrm{t}} = 173.1\,\mathrm{GeV} \quad \text{and} \quad v = (\sqrt{2}G_{\mathrm{F}})^{-1/2} = 246.221\,\mathrm{GeV}\,.$$

We adopted the scale $\mu = 2\pi T_{\mathrm{R}}$ with the reheating temperature $T_{\mathrm{R}} = 10^9\,\mathrm{GeV}$. Hence we can use the initial conditions for $t_0 \equiv \ln\frac{m_{\mathrm{Z}}}{2\pi T_{\mathrm{R}}}$ and thus need to evaluate the values of the couplings for $t = 0 = \ln\frac{2\pi T_{\mathrm{R}}}{2\pi T_{\mathrm{R}}}$. In contrast to the former taken value of the Higgs

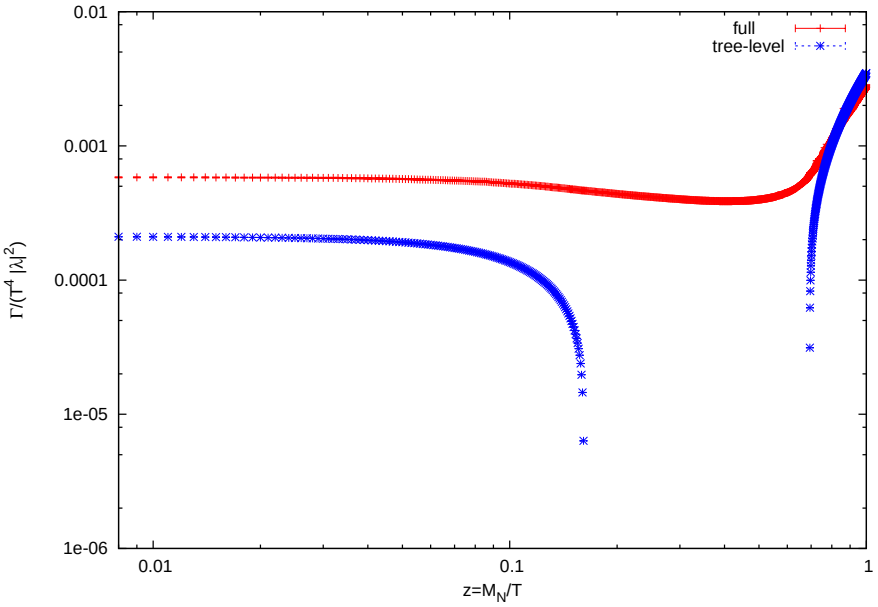

Figure 6.3: Majorana neutrino production rate as function of $z = M/T$ per unit time and volume. The blue line ($\times$) represents the tree-level contribution without including soft gauge interactions, the red line ($+$) depicts the full result.

mass of $m_{\mathrm{H}} = 150\,\mathrm{GeV}$, the results listed in appendix A.3 are obtained by implementing the current Higgs mass $m_{\mathrm{H}} = 126\,\mathrm{GeV}$, taken from [48,49], as an example. Furthermore, all values plotted are divided by the coupling $|\lambda|^2$ since the Majorana coupling is yet unknown. The dimension of the group representation is $d(r) = 2$.

Hence we can have a closer look at the functions $\mathbf{f}$ and ψ: The first one corresponds to helicity changing processes while the latter one to helicity conserving ones. The results of the two functions finally lead to the desired integrated production rate $\Gamma = \int \mathrm{d}^3k(\mathrm{d}\Gamma/\mathrm{d}^3k)$ in terms of $z = M/T$ which is depicted in fig. 6.2 for helicity changing and conserving processes both for tree-level and the full rate. We identify the different behaviour of the two: As mentioned earlier, the rate does not vanish in the case of $M \to 0$ for the former one whereas it does for ψ. Furthermore, one can see that the gauge corrected rates both for helicity changing as well as for helicity conserving processes do not vanish any more in the regime $m_\phi - m_l < M < m_\phi + m_l$. It even appears to be smooth in this interval where the decay of the Higgs is kinematically forbidden. This becomes more apparent by considering the total integrated production rate, i. e. the sum of both contributions, that is depicted in fig. 6.3. For small values of z one finds that the inclusion of gauge interactions is mandatory since their rate is larger than the tree-level result by a factor of 3. For large z the inverse decay is the dominating part, thus, the result is well described by the tree-level result.

We can also investigate the momentum spectrum of the produced Majorana neutrino. A thermal spectrum is proportional to the Fermi-Dirac distribution $f_{\mathrm{F}}(k)$. However, as

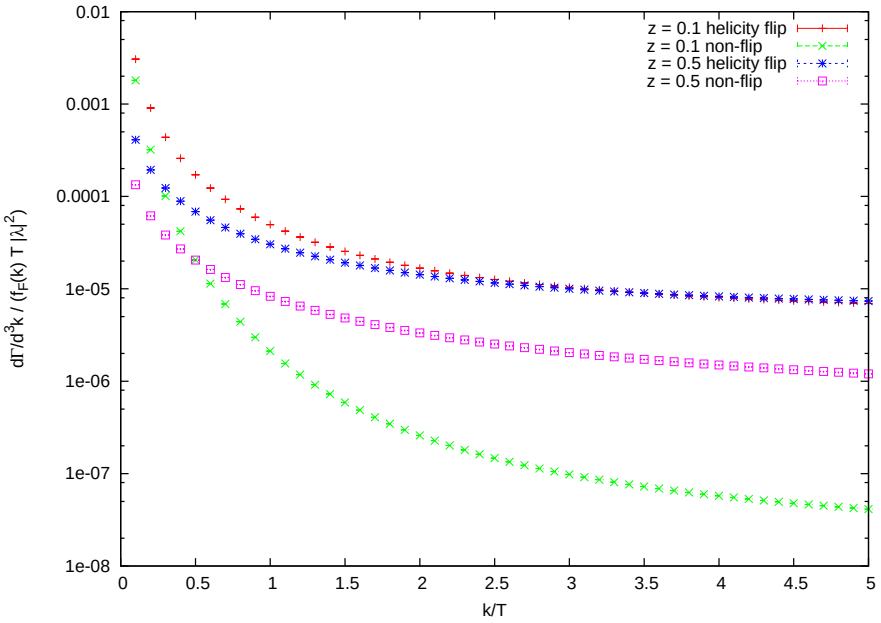

Figure 6.4: Differential production rate of the Majorana neutrino divided by the Fermi-Dirac distribution $f_{\mathrm{F}}(k)$ due to helicity changing/conserving processes as a function of momentum k for different temperatures.

can be seen in fig. 6.4, where the differential production rate divided by the Fermi-Dirac distribution is plotted for two temperatures, the spectrum is not thermal. It is peaked in the infrared which means that typical momenta of the Majorana neutrino are smaller than in equilibrium. This is true for both helicity changing and conserving processes. Furthermore, this behaviour occurs also in the region where tree-level processes and gauge corrected processes are allowed ($z = 0.1$) as well as in the region of pure multiple soft scatterings ($z = 0.5$).

7 Standard model corrections to thermal leptogenesis

Das entscheidende Kriterium ist Schönheit;
für häßliche Mathematik ist auf dieser Welt kein beständiger Platz.
Godfrey H. Hardy

In this chapter we finally include gauge corrections to the context of thermal leptogenesis systematically. In the first section naive considerations are presented in which the successive derivation of all possible Feynman diagrams that can contribute at three-loop level to the asymmetry-causing diagram, is shown. As already seen in the last section, this is not sufficient to gain all contributions since resummation schemes have to be used. Hence a cylindrical diagram is presented that contains all possible gauge corrected contributions to the lepton asymmetry. Afterwards the calculation of this diagram with the aid of the results of the last chapters is shown.

7.1 Including gauge interactions

7.1.1 Gauge corrected three-loop diagrams without resummation

Starting from the two diagrams in fig. 4.2 that are responsible for the lepton asymmetry, one can for a first approach look at all three-loop diagrams that include gauge corrections. The associated diagrams are shown in fig. 7.1 for the gauge corrected Higgs and lepton propagators as well as in fig. 7.2 for the vertex corrections. The result is checked with QGRAF[1] [125], a program that indicates all diagrams up to a given loop order by using the underlying Feynman rules only. One also has to keep in mind that the mirrored versions of all 17 diagrams contribute as well.

As we have seen in the last sections, only including three-loop diagrams is not sufficient for a consistent treatment of gauge corrections and thus, we have to use resummation schemes like HTL and CTL. This can be seen more easily by not integrating out the heavier Majorana neutrinos N_2 and N_3 (1), i. e. using the Lagrangian in eq. (2.6) instead of eq. (2.32), and closing the two outer lepton lines (2):

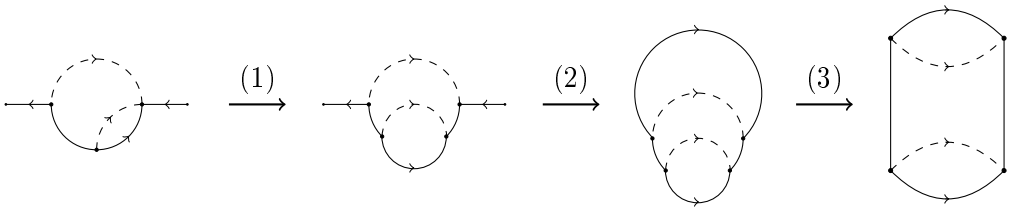

[1] http://cfif.ist.utl.pt/~paulo/qgraf.html

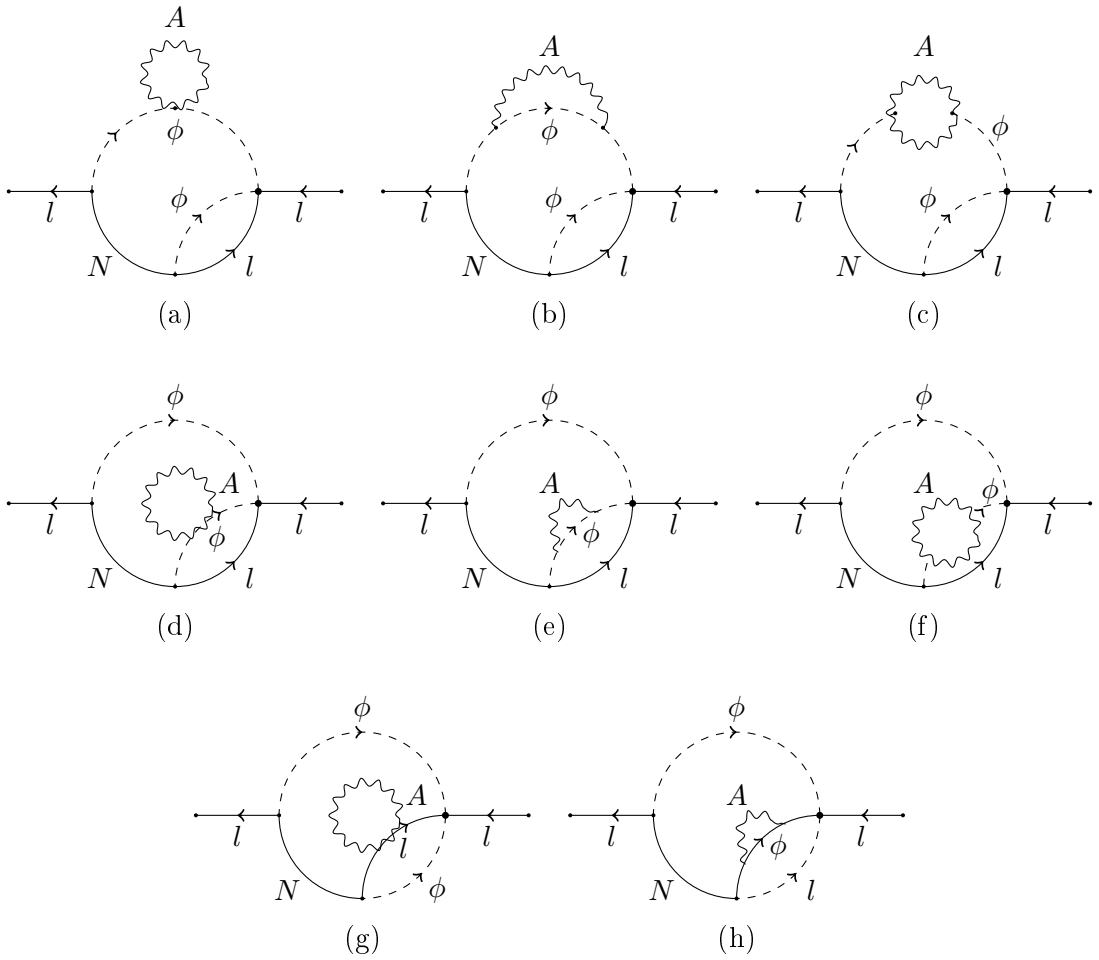

Figure 7.1: Three-loop diagrams containing gauge corrections for Higgs (a) - (f) and lepton (g) - (h) propagators.

After that, one is left with a new sort of diagram, the cylindrical diagram (3), that is depicted including the relevant gauge corrections in fig. 7.3. It consists of twice the resummed Majorana self-energy from fig. 5.5. The only difference is the feature of the Majorana propagators since now the two propagators are internal lines and thus do not have to fulfil the on-shell condition $p^2 = M^2$.

7.1.2 Gauge corrected diagram including resummation

To ensure that this cylindrical diagram really contains all contributions found in the last section, we have to compare it to those in fig. 7.1 and 7.2:

- Corrections to the Higgs and lepton propagator (fig. 7.1): These contributions are all included due to the HTL resummation and therefore the inclusion of asymptotic masses m_l and m_ϕ, cf. chap. 5.4.
- Vertex corrections (fig. 7.2 (a), (f), (g)): These three diagrams all lead to the same contribution when closing the outer lepton line and are obviously included, cf. fig. 5.5.

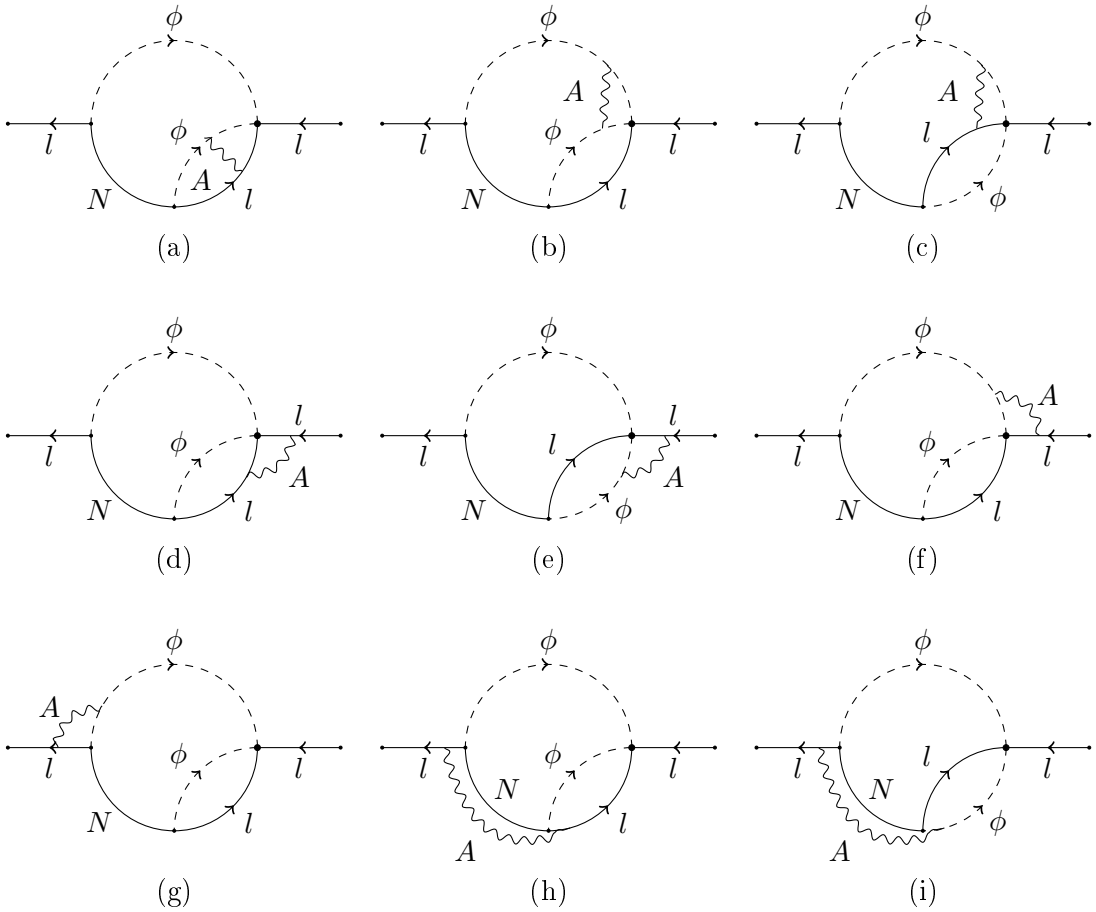

Figure 7.2: Three-loop diagrams containing gauge corrections for vertices.

- Vertex corrections (fig. 7.2, others): These diagrams are also included since these are the 'soft external gauge bosons' from the last section, cf. fig. 5.2. In the last step of the mentioned recipe in chap. 5.4, they are integrated out and thus the thermal width has to be included.

This shows that all contributions due to gauge corrections are enclosed in the cylindrical diagram fig. 7.3. After that, we can calculate it for obtaining the gauge corrected lepton asymmetry we are looking for. The whole diagram is only accessible numerically, as already seen in the last chapter by discussing the solutions of the functions $\mathbf{f}$ and ψ. Nevertheless, we start with some analytic considerations to simplify the expression.

7.2 Calculating the cylindrical diagram

Since we are interested in the hierarchical case of thermal leptogenesis (cf. chap. 4) we again have to integrate out the heavy neutrinos N_2 and N_3, respectively. As depicted in fig. 7.3, their corresponding momentum is $\mathbf{p}'$, so that we obtain an effective vertex on the right-hand side with $t_2 \equiv t_4$. Starting with the final expression for the lepton

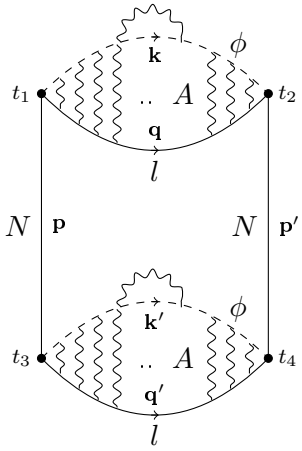

Figure 7.3: Cylindrical diagram containing all gauge contributions for a consistent treatment.

asymmetry from section 4.2 (cf. eq. (4.15)):

$$L_{\mathbf{k},ii}(t,t) = 12\,\lambda_{ii}\int_0^t \mathrm{d}t_1 \int_0^t \mathrm{d}t_2\,\mathrm{Re}\left(\mathrm{Tr}\left[\Pi^{(1)>}_{\mathbf{k}}(t_1,t_2)S^{<}_{\mathbf{k}}(t_2-t_1)\right]\right)\,, \tag{7.1}$$

with the lepton self-energy $\Pi^{>}$ containing all HTL-resummed terms and the resummed lepton propagator $S^{<}$. Using the relations of eq. (4.13) with $\widetilde{G}^{>} = \widetilde{G}^{22} \equiv \widetilde{G}$, we can rewrite the self-energy according to

$$\begin{aligned}\Pi^{(1)>}_{\mathbf{k}}(t_1,t_2) = \int_0^\infty \mathrm{d}t_3 \int_{\mathbf{q},\mathbf{q}',\mathbf{k}',\mathbf{p}} \widetilde{G}_{\mathbf{p}}(t_1,t_3)\Big[S^{11}_{\mathbf{k}'}(y_{23})\Delta^{11}_{\mathbf{q}'}(y_{23}) - S^{<}_{\mathbf{k}'}(y_{23})\Delta^{<}_{\mathbf{q}'}(y_{23})\Big]\Delta^{<}_{\mathbf{q}}(y_{21}) \\ \times (2\pi)^3\delta^3(\mathbf{p}-\mathbf{k}-\mathbf{q})(2\pi)^3\delta^3(\mathbf{p}-\mathbf{k}'-\mathbf{q}')P_L\,,\end{aligned} \tag{7.2}$$

where we introduced the notation $y_{ij} = t_i - t_j$. Applying properties of the lepton and Higgs propagators (cf. eqs. (3.17)) we can find a constraint for the integration of t_3 since

$$\begin{aligned}S^{11}_{\mathbf{k}'}(y_{23})\Delta^{11}_{\mathbf{q}'}(y_{23}) - S^{<}_{\mathbf{k}'}(y_{23})\Delta^{<}_{\mathbf{q}'}(y_{23}) = \theta(y_{23})\Big(S^{>}_{\mathbf{k}'}(y_{23})\Delta^{>}_{\mathbf{q}'}(y_{23}) \\ - S^{<}_{\mathbf{k}'}(y_{23})\Delta^{<}_{\mathbf{q}'}(y_{23})\Big)\,.\end{aligned}^{2} \tag{7.3}$$

Introducing also the notation

$$\Sigma^{<}_{\mathbf{p},\mathbf{q}}(y) \equiv S^{<}_{\mathbf{p}}(y)\Delta^{<}_{\mathbf{q}}(y) \tag{7.4}$$

and analogue for $\Sigma^{>}$, we can rewrite the asymmetry in a compact way

$$\begin{aligned}L_{\mathbf{k},ii}(t,t) =& 12\,\lambda_{ii}\int_0^t \mathrm{d}t_1 \int_0^t \mathrm{d}t_2 \int_0^{t_2} \mathrm{d}t_3 \int_{\mathbf{q},\mathbf{q}',\mathbf{k}',\mathbf{p}} \widetilde{G}_{\mathbf{p}}(t_1,t_3) \\ &\mathrm{Re}\left\{\mathrm{Tr}\left[\Sigma^{<}_{\mathbf{k},\mathbf{q}}(y_{21})\left(\Sigma^{>}_{\mathbf{k}',\mathbf{q}'}(y_{23}) - \Sigma^{<}_{\mathbf{k}',\mathbf{q}'}(y_{23})\right)P_L\right]\right\} \\ &\times (2\pi)^3\delta^3(\mathbf{p}-\mathbf{k}-\mathbf{q})(2\pi)^3\delta^3(\mathbf{p}-\mathbf{k}'-\mathbf{q}')\,.\end{aligned} \tag{7.5}$$

[2] Note that for the self-energy $\Pi^{(2)}$ this constraint would restrict t_3 to the interval $[0,t_1]$, instead.

Applying now the delta functions, defining momentum conservation $\mathbf{p} = \mathbf{k}+\mathbf{q} = \mathbf{p}'+\mathbf{k}'$ and using the relation (cf. e. g. [30])

$$S^{>}(y)^* = CS^{<}(y)C^{-1} = -(S^{<}(y))^T\,|_{M=0}\ , \tag{7.6}$$

and analogously for $\Delta^{>}$ with the charge conjugation matrix C, we can further simplify the expression. After performing a Fourier transform in y_{21} and y_{23} we obtain

$$\begin{aligned} L_{\mathbf{k},ii}(t,t) = &-12\lambda_{ii}\int_0^t \mathrm{d}t_1\int_0^t \mathrm{d}t_2\int_0^{t_2}\mathrm{d}t_3\int\frac{\mathrm{d}\omega_{21}}{2\pi}\int\frac{\mathrm{d}\omega_{23}}{2\pi}\int_{\mathbf{k}',\mathbf{p}}\widetilde{G}_{\mathbf{p}}(t_1,t_3)\\ &\times\mathrm{Tr}\Big\{\Big[\mathrm{Re}(\Sigma^{<}_{\mathbf{k},\mathbf{p}}(\omega_{21})\Sigma^{<}_{\mathbf{k}',\mathbf{p}}(\omega_{23}))\Big\{\cos(\omega_{21}y_{21})\cos(\omega_{23}y_{23})(1+\mathrm{e}^{2\beta\omega_{23}})\\ &\qquad-\sin(\omega_{21}y_{21})\sin(\omega_{23}y_{23})(1-\mathrm{e}^{2\beta\omega_{23}})\Big\}\\ &-\mathrm{Im}(\Sigma^{<}_{\mathbf{k},\mathbf{p}}(\omega_{21})\Sigma^{<}_{\mathbf{k}',\mathbf{p}}(\omega_{23}))\Big\{\cos(\omega_{21}y_{21})\sin(\omega_{23}y_{23})(1-\mathrm{e}^{2\beta\omega_{23}})\\ &\qquad+\sin(\omega_{21}y_{21})\cos(\omega_{23}y_{23})(1+\mathrm{e}^{2\beta\omega_{23}})\Big\}\Big]P_L\Big\}\ . \end{aligned} \tag{7.7}$$

Since the Fourier transform of a product in position space leads to a convolution in momentum space, we find for the self-energies $\Sigma^{\lessgtr}$:

$$\Sigma^{\lessgtr}_{\mathbf{p},\mathbf{q}}(\omega) = \int \mathrm{d}\omega' S^{\lessgtr}_{\mathbf{p}}(\omega')\Delta^{\lessgtr}_{\mathbf{p}-\mathbf{q}}(\omega-\omega')\,. \tag{7.8}$$

Finding the relation (cf. [86])

$$\Sigma^{<}(k) = -2f_{\mathrm{F}}(k_0)\,\mathrm{Im}\,\Sigma^{\mathrm{ret}}(k)\ , \tag{7.9}$$

with Σ^{ret} being the retarded self-energy, we are now able to connect the resummation scheme of chap. 5 with the lepton number matrix defined in chap. 4. The second part of eq. (7.7) then vanishes, since the imaginary part of a real value is zero. Thus we have to investigate the expression

$$\begin{aligned} L_{\mathbf{k},ii}(t,t) = &-96\lambda_{ii}\int_0^t \mathrm{d}t_1\int_0^t \mathrm{d}t_2\int_0^{t_2}\mathrm{d}t_3\int\frac{\mathrm{d}\omega_{21}}{2\pi}\int\frac{\mathrm{d}\omega_{23}}{2\pi}\int_{\mathbf{p}}\widetilde{G}_{\mathbf{p}}(t_1,t_3)f_{\mathrm{F}}(\omega_{21})f_{\mathrm{F}}(-\omega_{23})\\ &\times\big(\cos(\omega_{21}y_{21})\cos(\omega_{23}y_{23})\cosh(\beta\omega_{23})+\sin(\omega_{21}y_{21})\sin(\omega_{23}y_{23})\sinh(\beta\omega_{23})\big)\\ &\times\mathrm{Tr}\Big\{\mathrm{Im}\,\Sigma^{\mathrm{R,ret}}_{\mathbf{k}}(\omega_{21},\omega_{\mathbf{p}},\mathbf{p})\,\mathrm{Im}\,\Sigma^{\mathrm{R,ret}}(\omega_{23},\omega_{\mathbf{p}},\mathbf{p})P_L\Big\}\ , \end{aligned} \tag{7.10}$$

where

$$\mathrm{Im}\,\Sigma^{\mathrm{R,ret}}(\omega_{23},\omega_{\mathbf{p}},\mathbf{p}) = \int\frac{\mathrm{d}^3k'}{(2\pi)^3}\,\mathrm{Im}\,\Sigma^{\mathrm{R,ret}}_{\mathbf{k}'}(\omega_{23},\omega_{\mathbf{p}},\mathbf{p})\ . \tag{7.11}$$

In analogy to chap. 5 the index R denotes the 2×2 matrix in Weyl representation, but now the momenta k and p are interchanged due to the momentum distribution in fig. 7.3. Again, we can use the collinearity of the inner momenta so that $k'_{\parallel}\sim k'_0\equiv\omega_{23}$ and $k_{\parallel}\sim k_0\equiv\omega_{21}$, respectively. This corresponds to an error of $\mathcal{O}(g^2T)$ and thus can be neglected for a first approach.

Starting with the ansatz eq. (5.35) we can compute the retarded self-energy

$$\Sigma^{\mathrm{R,ret}}(p) = \mathrm{i}\int \frac{\mathrm{d}^3k}{(2\pi)^3}\frac{\mathcal{F}(p_\parallel,k_\parallel)}{k_\parallel - p_\parallel}\eta(k)\left(-\frac{f_1+\mathrm{i}f_2}{4k_\parallel},\psi\right)\,, \tag{7.12}$$

and therefore the imaginary part of it:

$$\operatorname{Im}\Sigma^{\mathrm{R,ret}}(p) = \int \frac{\mathrm{d}^3k}{(2\pi)^3}\frac{\mathcal{F}(p_\parallel,k_\parallel)}{k_\parallel - p_\parallel}\begin{pmatrix} \frac{\operatorname{Re}\mathbf{k}_\perp\mathbf{f}}{8k_\parallel^2} & -\frac{k_1}{2k_\parallel}\operatorname{Re}\psi \\ -\frac{\operatorname{Re}f_1}{4k_\parallel} & \operatorname{Re}\psi \end{pmatrix}\,. \tag{7.13}$$

The detailed calculation can be found in app. B.3.3.

Since for leptogenesis, only temperature dependent parts of the self-energy are of interest (cf. sec. 2.1.1), we can have a further look at the off-diagonal elements and the integrals

$$\int \frac{\mathrm{d}^2k_\perp}{(2\pi)^3}\operatorname{Re}f_1(\mathbf{k}_\perp) = 0\,, \quad \text{and} \quad \int \frac{\mathrm{d}^2k_\perp}{(2\pi)^3}\,k_1\operatorname{Re}\psi(\mathbf{k}_\perp) = 0\,. \tag{7.14}$$

Applying the same procedure on these integrals as shown in app. B.3.3, we find that the two integrals diverge, in detail:

$$\int \frac{\mathrm{d}^2k_\perp}{(2\pi)^3}\operatorname{Re}f_1(\mathbf{k}_\perp) = \lim_{b\to 0} b_1 \operatorname{Re}h(b)\,, \tag{7.15a}$$

$$\int \frac{\mathrm{d}^2k_\perp}{(2\pi)^3}\,k_1\operatorname{Re}\psi(\mathbf{k}_\perp) = \lim_{b\to 0}\frac{b_1}{b}\operatorname{Im}\psi'(b)\,, \tag{7.15b}$$

with the diverging functions $\operatorname{Re}h(b)$ and $\operatorname{Im}\psi'(b)$. Their exact behaviour for $b\to 0$ can be derived by comparing the right hand side of both integrals with the boundary conditions (B.39):

$$\lim_{b\to 0} b_i \operatorname{Re}h(b) \sim \frac{b_i}{b^2} + \mathcal{O}(b)\,, \tag{7.16a}$$

$$\lim_{b\to 0}\operatorname{Im}\psi(b) \sim \ln b + \mathcal{O}(b^0) \quad \Rightarrow \quad \lim_{b\to 0}\operatorname{Im}\psi'(b) \sim \frac{1}{b} + \mathcal{O}(b^0)\,. \tag{7.16b}$$

Thus for $b\to 0$ both terms behave like $\mathcal{O}(\frac{1}{b})$. However, this is no problem, since the divergence occurs in the temperature independent part of the self-energy. This can be seen by a particular consideration of the function $\mathcal{F}(p_\parallel,k_\parallel)$, because it is the only part of the self-energy, which directly depends on T:

$$\begin{aligned}\mathcal{F}(p_\parallel,k_\parallel) &= f_{\mathrm{F}}(p_\parallel) + f_{\mathrm{B}}(k_\parallel - p_\parallel) \\ &= \frac{1}{\mathrm{e}^{\beta k_\parallel}+1} + \frac{1}{\mathrm{e}^{\beta(k_\parallel - p_\parallel)}+1} \\ &\overset{T=0}{=} \theta(-k_\parallel) - \theta(p_\parallel - k_\parallel)\,.\end{aligned} \tag{7.17}$$

Obviously this only concerns the $k_\parallel$-integration[3] and thus the divergence in the $\mathbf{k}_\perp$-integration still holds and is temperature independent. This divergent part gets removed

[3] Using the θ-functions leads to a restriction to the interval $[0, p_\parallel]$.

by the renormalisation at $T = 0$. Hence, we can restrict our considerations to the temperature dependent part of the self-energy, omitting this divergent part.

Altogether we can rewrite the integrated lepton number matrix according to

$$\begin{aligned} L_{ii}(t,t) = &-\frac{3}{2}\lambda_{ii}\int_0^t \mathrm{d}t_1 \int_0^t \mathrm{d}t_2 \int_0^{t_2} \mathrm{d}t_3 \int \frac{\mathrm{d}\omega_{21}}{2\pi} \int \frac{\mathrm{d}\omega_{23}}{2\pi} \int_{\mathbf{p}} \widetilde{G}_{\mathbf{p}}(t_1,t_3) f_{\mathrm{F}}(\omega_{21}) f_{\mathrm{F}}(-\omega_{23}) \\ &\times \big(\cos(\omega_{21}y_{21})\cos(\omega_{23}y_{23})\cosh(\beta\omega_{23}) + \sin(\omega_{21}y_{21})\sin(\omega_{23}y_{23})\sinh(\beta\omega_{23})\big) \\ &\times \frac{\mathcal{F}(p_\parallel,\omega_{21})\mathcal{F}(p_\parallel,\omega_{23})}{\omega_{21}^2\omega_{23}^2(p_\parallel-\omega_{21})(p_\parallel-\omega_{23})} \operatorname{Im} c_2(\omega_{21},\omega_{\mathbf{p}},\mathbf{p}) \operatorname{Im} c_2(\omega_{23},\omega_{\mathbf{p}},\mathbf{p}) \,, \end{aligned} \tag{7.18}$$

where we used the result of appendix B.3.2

$$\operatorname{Im} c_2(\omega,\omega_{\mathbf{p}},\mathbf{p}) = \int \frac{\mathrm{d}^2 q_\perp}{(2\pi)^2} \operatorname{Re}[\mathbf{q}_\perp \cdot \mathbf{f}(\omega,\omega_{\mathbf{p}},\mathbf{p})] \,. \tag{7.19}$$

Let us recall the nonequilibrium scalar part of the Majorana propagator (cf. (4.13))

$$\widetilde{G}_{\mathbf{p}}(t_1,t_3) = \frac{M}{\omega_{\mathbf{p}}} \cos(\omega_{\mathbf{p}}(t_1-t_3)) f_{\mathrm{F}}(\omega_{\mathbf{p}}) \exp\left\{-\Gamma_{\mathbf{p}}\frac{t_1+t_3}{2}\right\} ,$$

with the Majorana neutrino production rate $\Gamma_{\mathbf{p}}$ discussed in chapter 6. Thus the t_3- and the t_1-integration can only be performed analytically if one deals with a constant production rate. This leads to very lengthy terms that will not be presented here, since they do not provide an additional benefit for a numerical analysis of the expression. Furthermore, the t_2- and the t_3-integration are linked, hence one also cannot perform the former.

Finally, we find the following for the integrated lepton number matrix:

$$\begin{aligned} L_{ii}(t,t) = &-\frac{3}{2}\lambda_{ii}\int_0^t \mathrm{d}t_1 \int_0^t \mathrm{d}t_2 \int_0^{t_2} \mathrm{d}t_3 \int \frac{\mathrm{d}\omega_{21}}{2\pi} \int \frac{\mathrm{d}\omega_{23}}{2\pi} \int \frac{\mathrm{d}^3 p\, M}{(2\pi)^3 2\,\omega_{\mathbf{p}}^2} \\ &\times f_{\mathrm{F}}(\omega_{\mathbf{p}}) f_{\mathrm{F}}(\omega_{21}) f_{\mathrm{F}}(-\omega_{23}) \cos(\omega_{\mathbf{p}} y_{13}) \exp\left\{-\Gamma_{\mathbf{p}}\frac{t_1+t_3}{2}\right\} \\ &\times \big(\cos(\omega_{21}y_{21})\cos(\omega_{23}y_{23})\cosh(\beta\omega_{23}) + \sin(\omega_{21}y_{21})\sin(\omega_{23}y_{23})\sinh(\beta\omega_{23})\big) \\ &\times \frac{\mathcal{F}(p_\parallel,\omega_{21})\mathcal{F}(p_\parallel,\omega_{23})}{\omega_{21}^2\omega_{23}^2(p_\parallel-\omega_{21})(p_\parallel-\omega_{23})} \operatorname{Im} c_2(\omega_{21},\omega_{\mathbf{p}},\mathbf{p}) \operatorname{Im} c_2(\omega_{23},\omega_{\mathbf{p}},\mathbf{p}) \,. \end{aligned} \tag{7.20}$$

This expression is the first complete result for the lepton number matrix including systematically all gauge interactions up to one-loop order. As already mentioned the coefficients $\operatorname{Im} c_2(\omega_{21},\omega_{\mathbf{p}},\mathbf{p})$ and $\operatorname{Im} c_2(\omega_{23},\omega_{\mathbf{p}},\mathbf{p})$ are only numerically available, one has to continue with a numerical analysis. For the eight-dimensional integral, that needs to be solved, a Monte Carlo integration routine like the one used for obtaining the results in chap. 6 (cf. app. B.2.5) appears to be useful. However, since the integrand has to be evaluated for each point the integration routine needs, both coefficients $\operatorname{Im} c_2$ need to be calculated. This corresponds to solving the related ordinary differential equation twice, which means a great computational effort. Thus the full numerical evaluation of the lepton number matrix is yet beyond reach and needs much more considerations.

8 Conclusions and research perspectives

I may not have gone where I intended to go,
but I think I have ended up where I needed to be.
Douglas Adams

Conclusions

This thesis provides the first approach of a systematic inclusion of gauge corrections to leading order to the ansatz of thermal leptogenesis. We have derived a complete expression for the integrated lepton number matrix including all resummations needed. For this purpose, a new class of diagram has been invented, namely the cylindrical diagram, which allows diverse investigations into the topic of leptogenesis such as the case of resonant leptogenesis.

After a brief introduction of the topic of the baryon asymmetry in the universe and a discussion of its most promising solutions as well as their advantages and disadvantages, we have presented our framework of thermal leptogenesis. An effective model was described as well as the associated Feynman rules. The basis for using nonequilibrium quantum field theory has been built in chapter 3. At first, the main definitions have been presented for equilibrium thermal field theory, afterwards we have discussed the Kadanoff-Baym equations for systems out of equilibrium using the example of the Majorana neutrino. The equations have also been solved in the context of leptogenesis in chapter 4. Since gauge corrections play a crucial role throughout this thesis, we have also repeated the naive ansatz by replacing the free equilibrium propagator by propagators including thermal damping rates due to the Standard Model damping widths for lepton and Higgs fields. It is shown that this leads to a comparable result to the solutions of the Boltzmann equations for thermal leptogenesis. Thus it becomes obvious that Standard Model corrections are not negligible for thermal leptogenesis and therefore need to be included systematically from first principles.

In order to achieve this we have started discussing the calculation of ladder rung diagrams for Majorana neutrinos using the HTL and the CTL approach in chapter 5. All gauge corrections are included in this framework and thus it has become the basis for the following considerations. Furthermore, we have computed the Majorana neutrino production rate itself in chapter 6 to test our numerical procedure. In this context we have reproduced and extended the results of Anisimov, Besak and Bödeker [17] by calculating the tree-level result as well as the gauge corrected result for the Majorana neutrino production rate. As can be seen by comparison our numerical algorithm works correctly since the results coincide.

Finally in chapter 7, we have implemented the Majorana neutrino ladder rung diagram into our setup for leptogenesis: As a first consideration, we have collected all gauge corrected diagrams up to three-loop order for the asymmetry-causing two-loop diagrams. However, the results of chap. 5 showed that it is not sufficient to just include diagrams

up to three-loop level. Due to the necessity of resumming all n-loop diagrams, we have constructed a cylindrical diagram that fulfils this condition. This diagram is the link between the Majorana neutrino ladder rung diagram calculated before on the one hand and the lepton asymmetry on the other. Therefore we have been able to derive a complete expression for the integrated lepton number matrix including all leading order corrections by plugging in the results of chapter 6 into the analytic expression of Buchmüller et al. [16]. The numerical analysis of this lepton number matrix needs a great computational effort since for the resulting eight-dimensional integral two ordinary differential equations have to be computed for each point the routine evaluates. Thus the result remains yet inaccessible.

Research perspectives

Summarising, this thesis provides the basis for a systematic inclusion of gauge interactions in thermal leptogenesis scenarios. As a next step, one should evaluate the expression for the integrated lepton number numerically to gain a value, which can be used for comparison to earlier results such as the solutions of the Boltzmann equations as well as the Kadanoff-Baym ansatz with the implemented Standard Model widths. This numerical result would be the first quantitative number, which contains leading order corrections due to *all* interactions of the Majorana neutrino with the Standard Model particles. Further corrections by means of including washout effects and the Hubble expansion are expected to be reasonably small.

Furthermore, it is very interesting to apply this result to the case of resonant leptogenesis [126–128]. This is the scenario where there is degeneracy or quasi-degeneracy of the Majorana masses, thus none of the heavy neutrino masses can be integrated out. By using the versatile cylindrical diagram first described in this thesis, it is not far to seek that this case can be considered easily.

For the sake of completeness one has to mention that it is also possible to give constraints of the gravitino production [129,130] and, thus, to test supersymmetric theories. If the lightest superparticle is the gravitino, which can be a dominant component of dark matter [131, 132], also supergravity might be tested at the LHC in the near future.

A Conventions and Feynman rules

Many errors, of a truth, consist merely in the application of the wrong names of things.
Baruch Spinoza

A.1 Conventions

A.1.1 Natural units

In this thesis, natural units are used, i. e.

$$\hbar = c = k_\mathrm{B} = 1\,. \tag{A.1}$$

A conversion to other systems of unit e. g. to the standard SI-system can be achieved by [25]

$$\hbar = 1.054\,571\,628\,(53)\ \cdot 10^{-34}\mathrm{J\,s} \tag{A.2a}$$
$$c = 299\,792\,458\,\mathrm{m/s} \tag{A.2b}$$
$$k = 8.617\,343\,(15) \cdot 10^{-5}\,\mathrm{eV/K}. \tag{A.2c}$$

For the calculation forth and back multiplying with

$$\hbar c = 197.326\,963\,1(49)\,\mathrm{MeV\,fm} \tag{A.3}$$

is useful.

A.1.2 Metric

We use the Minkowski metric

$$g_{\mu\nu} = \mathrm{diag}\{1, -1, -1, -1\} \tag{A.4}$$

and the four-vectors

$$x_\mu = g_{\mu\nu} x^\nu = (x_0, -x_1, -x_2, -x_3)\,, \tag{A.5}$$

with the scalar product

$$x \cdot y = x^\mu y_\mu = x_0 y_0 - \mathbf{x}\mathbf{y}\,. \tag{A.6}$$

The Einstein convention, i. e. summation over equal greek indices, is always used unless stated elsewise. For on-shell particles with momentum k_μ we then have $k^2 = m^2$. Going to imaginary times $k^0 = \mathrm{i}\omega_n$, we find discrete Matsubara frequencies

$$\omega_n = \begin{cases} \frac{2n\pi}{\beta}\,, & \text{for Bosons} \\ \frac{(2n+1)\pi}{\beta}\,, & \text{for Fermions,} \end{cases} \tag{A.7}$$

with β the inverse temperature and $n \in \mathbb{N}$.

A.1.3 Lightcone coordinates

In this thesis lightcone coordinates are frequently used. Therefore a light-like four-vector $v \equiv (1, \mathbf{v})$, $\mathbf{v}^2 = 1$ is eminent. Then we can define the parallel component of a vector k according to $k_\parallel \equiv \mathbf{kv}$, while the 2-momentum perpendicular to $\mathbf{v}$ is denoted by $\mathbf{k}_\perp$. Thus we can rewrite

$$k = (k_0, k_1, k_2, k_3) = (k_0, \mathbf{k}_\perp, k_\parallel) \equiv (k_+, k_-, \mathbf{k}_\perp) \tag{A.8}$$

with $k_+ = k_0 + k_\parallel$ and $k_- = k_0 - k_\parallel$. The scalar product becomes $k^2 = k_+ k_- - \mathbf{k}_\perp^2$ and the measure remains $\mathrm{d}^4k \sim \mathrm{d}k_+ \mathrm{d}k_- \mathrm{d}^k_\perp$.

A.1.4 Gamma matrices

The gamma matrices are a matrix representation of a Clifford algebra. They fulfil the anticommutator relation

$$\{\gamma^\mu, \gamma^\nu\} = 2g^{\mu\nu} \mathbb{1}_4 \tag{A.9}$$

in Minkowski space. The normalization is defined as

$$(\gamma^\mu)^\dagger = \gamma^0 \gamma^\mu \gamma^0 \tag{A.10}$$

and the matrices obey varies identities and trace identities such as

$$\gamma^\mu \gamma_\mu = 4 \cdot \mathbb{1}_4 \,, \qquad \mathrm{Tr}(\gamma^\mu) = 0 \,. \tag{A.11}$$

For more identities consult [133, Appendix A].

Normally the gamma matrices are given in the Dirac basis for an easy way of acting on Dirac spinors. There they are defined according to

$$\gamma^0 = \begin{pmatrix} \mathbb{1}_2 & 0 \\ 0 & \mathbb{1}_2 \end{pmatrix} , \qquad \gamma^k = \begin{pmatrix} 0 & \sigma^k \\ -\sigma^k & 0 \end{pmatrix} , \qquad \gamma^5 = \mathrm{i}\gamma^0\gamma^1\gamma^2\gamma^3 = \begin{pmatrix} 0 & \mathbb{1}_2 \\ \mathbb{1}_2 & 0 \end{pmatrix} , \tag{A.12}$$

with the Pauli matrices

$$\sigma^1 = \begin{pmatrix} 0 & 1 \\ 1 & 0 \end{pmatrix} , \qquad \sigma^2 = \begin{pmatrix} 0 & -\mathrm{i} \\ \mathrm{i} & 0 \end{pmatrix} , \qquad \sigma^3 = \begin{pmatrix} 1 & 0 \\ 0 & -1 \end{pmatrix} . \tag{A.13}$$

Since for this thesis mainly the chiral basis is applied, we use the Weyl representation for gamma matrices, where γ^k stays equal but γ^0 changes and thus does γ^5:

$$\gamma^0 = \begin{pmatrix} 0 & \mathbb{1}_2 \\ \mathbb{1}_2 & 0 \end{pmatrix} \quad \text{and} \quad \gamma^5 = \begin{pmatrix} -\mathbb{1}_2 & 0 \\ 0 & \mathbb{1}_2 \end{pmatrix} . \tag{A.14}$$

Then the chrial projectors simply become

$$P_L \psi = \frac{1}{2}(1 - \gamma^5)\psi = \psi_L \,, \qquad P_R \psi = \frac{1}{2}(1 + \gamma^5)\psi = \psi_R \,, \tag{A.15}$$

with the two-component Weyl spinor $\psi = (\psi_L, \psi_R)$.

Furthermore the charge conjugation matrix is given by $C = \mathrm{i}\gamma_2\gamma_0$.

A.2 Feynman rules

For a summary, all in this thesis used Feynman rules are listed here. We only present the spectral and statistical propagators, since the others can be calculated using the relations between the propagators (3.17). As an application we calculate the asymmetry-causing diagrams in A.2.2. The derivation of the resummed propagators (HTL/CTL) is also presented in A.2.3.

A.2.1 Effective theory

From the Lagrangian of the effective theory eq. (2.32) we can derive the following Feynman rules for propagators and vertices [16]:

- Majorana neutrino propagator:

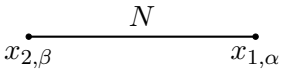

$\mathrm{i}\, G_{\alpha\beta}(x_1, x_2)$

- Lepton propagator:

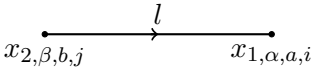

$\mathrm{i}\, \delta_{ij}\, \delta_{ab}\, S_{\alpha\beta}(x_1, x_2)$

- Scalar propagator:

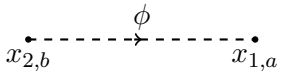

$\mathrm{i}\, \delta_{ab}\, \Delta(x_1, x_2)$

- Majorana-lepton-scalar-vertices:

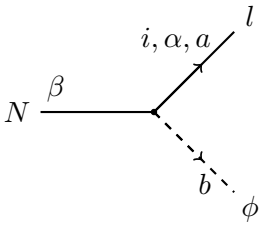

$\mathrm{i}\, \lambda^*_{i1} \epsilon_{ab} (P_R)_{\alpha\beta}$

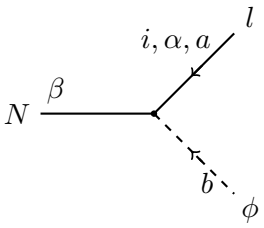

$\mathrm{i}\, \lambda_{i1} \epsilon_{ab} (C P_L)_{\beta\alpha}$

- Lepton-lepton-scalar-scalar-vertices:

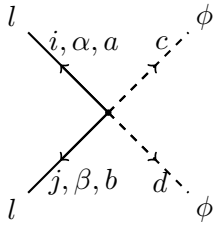

$\mathrm{i}\, \eta^*_{ij} (\epsilon_{ac}\epsilon_{bd} + \epsilon_{ad}\epsilon_{bc}) (P_R C)_{\alpha\beta}$

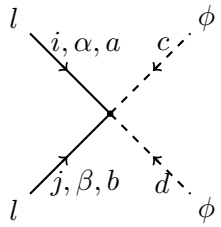

$$\mathrm{i}\,\eta_{ij}(\epsilon_{ac}\epsilon_{bd}+\epsilon_{ad}\epsilon_{bc})(CP_L)_{\alpha\beta}$$

The Levi-Civita tensor in 2 dimensions is denoted by ϵ_{ab} and the propagators are defined in the following:

- Free propagators for scalars and leptons:

$$\begin{aligned}
\Delta^-_{\mathbf{q}}(y) &= \frac{1}{\omega_{\mathbf{q}}}\sin(\omega_{\mathbf{q}}y)\,,\\
\Delta^+_{\mathbf{q}}(y) &= \frac{1}{2\omega_{\mathbf{q}}}\coth\left(\frac{\beta\omega_{\mathbf{q}}}{2}\right)\cos(\omega_{\mathbf{q}}y)\,,\\
S^-_{\mathbf{k}}(y) &= \mathrm{i}\,\gamma_0\cos(\omega_{\mathbf{k}}y)+\frac{M-\mathbf{k}\boldsymbol{\gamma}}{\omega_{\mathbf{k}}}\sin(\omega_{\mathbf{k}}y)\,,\\
S^+_{\mathbf{k}}(y) &= -\frac{1}{2}\tanh\left(\frac{\beta\omega_{\mathbf{k}}}{2}\right)\left(\mathrm{i}\gamma_0\sin(\omega_{\mathbf{k}}y)-\frac{M-\mathbf{k}\boldsymbol{\gamma}}{\omega_{\mathbf{k}}}\cos(\omega_{\mathbf{k}}y)\right)\,,
\end{aligned}$$

  with the dispersion relation $\omega^2_{\mathbf{q}} = \mathbf{q}^2 + M^2$ and analogue for the lepton with momentum $\mathbf{k}$.

  For getting the equilibrium versions of the propagators multiply the listed ones with $\mathrm{e}^{-\Gamma_{\mathbf{q}}|y|/2}$, where $\mathbf{q}$ is the corresponding momentum of the propagator. For the Majorana neutrino propagator, one has to multiply with C^{-1} from the right to the lepton propagators $S^{\pm}$ in the free and the equilibrium cases as well.

- Non-equilibrium Majorana neutrino propagators:

$$\begin{aligned}
G^-_{\mathbf{p}}(y) &= \left(\mathrm{i}\gamma_0\cos(\omega_{\mathbf{p}}y)-\frac{M-\mathbf{p}\boldsymbol{\gamma}}{\omega_{\mathbf{p}}}\sin(\omega_{\mathbf{p}}y)\right)\mathrm{e}^{-\Gamma_{\mathbf{p}}|y|/2}C^{-1}\,,\\
G^+_{\mathbf{p}}(y) &= -\left(\mathrm{i}\gamma_0\sin(\omega_{\mathbf{p}}y)-\frac{M-\mathbf{p}\boldsymbol{\gamma}}{\omega_{\mathbf{p}}}\cos(\omega_{\mathbf{p}}y)\right)\\
&\quad\times\left[\frac{1}{2}\tanh\left(\frac{\beta\omega_{\mathbf{p}}}{2}\right)\mathrm{e}^{-\Gamma_{\mathbf{p}}|y|/2}+f^{\mathrm{eq}}_N(\omega_{\mathbf{p}})\mathrm{e}^{-\Gamma_{\mathbf{p}}t}\right]C^{-1}\,.
\end{aligned}$$

  with the dispersion relation $\omega^2_{\mathbf{p}} = \mathbf{p}^2 + M^2$ and the sum of decay and inverse decay width

$$\Gamma_{\mathbf{p}} \equiv \Gamma_{\mathbf{p}}(\omega_{\mathbf{p}}) = (\lambda^\dagger\lambda)_{11}\frac{2}{\omega_{\mathbf{p}}}\int_{\mathbf{q},\mathbf{k}} p\cdot k\, f_{l\phi}(k,q)(2\pi)^4\delta^4(p-k-q)$$

  and momentum integration $\int_{\mathbf{p}} = \int \mathrm{d}^3p/((2\pi)^3\,2\,\omega_{\mathbf{p}})$.

A.2.2 Calculation of the asymmetry-causing diagrams

In this section we explicitly calculate one of the Feynman diagrams that cause the lepton asymmetry, namely the one in fig. A.1.

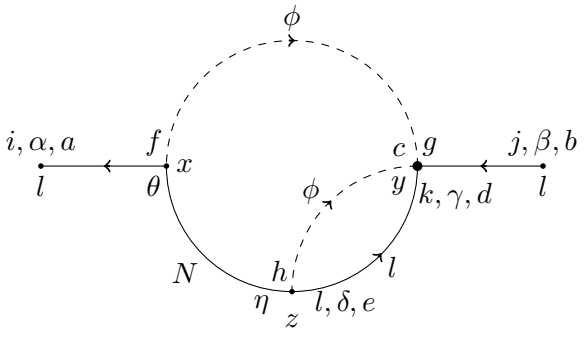

Figure A.1: Two-loop contribution to the lepton self-energy.

Using the above-listed Feynman rules we obtain:

$$\begin{aligned}\Pi_{ij}^{ab}(x,y) = -\frac{1}{2}\int \mathrm{d}^4 z\, (\mathrm{i}\lambda_{i1}^* \epsilon_{af} (P_R)_{\alpha\theta})\, (\mathrm{i}G_{\eta\theta}(z,x))\, (\mathrm{i}\lambda_{l1}^* \epsilon_{eh} (P_R)_{\delta\eta})\, (\mathrm{i}\delta_{lk}\delta_{de} S_{\gamma\delta}(y,z)) \\ \times (\mathrm{i}\eta_{kj}[\epsilon_{dc}\epsilon_{bg} + \epsilon_{bc}\epsilon_{dg}](CP_L)_{\gamma\beta})(\mathrm{i}\delta_{ch}\Delta(y,z))(\mathrm{i}\delta_{gf}\Delta(y,x)) \\ = \frac{\mathrm{i}}{2}\int \mathrm{d}^4 z\, \epsilon_{ag}\epsilon_{ec}[\epsilon_{ec}\epsilon_{bg} + \epsilon_{bc}\epsilon_{eg}]\lambda_{i1}^*\lambda_{k1}^*\eta_{kj} P_R G^T(z,x) P_R^T S^T(y,z)(CP_L)\Delta(y,z)\Delta(y,x),\end{aligned} \tag{A.16}$$

where in the second line we made use of the Kronecker deltas and rewrote everything in matrix form. With the definition of η_{kj}, the properties of the Levi-Civita tensor

$$\epsilon_{ac}\epsilon_{bc} = \delta_{ab} \tag{A.17a}$$

$$\epsilon_{ab}\epsilon_{cd} = \delta_{ac}\delta_{bd} - \delta_{ad}\delta_{bc}\,, \tag{A.17b}$$

the properties of the projection operators

$$P_L^T C = C P_L\,, \qquad P_R^T C = C P_R \tag{A.18}$$

and the properties of the propagators

$$G^T(z,x) = -G(x,z)\,, \qquad S^T C = -CS \quad (\text{for } m_l = 0)\,, \tag{A.19}$$

we receive

$$\Pi_{ij}^{ab}(x,y) = \frac{3\mathrm{i}}{2}\delta^{ab}\sum_{k,m}\int \mathrm{d}^4 z \frac{1}{M_m}\lambda_{i1}^*\lambda_{k1}^*\lambda_{km}\lambda_{mj}^T P_R G(x,z) C P_R S(y,z) P_L \Delta(y,z)\Delta(y,x)\,. \tag{A.20}$$

One can show that only the scalar part of the Majorana neutrino propagator contributes here since starting from the general form of the propagator

$$G \sim (T_{\mu\nu}\sigma^{\mu\nu} + V_\mu\gamma^\mu + S)\, C^{-1}\,, \tag{A.21}$$

we can see that there is no tensor part $T_{\mu\nu}$ for our propagator (cf. last section), but only a vector part V_μ and a scalar one S. For the remaining parts one finds

$$P_R\,(V_\mu\gamma^\mu + S)\, C^{-1} C P_R = S P_R \equiv \widetilde{G} P_R\,, \tag{A.22}$$

with $\widetilde{G}$ the scalar part of the Majorana neutrino propagator. Now we can define some abbreviations

$$\lambda_{ij}^{ab} \equiv -\frac{3\mathrm{i}}{2}\delta^{ab}\sum_{k,m}\lambda_{i1}^{*}\lambda_{k1}^{*}\lambda_{km}\lambda_{mj}^{T} \tag{A.23}$$

and $\mathrm{d}Z \equiv \mathrm{d}t_z\mathrm{d}\mathbf{z}$ and we can perform a Fourier transform which leads to a δ-function. Performing one of the momentum integrations with it yields

$$\begin{aligned}\Pi_{ij}^{ab}(x,y) = \mathrm{i}\lambda_{ij}^{ab}\int \mathrm{d}t_z \frac{\mathrm{d}^3q}{(2\pi)^3}\frac{\mathrm{d}^3q'}{(2\pi)^3}\frac{\mathrm{d}^3p}{(2\pi)^3}\mathrm{e}^{\mathrm{i}(\mathbf{p}-\mathbf{q})(\mathbf{y}-\mathbf{x})}\widetilde{G}_{\mathbf{p}}(t_x,t_z)P_R S_{-(\mathbf{p}+\mathbf{q}')}(t_y-t_z)\\ \times P_L\Delta_{\mathbf{q}'}(t_y-t_z)\Delta_{\mathbf{q}}(t_y-t_x)\,.\end{aligned} \tag{A.24}$$

Performing now a Fourier transform of the whole self-energy with the external momentum $\mathbf{k} = \mathbf{p} - \mathbf{q}$ then leads to

$$\begin{aligned}\Pi_{\mathbf{k}ij}^{ab}(t_x,t_y) &= \int \mathrm{d}^3[y-x]\mathrm{e}^{\mathrm{i}\mathbf{k}(\mathbf{y}-\mathbf{x})}\Pi_{ij}^{ab}(x,y)\\ &= \mathrm{i}\lambda_{ij}^{ab}\int \mathrm{d}t_z\frac{\mathrm{d}^3q}{(2\pi)^3}\frac{\mathrm{d}^3q'}{(2\pi)^3}\frac{\mathrm{d}^3p}{(2\pi)^3}\mathrm{d}^3[y-x]\mathrm{e}^{(\mathbf{k}+\mathbf{p}-\mathbf{q})(\mathbf{y}-\mathbf{x})}\widetilde{G}_{\mathbf{p}}(t_x,t_z)\\ &\quad\times S_{-(\mathbf{p}+\mathbf{q}')}(t_y-t_z)P_L\Delta_{\mathbf{q}'}(t_y-t_z)\Delta_{\mathbf{q}}(t_y-t_x)\,.\end{aligned} \tag{A.25}$$

We again develop a δ-function for the $\mathrm{d}^3[y-x]$-integration. Performing the integration over $\mathbf{q} = \mathbf{p} + \mathbf{k}$ then results in

$$\begin{aligned}\Pi_{\mathbf{k}ij}^{ab}(t_x,t_y) = \mathrm{i}\lambda_{ij}^{ab}\int \mathrm{d}t_z\frac{\mathrm{d}^3q'}{(2\pi)^3}\frac{\mathrm{d}^3p}{(2\pi)^3}\widetilde{G}_{\mathbf{p}}(t_x,t_z)S_{-(\mathbf{p}+\mathbf{q}')}(t_y-t_z)\\ \times P_L\Delta_{\mathbf{q}'}(t_y-t_z)\Delta_{\mathbf{p}+\mathbf{k}}(t_y-t_x)\,.\end{aligned} \tag{A.26}$$

The last step missing remains the inclusion of the Keldysh contour. Since we are only interested in the terms for $\Pi_{\mathbf{k}ij}^{ab\gtrless}(t_x,t_y)$ (cf. eq. (4.11)), we can restrict our considerations to the diagrams with two different kinds of outer vertices:

$\Pi^{>}$ =

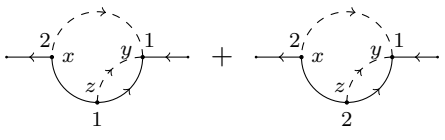

$\Pi^{<}$ =

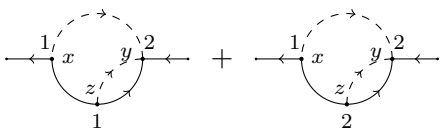

.

So we can read off the contributions for the self-energy

$$\Pi^{ab\,>}_{\mathbf{k}ij}(t_x,t_y) = \mathrm{i}\lambda^{ab}_{ij}\int \mathrm{d}t_z \frac{\mathrm{d}^3q'}{(2\pi)^3}\frac{\mathrm{d}^3p}{(2\pi)^3} \tag{A.27a}$$
$$\times\Big\{\widetilde{G}^{>}_{\mathbf{p}}(t_x,t_z)S^{11}_{-(\mathbf{p}+\mathbf{q}')}(t_y-t_z)P_L\Delta^{11}_{\mathbf{q}'}(t_y-t_z)\Delta^{<}_{\mathbf{p}+\mathbf{k}}(t_y-t_x)$$
$$-\widetilde{G}^{22}_{\mathbf{p}}(t_x,t_z)S^{<}_{-(\mathbf{p}+\mathbf{q}')}(t_y-t_z)P_L\Delta^{<}_{\mathbf{q}'}(t_y-t_z)\Delta^{<}_{\mathbf{p}+\mathbf{k}}(t_y-t_x)\Big\}$$
$$\Pi^{ab\,<}_{\mathbf{k}ij}(t_x,t_y) = \mathrm{i}\lambda^{ab}_{ij}\int \mathrm{d}t_z \frac{\mathrm{d}^3q'}{(2\pi)^3}\frac{\mathrm{d}^3p}{(2\pi)^3} \tag{A.27b}$$
$$\times\Big\{\widetilde{G}^{11}_{\mathbf{p}}(t_x,t_z)S^{>}_{-(\mathbf{p}+\mathbf{q}')}(t_y-t_z)P_L\Delta^{>}_{\mathbf{q}'}(t_y-t_z)\Delta^{>}_{\mathbf{p}+\mathbf{k}}(t_y-t_x)$$
$$-\widetilde{G}^{<}_{\mathbf{p}}(t_x,t_z)S^{22}_{-(\mathbf{p}+\mathbf{q}')}(t_y-t_z)P_L\Delta^{22}_{\mathbf{q}'}(t_y-t_z)\Delta^{>}_{\mathbf{p}+\mathbf{k}}(t_y-t_x)\Big\}\,.$$

The result for the second diagram, i. e. the mirrored version of fig. A.1, can be obtained in exactly the same way. Since it is sufficient to know the contribution of one diagram (cf. (4.15)), it is not listed here.

A.2.3 HTL and CTL Propagators

In this appendix we derive the finite temperature propagators both for soft (HTL) as well as for hard and light-like (CTL) external momenta including all one-loop contributions. Therefore we can display the results for the thermal and asymptotic masses.

Scalar propagator

The resummed scalar propagator is defined as

$$\Delta(k) = \frac{-1}{k^2-\Pi(k_0,\mathbf{k})}\,, \tag{A.28}$$

including the self-energy $\Pi(k_0,\mathbf{k})$. At one-loop level, we can determine the resummed propagator by adding the following contributions of the Higgs self-energy:

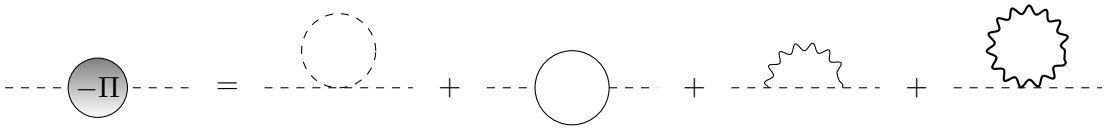

which are computed in the following.

(a) Higgs self-coupling: With outer momentum k and loop momentum q it is

$$-\Pi_\phi(k_0,\mathbf{k}) = 6\Lambda T\sum_{q_0}\int\frac{\mathrm{d}^3q}{(2\pi)^3}\Delta(q) \tag{A.29}$$

with Higgs self-coupling Λ. The factor 6 arises due to multiplicity. The massless propagator[1] $\Delta(q) = -(q_0^2-q^2)^{-1}$ has poles for $q_0 = \pm q$ so that we can evaluate

[1] This is a valid approximation as long as $m \sim \mathcal{O}(gT)$ is a thermal mass since we neglect terms of $\mathcal{O}(m/T)$.

the Matsubara sum:

$$T\sum_{q_0=\mathrm{i}\omega_n}\Delta(q_0)=\int_C\frac{\mathrm{d}q_0}{2\pi\mathrm{i}}\left(\frac{1}{2}+f_\mathrm{B}(q_0)\right)\Delta(q_0)=-\left(1+2f_\mathrm{B}(q)\right)\frac{1}{2q}\,. \tag{A.30}$$

Plugging this into the expression for the self-energy yields

$$-\Pi_\phi(k_0,\mathbf{k})=-6\Lambda\int\frac{\mathrm{d}^3q}{(2\pi)^3}\frac{1+2f_\mathrm{B}}{2q}\quad\rightarrow\quad-6\Lambda\int\frac{\mathrm{d}^3q}{(2\pi)^3}\frac{2f_\mathrm{B}}{2q}\,, \tag{A.31}$$

where in the last step we omitted the temperature independent term due to renormalization. Now we can finish the calculation with

$$-\Pi_\phi(k_0,\mathbf{k})=-\frac{3\Lambda}{\pi^2}\int_0^\infty\mathrm{d}q\frac{q}{\mathrm{e}^{\beta q}-1}=-\frac{\Lambda}{2}T^2\,. \tag{A.32}$$

This result stays the same for both the HTL and the CTL resummation scheme.

(b) Fermion loop: Therefore, we find for outer momentum k and loop momentum q:

$$-\Pi_f(k_0,\mathbf{k})=-\lambda_f^2N_\mathrm{c,f}T\sum_{\widetilde{q_0}}\int\frac{\mathrm{d}^3q}{(2\pi)^3}\,\mathrm{Tr}\left[P_L\not{q}(\not{q}-\not{k})\right]\Delta(q)\Delta(q-k)\,, \tag{A.33}$$

with the minus occuring due to the closed fermion loop, N_c numbers of colours and N_f numbers of flavours. The $\widetilde{q_0}$ are the fermionic Matsubara modes, i. e. $\widetilde{\omega}_n=2\pi(n+\frac{1}{2})T$. Computing the trace with the properties of the gamma matrices, we get $\mathrm{Tr}[P_L\not{q}(\not{q}-\not{k})]=q^2+(q-k)^2-k^2$, which leads us to

$$-\Pi_f(k_0,\mathbf{k})=-\lambda_f^2N_\mathrm{c,f}T\sum_{\widetilde{q_0}}\int\frac{\mathrm{d}^3q}{(2\pi)^3}\left(\Delta(q-k)+\Delta(q)-k^2\Delta(q)\Delta(q-k)\right)\,. \tag{A.34}$$

Neglecting the hard and light-like external momentum $k^2\sim\mathcal{O}(g^2T^2)$ yields

$$-\Pi_f(k_0,\mathbf{k})=-\lambda_f^2N_\mathrm{c,f}T\sum_{\widetilde{q_0}}\int\frac{\mathrm{d}^3q}{(2\pi)^3}\left(\Delta(q-k)+\Delta(q)\right)=-\frac{\lambda_f^2N_\mathrm{c,f}}{12}T^2\,, \tag{A.35}$$

since the evaluation of the fermionic Matsubara sum leads to a factor -2.

For the HTL ansatz, the computation of the trace would have given a factor $2q^2$, since k is soft then. Nevertheless one obtains the same result as in the CTL resummation scheme after evaluating the Matsubara sum.

(c) Gauge boson contributions: For these two diagrams we obtain with again outer momentum k and loop momentum q:

$$-\Pi_{G_r}(k_0,\mathbf{k})=g_r^2\,t_r^a\,t_r^b\,T\sum_{q_0}\int\frac{\mathrm{d}^3q}{(2\pi)^3}\Big[(2k-q)^\mu\Delta^{ab}_{\mu\nu}(q)(2k-q)^\nu\Delta(k-q)+\frac{1}{2}(-2g^{\mu\nu})\Delta^{ab}_{\mu\nu}(q)\Big]\,, \tag{A.36}$$

with the gauge boson propagator $\Delta^{ab}_{\mu\nu}(q) = -g_{\mu\nu}\delta^{ab}\Delta(q)$ and the indices $r = \mathrm{w}, \mathrm{Y}$ representing SU(2) or U(1) gauge bosons, respectively. Hence we can also use the Casimir operator $C_2(r) = t^a_r\, t^b_r\, \delta^{ab}$ and apply for the momenta $(2k-q)^2 = 2k^2 - q^2 + 2(k-q)^2$, so that again k^2 can be omitted in the hard and light-like approach:

$$-\Pi_{G_r}(k_0, \mathbf{k}) = g_r^2 C_2(r) T \sum_{q_0} \int \frac{\mathrm{d}^3 q}{(2\pi)^3} \left[2\Delta(q) + \Delta(k-q)\right] = -\frac{g_r^2 C_2(r)}{4} T^2 \,. \tag{A.37}$$

For soft external momenta it is $(2k-q)^2 \sim q^2$ so that we again obtain the same result for both schemes.

Fermion propagator

For the resummed fermion propagator, we start with the definition

$$S(p) = \frac{-1}{\not{p} - \Sigma(p_0, \mathbf{p})} \,, \tag{A.38}$$

and we again consider only one-loop contributions to the self-energy, that we display in the common so-called plasma rest frame using the four-velocity $u^\mu = (1, \mathbf{0})$:

$$\begin{aligned} \Sigma(p_0, \mathbf{p}) &= \tilde{a}(p_0, \mathbf{p})\not{p} + \tilde{b}(p_0, \mathbf{p})\not{u} \\ &= \tilde{a}(p_0, \mathbf{p})\not{p} + \tilde{b}(p_0, \mathbf{p})\gamma^0 \,. \end{aligned} \tag{A.39}$$

With this notation we can rewrite the propagator up to one-loop order according to

$$S(p) = \frac{-(1 - \tilde{a}(p_0, \mathbf{p}))\not{p} + \tilde{b}(p_0, \mathbf{p})\gamma^0}{(1 - \tilde{a}(p_0, \mathbf{p}))^2 p^2 + \tilde{b}^2(p_0, \mathbf{p}) - 2\tilde{b}(p_0, \mathbf{p})(1 - \tilde{a}(p_0, \mathbf{p}))p^0} \,. \tag{A.40}$$

Applying now hard and light-like momenta, we can read of the behaviour $\tilde{a} \sim g^2 \ll 1$ and $\tilde{b} \sim g^2 T$, since $\Sigma \sim g^2 T$. Hence we can neglect terms proportional to $\tilde{a}$ and $\tilde{b}^2$. Using now the discussion in sec. 5.3.1, i. e. the definition of the asymptotic thermal mass and the vanishing thermal width in this case, we find $\tilde{b}$ to be real

$$\tilde{b}(p_0, \mathbf{p}) \simeq \frac{m_\infty^2}{2p^0} \,. \tag{A.41}$$

Therefore and using $p^0 \equiv p_\parallel$ we can rewrite the propagator in the CTL resummation scheme as given in eq. (5.5), namely

$$S(p) \simeq -\frac{\not{p} - \frac{m_\infty^2}{2p_0}\gamma^0}{p^2 - m_\infty^2} \,.$$

We still need to compute the asymptotic mass, i. e. the coefficient $\tilde{b}$, what can be done by calculating the following Feynman diagram:

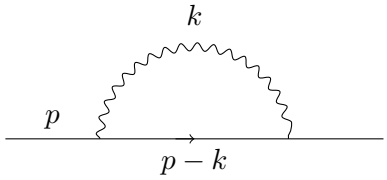

In Feynman gauge we obtain

$$-\Sigma(p) = -g_r^2 C_2(r) T \sum_{k_0} \int \frac{\mathrm{d}^3 k}{(2\pi)^3} \gamma^\mu (\not{p} - \not{k}) \gamma_\mu \Delta(p-k)\,. \tag{A.42}$$

If we now define two traces

$$T_1 \equiv \frac{1}{4} \operatorname{Tr}[\not{p} \Sigma(p_0, \mathbf{p})] \tag{A.43a}$$

$$T_2 \equiv \frac{1}{4} \operatorname{Tr}[\gamma^0 \Sigma(p_0, \mathbf{p})]\,, \tag{A.43b}$$

we find by comparing with the definitions (cf. (A.39)) for the coefficients $\tilde{a}$ and $\tilde{b}$:

$$\tilde{a}(p_0, \mathbf{p}) = -\frac{1}{\mathbf{p}^2}(T_1 - p_0 T_2) \tag{A.44a}$$

$$\tilde{b}(p_0, \mathbf{p}) = \frac{1}{\mathbf{p}^2}(p_0 T_1 - p^2 T_2)\,. \tag{A.44b}$$

So we just have to calculate the contribution of T_1 for $\tilde{b}$, since again $p^2 \sim g^2 T^2$. Using $\frac{1}{4}\operatorname{Tr}[\not{p}\gamma^\mu(\not{p} - \not{k})\gamma_\mu] = -2(p^2 - pk) = -(p^2 + (p-k)^2 - k^2)$ yields (again neglecting contributions $p^2 \sim g^2 T^2$)

$$\begin{aligned} T_1 &= -g_r^2 C_2(r) T \sum_{k_0} \int \frac{\mathrm{d}^3 k}{(2\pi)^3} (\Delta(k) - \Delta(p-k)) \\ &= -g_r^2 C_2(r) \left(-\frac{T^2}{12} - \frac{T^2}{24} \right) \\ &= \frac{g_r^2 C_2(r)}{8} T^2\,. \end{aligned} \tag{A.45}$$

The asmptotic thermal mass then becomes

$$\begin{aligned} m_{l,\infty} &= 2\, p_0\, \tilde{b}(p_0, \mathbf{p}) \\ &= 2\, \frac{p_0^2}{\mathbf{p}^2}\, T_1 \simeq \frac{g_r^2 C_2(r)}{4} T^2\,, \end{aligned} \tag{A.46}$$

with again using the CTL approximation in the second step.

Now we only have to calculate the HTL fermion propagator. Therefore the external momentum is soft so that we need to compute both contributions $\tilde{a}$ and $\tilde{b}$. The result for T_1 stays the same (cf. scalar case) and for T_2 we obtain with $\frac{1}{4}\operatorname{Tr}[\gamma^0\gamma^\mu(\not{p} - \not{k})\gamma_\mu] = -2(p^0 - k^0) \simeq 2k^0$ for soft outer momentum p:

$$T_2 = 2 g_r^2 C_2(r) T \sum_{k_0} \int \frac{\mathrm{d}^3 k}{(2\pi)^3} k^0 \Delta(k) \Delta(p-k)\,. \tag{A.47}$$

Computing the thermal sums according to the textbooks (cf. [86]) and using again the soft outer momentum we are in leading order left with

$$T_2 = 2g_r^2 C_2(r) \int \frac{\mathrm{d}^3k}{(2\pi)^3} \frac{f_\mathrm{B}(k) + f_\mathrm{F}(k)}{2k(p^0 + p\cos\theta)} = \frac{g_r^2 C_2(r)}{8p} T^2 Q_0(\tfrac{p_0}{p}) \,, \tag{A.48}$$

with the Legendre function of the second kind $Q_0(x) = \frac{1}{2}\ln\frac{x+1}{x-1}$. So we find

$$\tilde{a} = -\frac{m_{l,\mathrm{th}}^2}{p^2}(1 - xQ_0(x)) \tag{A.49a}$$

$$\tilde{b} = \frac{m_{l,\mathrm{th}}^2}{p}(x(1 - xQ_0(x)) + Q_0(x) \,, \tag{A.49b}$$

using $x = \frac{p_0}{p}$ and defining the thermal mass $m_{l,\mathrm{th}} \equiv T_1$, so that we obtain with (A.39) for the self-energy the well-known result

$$\Sigma(p_0, \mathbf{p}) = \frac{m_{l,\mathrm{th}}}{p}\Big(Q_0(x)\gamma^0 + (1 - xQ_0(x))\boldsymbol{\gamma}\hat{\mathbf{p}}\Big) \,, \tag{A.50}$$

and $\hat{\mathbf{p}}$ denotes the unit vector in $\mathbf{p}$-direction.

A.2.4 Thermal and asymptotic masses

As already discussed, the thermal and asymptotic mass are the same for the scalar propagator as can be seen in the last section $m_\phi \equiv m_{\phi,\mathrm{th}} = m_{\phi,\infty}$. We therefore have to sum up all contributions of the one-loop self-energy which leads to

$$\begin{aligned}\Pi(k_0, \mathbf{k}) &= \Pi_\phi(k_0, \mathbf{k}) + \Pi_\mathrm{w}(k_0, \mathbf{k}) + \Pi_\mathrm{Y}(k_0, \mathbf{k}) + \Pi_f(k_0, \mathbf{k}) \equiv m_\phi^2 \\ &= \left(\frac{1}{2}\Lambda^2 + \frac{3}{16}g_\mathrm{w}^2 + \frac{1}{16}g_\mathrm{Y}^2 + \frac{1}{4}\lambda_\mathrm{t}^2\right) T^2 \\ &= \frac{1}{16}\left(8\Lambda + 3g_\mathrm{w}^2 + g_\mathrm{Y}^2 + 4\lambda_\mathrm{t}^2\right) T^2 \,, \end{aligned} \tag{A.51}$$

where we used the Casimir operators in the fundamental representation

$$t_\mathrm{Y} = \frac{1}{2}\,\mathbb{1} \quad \longrightarrow \quad C_2(\mathrm{Y}) = \frac{1}{4} \,, \tag{A.52a}$$

$$t_\mathrm{w}^a = \frac{1}{2}\sigma^a \quad \longrightarrow \quad C_2(\mathrm{w}) = \frac{3}{4} \,, \tag{A.52b}$$

$N_\mathrm{c,f} = 3$ due to the number of light quark flavours and only taking into account the top quark contribution due to the weakness of the small Yukawa couplings of the other quarks.

Summarising, for the fermion propagator we find different contributions for the asymptotic and the thermal mass as seen in the last section. We obtain for the asymptotic mass

$$m_{l,\infty}^2 = \frac{1}{16}\left(3g_\mathrm{w}^2 + g_\mathrm{Y}^2\right) T^2 \,, \tag{A.53}$$

with again summing up the contributions due to SU(2) and U(1). For the thermal mass we get in total

$$m_{l,\mathrm{th}}^2 = \frac{1}{32}\left(3g_\mathrm{w}^2 + g_\mathrm{Y}^2\right) T^2 \,, \tag{A.54}$$

so that we find the two masses differ from each other by a factor $\sqrt{2}$.

A.3 Standard Model couplings

As already described in section 6.2 we used the one-loop renormalization group equations eqs. (6.4) for calculating the values of the couplings at the scale $\mu = 2\pi T_\mathrm{R}$. The calculations were done with Mathematica®[2]. We found for

- α_1 with initial condition (i. c.) $g_1^2(m_\mathrm{Z}) = 4\pi\alpha_\mathrm{em}(m_\mathrm{Z})/\cos^2\theta_\mathrm{W}(m_\mathrm{Z}) = 0.127692$:

$$g_1^2(t) = \frac{789.568}{5443.41 - 41t} \quad \Rightarrow \quad g_1^2(0) = g_\mathrm{Y}^2 = 0.14505\,,$$

  so that for the calculation $g' = g_\mathrm{Y} = 0.380855$.

- α_2 with i. c. $g_2^2(m_\mathrm{Z}) = 4\pi\alpha_\mathrm{em}(m_\mathrm{Z})/\sin^2\theta_\mathrm{W}(m_\mathrm{Z}) = 0.424705$:

$$g_2^2(t) = \frac{473.741}{1458.37 + 19t} \quad \Rightarrow \quad g_2^2(0) = g_\mathrm{w}^2 = 0.324843\,,$$

  so that for the calculation $g = g_\mathrm{w} = 0.56995$.

- α_3 with i. c. $g_3^2(m_\mathrm{Z}) = 4\pi\alpha_\mathrm{s}(m_\mathrm{Z}) = 1.48786$:

$$g_3^2(t) = \frac{78.9568}{179.405 + 7t} \quad \Rightarrow \quad g_3^2(0) = 0.440104\,,$$

  which is not needed explicitly, but for the next two calculations.

- λ_t^2 with i. c. $\lambda_\mathrm{t}^2(m_\mathrm{Z}) = 2m_\mathrm{t}^2/v^2 = 0.988494$ we only get the numerical solution:

$$\lambda_\mathrm{t}^2(0) = 0.352087\,,$$

  so that for the calculation $\lambda_\mathrm{t} = 0.593369$.

- Λ with i. c. $\Lambda(m_\mathrm{Z}) = m_\mathrm{H}^2/(2v^2) = 0.130937$ we again only get a numerical solution:

$$\Lambda(0) = \Lambda = 0.063161\,.$$

[2] http://www.wolfram.com/mathematica/

B Numerics

There is no reason for any individual
to have a computer in their home.
Ken Olsen
(president and founder of Digital, 1977)

B.1 Deriving the Majorana neutrino production rate

In the following, the derivation of eq. (5.36) is presented in detail. Starting from eq. (5.11) we can derive eq. (5.12) by using the gamma matrices in Weyl representation (cf. app. A.1.4) and applying

$$\overline{\sigma} \cdot k = \sigma_0 k_0 + \boldsymbol{\sigma}\mathbf{k}\,, \tag{B.1}$$

since $\overline{\sigma}^0 = \mathbb{1}$, $\overline{\boldsymbol{\sigma}} = -\boldsymbol{\sigma}$. Then we can rewrite (5.11) with the 2×2 matrix Σ_R after multiplying by a factor of 2.

With the expansion for a Weyl spinor in terms of the coupling

$$\eta = \eta_0 + \eta_1 + \mathcal{O}(g^2)\,, \qquad \eta_0 = \begin{pmatrix} 0 \\ 1 \end{pmatrix}\,, \qquad \eta_1 = -\frac{\boldsymbol{\sigma}\mathbf{p}_\perp}{2p_\parallel}\eta_0\,, \tag{B.2}$$

we obtain the result (5.17). If we now put this into eq. (5.22) and use an auxiliary vector $\mathbf{w} = (1, \mathrm{i})$ so that $\mathbf{w} \cdot \mathbf{f} = (f_1 + \mathrm{i}f_2)$, we are left with eq. (5.36) after applying

$$\mathcal{F}(k_\parallel, p_\parallel) \equiv f_\mathrm{F}(p_\parallel) + f_\mathrm{B}(p_\parallel - k_\parallel) = -\frac{f_\mathrm{F}(p_\parallel) f_\mathrm{B}(k_\parallel - p_\parallel)}{f_\mathrm{F}(k_\parallel)} \tag{B.3}$$

and

$$\overline{\sigma}k = \begin{pmatrix} k_0 + k_3 & k_1 - \mathrm{i}k_2 \\ k_1 + \mathrm{i}k_2 & k_0 - k_3 \end{pmatrix} \overset{\mathbf{k}_\perp = \mathbf{0}}{=} \begin{pmatrix} k_+ & 0 \\ 0 & k_- \end{pmatrix} = \begin{pmatrix} 2k_\parallel & 0 \\ 0 & \frac{M^2}{2k_\parallel} \end{pmatrix} + \mathcal{O}(g^3 T)\,. \tag{B.4}$$

In the last step, we used the approximation $k_0 \simeq k_\parallel$ since the difference is $k_- \sim g^2 T$ and the on-shell condition for the Majorana neutrino $M^2 = k_0^2 - k_\parallel^2 \simeq 2k_\parallel k_-$. Hence it is

$$\begin{aligned} \frac{\mathrm{d}\Gamma}{\mathrm{d}^3 k} &\sim \mathrm{Tr}\left[\overline{\sigma} \cdot k\, \mathrm{Im}\, \Sigma_\mathrm{R,ret}(k)\right] \\ &= -\frac{|\lambda|^2 d(r)}{2} \int \frac{\mathrm{d}^3 p}{(2\pi)^3} \frac{\mathcal{F}(k_\parallel, p_\parallel)}{p_\parallel - k_\parallel} \underbrace{\mathrm{Tr}\left[\begin{pmatrix} k_+ & 0 \\ 0 & k_- \end{pmatrix} \mathrm{Re}\left\{\eta(p)\left(-\frac{\mathbf{wf}}{2p_\parallel}, \psi\right)\right\}\right]}_{= k_+ \mathrm{Re}\left\{\mathbf{p}_\perp \mathbf{f}/(4p_\parallel^2)\right\} + k_- \mathrm{Re}\,\psi} \end{aligned} \tag{B.5}$$

and after again using $k_+ \simeq 2k_\parallel$ we recover eq. (5.36):

$$\frac{\mathrm{d}\Gamma}{\mathrm{d}^3 k} = -\frac{d(r)|\lambda|^2}{(2\pi)^3 2k} \int \frac{\mathrm{d}^3 p}{(2\pi)^3} \frac{f_\mathrm{F}(p_\parallel) f_\mathrm{B}(k - p_\parallel)}{k - p_\parallel} \mathrm{Re}\left[\frac{k}{2p_\parallel^2}\mathbf{p}_\perp \cdot \mathbf{f} + \frac{M^2}{k}\psi\right]\,.$$

B.1.1 Tree-level expression

Thus we can continue deriving the tree-level expression eq. (6.2) from the above equation. Therefore we neglect the integral terms in eq. (5.34) which yields

$$\mathbf{f}(\mathbf{p}_\perp) = \frac{2\mathbf{p}_\perp}{\mathrm{i}\epsilon(k,\mathbf{p}_\perp)} \quad \text{and} \quad \psi(\mathbf{p}_\perp) = \frac{1}{\mathrm{i}\epsilon(k,\mathbf{p}_\perp)}\,, \tag{B.6}$$

with ϵ from eq. (5.18). In the following we restrict ourselves to the case of interest $\mathbf{k}_\perp = 0$, $k^2 = M^2$ and $k_0 \sim k_\parallel$. Hence we can rewrite

$$\epsilon(k,\mathbf{p}) \equiv \alpha(p_\parallel, k_\parallel) + \beta(p_\parallel, k_\parallel)\mathbf{p}_\perp^2\,, \tag{B.7}$$

with

$$\alpha \equiv -\frac{m_l^2}{2p_\parallel} + \frac{m_\phi^2}{2(p_\parallel - k_\parallel)} + \frac{M^2}{2k_\parallel}\,, \qquad \beta \equiv \frac{k_\parallel}{2p_\parallel(p_\parallel - k_\parallel)}\,. \tag{B.8}$$

For the real part in eq. (5.36) we then obtain

$$\mathrm{Re}\left[\frac{k}{2p_\parallel^2}\mathbf{p}_\perp\cdot\mathbf{f} + \frac{M^2}{k}\psi\right] \overset{\text{tree-level}}{=} \left(\frac{k\,\mathbf{p}_\perp^2}{p_\parallel^2} + \frac{M^2}{k}\right) \underbrace{\mathrm{Im}\left[\frac{1}{\epsilon}\right]}_{=\,\pi\delta(\epsilon)}\,, \tag{B.9}$$

where the definition of the principal value is used:

$$\frac{1}{A \pm \mathrm{i}\varepsilon} \overset{\varepsilon\to 0^+}{=} \mathbb{P}\left(\frac{1}{A}\right) \mp \mathrm{i}\pi\delta(A)\,. \tag{B.10}$$

Using the property of the δ-function

$$\delta(\epsilon) = \frac{1}{|\beta|}\,\delta\!\left(\frac{\alpha}{\beta} + \mathbf{p}_\perp^2\right)\,, \tag{B.11}$$

leads to the restriction for the limits of the $p_\parallel$-integration $\mathbf{p}_\perp^2 = -\frac{\alpha}{\beta} \overset{!}{\geq} 0$ due to assuming a positive solution of $\epsilon = 0$. After applying $\mathrm{d}^2p_\perp = \pi\mathrm{d}(\mathbf{p}_\perp^2)$ we derive eq. (6.2) by simply expanding the products.

B.1.2 Domain of integration

For the limits of the integration we have to solve $\mathbf{p}_\perp^2 = -\frac{\alpha}{\beta}$ with assuming real values for $\sqrt{\mathbf{p}_\perp^2}$ due to positivity of the lepton energy :

$$\begin{aligned}
\mathbf{p}_\perp^2 &= -\frac{\alpha}{\beta} \\
&= -\frac{2p_\parallel(p_\parallel - k_\parallel)}{k_\parallel}\left(\frac{M^2}{2k_\parallel} + \frac{m_\phi^2}{2(p_\parallel - k_\parallel)} - \frac{m_l^2}{2p_\parallel}\right) \\
&= -\frac{M^2}{k_\parallel}p_\parallel^2 + \underbrace{(m_l^2 - m_\phi^2 + M^2)}_{\equiv\, X}p_\parallel - m_l^2 k_\parallel \overset{!}{\geq} 0\,.
\end{aligned} \tag{B.12}$$

The zeros of this expression are

$$p_\pm = \frac{X}{2M^2}k_\parallel \pm \frac{k_\parallel}{2M^2}\underbrace{\sqrt{X^2 - 4m_l^2M^2}}_{\equiv\sqrt{Y}}, \tag{B.13}$$

so that the constraints are

$$\frac{X-\sqrt{Y}}{2M^2}k_\parallel \leq p_\parallel \leq \frac{X+\sqrt{Y}}{2M^2}k_\parallel\,, \tag{B.14}$$

what had to be shown (cf. eq. (6.3)).

B.2 Solving the integral equations

The receipt for solving the integral equations closely follows [108,117,118]. The main steps are presented in the following.

B.2.1 From integral equations to differential equations

As a first step we transform the integral equations (5.34)

$$\begin{aligned}
\mathrm{i}\epsilon(k,\mathbf{p})\psi(\mathbf{p}_\perp) - \int \frac{\mathrm{d}^2q_\perp}{(2\pi)^2}\,\mathcal{C}(\mathbf{q}_\perp)\,[\psi(\mathbf{q}_\perp) - \psi(\mathbf{p}_\perp - \mathbf{q}_\perp)] &= 1\\
\mathrm{i}\epsilon(k,\mathbf{p})\,\mathbf{f}(\mathbf{p}_\perp) - \int \frac{\mathrm{d}^2q_\perp}{(2\pi)^2}\,\mathcal{C}(\mathbf{q}_\perp)\,[\mathbf{f}(\mathbf{q}_\perp) - \mathbf{f}(\mathbf{p}_\perp - \mathbf{q}_\perp)] &= 2\mathbf{p}_\perp
\end{aligned}$$

into differential equations that will be solved afterwards numerically. Since this procedure is analgue for both equations, we only present the elaboration for the equation for ψ and give the results for $\mathbf{f}$. Furthermore we use again $\mathbf{k}_\perp = 0$ and $k_\parallel = k = |\mathbf{k}|$. Then we can define an effective mass M_{eff} (cf. (B.45)) via

$$\epsilon(k,\mathbf{p}) = \beta(M_{\text{eff}}^2 + \mathbf{p}_\perp^2)\,, \quad \text{with} \quad M_{\text{eff}} \equiv \frac{\alpha}{\beta}\,, \tag{B.15}$$

using the definitions from eq. (B.8). We can perform a Fourier transform

$$\psi(\mathbf{p}_\perp) = \int \mathrm{d}^2b\,\mathrm{e}^{-\mathrm{i}\mathbf{p}_\perp\mathbf{b}}\psi(\mathbf{b}) \qquad \psi(\mathbf{b}) = \int \frac{\mathrm{d}^2\mathbf{p}_\perp}{(2\pi)^2}\mathrm{e}^{\mathrm{i}\mathbf{p}_\perp\mathbf{b}}\psi(\mathbf{p}_\perp)\,, \tag{B.16}$$

so that the integral over the perpendicular momentum in the production rate (5.36) simplifies in terms of the Fourier transfom for $b \to 0$ according to

$$\int \frac{\mathrm{d}^2p_\perp}{(2\pi)^2}\,\mathrm{Re}\,[\mathbf{p}_\perp\cdot\mathbf{f}(\mathbf{p}_\perp)] = \lim_{b\to 0}\mathrm{Im}\,\nabla\cdot\mathbf{f}(\mathbf{b})\,, \tag{B.17a}$$

$$\int \frac{\mathrm{d}^2p_\perp}{(2\pi)^2}\,\mathrm{Re}\,\psi(\mathbf{p}_\perp) = \lim_{b\to 0}\mathrm{Re}\,\psi(\mathbf{b})\,. \tag{B.17b}$$

The relations are proven in app. B.3.2. Now we can continue applying a representation of the δ-function

$$1 = \int \mathrm{d}^2b\,\delta^2(\mathbf{b})\,\mathrm{e}^{-\mathrm{i}\mathbf{p}_\perp\mathbf{b}} \tag{B.18}$$

as well as the relation

$$\Delta_{\mathbf{b}}\psi(\mathbf{b}) = \int \frac{\mathrm{d}^2\mathbf{p}_\perp}{(2\pi)^2}\,(-\mathbf{p}_\perp^2)\,\mathrm{e}^{-\mathrm{i}\mathbf{p}_\perp\mathbf{b}}\psi(\mathbf{p}_\perp) \tag{B.19}$$

to rewrite the integral equation as

$$-\mathrm{i}\beta(\Delta_{\mathbf{b}} - M_{\mathrm{eff}}^2)\psi(\mathbf{b}) - \underbrace{\left(\int \frac{\mathrm{d}^2\mathbf{p}_\perp}{(2\pi)^2}\mathcal{C}(\mathbf{p}_\perp) - \mathcal{C}(\mathbf{b})\right)}_{\equiv\ \mathcal{K}(b)}\psi(\mathbf{b}) = \delta^2(\mathbf{b})\,, \tag{B.20}$$

recapitulating

$$\mathcal{C}(\mathbf{q}_\perp) \equiv T\left[C_2(r)g^2\left(\frac{1}{\mathbf{q}_\perp^2} - \frac{1}{\mathbf{q}_\perp^2 + m_{\mathrm{D}}^2}\right) + y_l^2 g'^2\left(\frac{1}{\mathbf{q}_\perp^2} - \frac{1}{\mathbf{q}_\perp^2 + m_{\mathrm{D}}'^2}\right)\right] \tag{B.21}$$

and $\mathcal{C}(\mathbf{b}) = \int \mathrm{d}^2\mathbf{q}_\perp/(2\pi)^2\mathcal{C}(\mathbf{q}_\perp)\,\exp\{-\mathrm{i}\mathbf{p}_\perp\mathbf{b}\}$ the Fourier transform of the kernel. Since $\psi(\mathbf{b}) = \psi(b)$ due to rotational invariance, we can rewrite the derivative $\Delta_{\mathbf{b}} = \partial_b^2 + \frac{1}{b}\partial_b$. Thus we numerically have to solve the differential equation

$$-\mathrm{i}\beta\left(\partial_b^2 + \frac{1}{b}\partial_b - M_{\mathrm{eff}}^2\right)\psi(b) - \mathcal{K}(b)\psi(b) = 0\,. \tag{B.22}$$

For $\mathbf{f}(\mathbf{b}) = h(b)\mathbf{b}$ we obtain a similar equation using $\Delta_{\mathbf{b}}\mathbf{f}(\mathbf{b}) = \frac{3}{b}h'(b)\mathbf{b} + h''(b)\mathbf{b}$. After multiplying with one and rewriting

$$2\mathbf{p}_\perp\int \mathrm{d}^2 b\,\delta^2(\mathbf{b})\,\mathrm{e}^{+\mathrm{i}\mathbf{p}_\perp\mathbf{b}} \to -2\,\mathrm{i}\,\nabla_{\mathbf{b}}\,\delta^2(\mathbf{b})\,, \tag{B.23}$$

we get for the rhs the differential equation

$$-\mathrm{i}\beta\left(\partial_b^2 + \frac{3}{b}\partial_b - M_{\mathrm{eff}}^2\right)h(b) - \mathcal{K}(b)h(b) = 0\,. \tag{B.24}$$

These two equations will be solved in the following for $b > 0$.

Before that we only have to prove

$$\int \frac{\mathrm{d}^2\mathbf{q}_\perp}{(2\pi)^2}\mathcal{C}(\mathbf{q}_\perp) - \mathcal{C}(b) \equiv \mathcal{K}(b) = T\left[C_2(r)g^2 D(m_{\mathrm{D}}b) + y_l^2 g'^2 D(m_{\mathrm{D}}'b)\right]\,, \tag{B.25}$$

with $D(x) = \frac{1}{2\pi}(\gamma_{\mathrm{E}} + \ln\frac{x}{2} + K_0(x))$, $K_0(x)$ the modified Bessel function of second kind and $\gamma_{\mathrm{E}} = 0.57721\ldots$ the Euler-Mascheroni constant. Therefore we need to calculate the (divergent) integral

$$I(b) \equiv \int \frac{\mathrm{d}^2 q}{(2\pi)^2}\left(\frac{1}{q^2} - \frac{1}{q^2 + m^2}\right)\left(1 - \mathrm{e}^{-\mathrm{i}qb}\right)\,. \tag{B.26}$$

In dimensional regularization in $n = 2 - 2\varepsilon$ dimension (cf. [134]), we obtain

1. $$\int \frac{\mathrm{d}^n q}{(2\pi)^2}\,\frac{\mathrm{e}^{\pm\mathrm{i}qb}}{q^2} = \frac{\Gamma(\frac{n}{2} - 1)}{(4\pi)^{\frac{n}{2}}b^{n-2}} \sim \Gamma(\varepsilon)\,. \tag{B.27a}$$

2. $$\int \frac{\mathrm{d}^n q}{(2\pi)^2}\,\frac{1}{q^2} = 0\,. \tag{B.27b}$$

3. $$\int \frac{\mathrm{d}^n q}{(2\pi)^2}\,\frac{1}{q^2 + m^2} = \frac{\Gamma(1 - \frac{n}{2})}{(4\pi)^{\frac{n}{2}}m^{2-n}} \sim \Gamma(\varepsilon)\,. \tag{B.27c}$$

4. $$\int \frac{\mathrm{d}^n q}{(2\pi)^2}\,\frac{\mathrm{e}^{\pm\mathrm{i}qb}}{q^2 + m^2} = \frac{b^{1-\frac{n}{2}}}{(2\pi)^{\frac{n}{2}}}K_{\frac{n}{2}-1}(mb) \overset{n=2}{\longrightarrow} \frac{1}{2\pi}K_0(mb)\,. \tag{B.27d}$$

For a more detailed calculation of the integrals and the usa of dimensional regularization consult [135]. Considering the divergent terms (B.27a) and (B.27c) we can use the following expansions in powers of ε

$$\Gamma\left(1-\frac{n}{2}\right) = \Gamma(\varepsilon) = \frac{1}{\varepsilon} - \gamma_{\mathrm{E}} + \mathcal{O}(\varepsilon)\,, \tag{B.28}$$

$$\Gamma\left(\frac{n}{2}-1\right) = \Gamma(-\varepsilon) = -\frac{1}{\varepsilon}\Gamma(1-\varepsilon) = -\frac{1}{\varepsilon} - \gamma_{\mathrm{E}} + \mathcal{O}(\varepsilon)\,, \tag{B.29}$$

$$x^{\varepsilon} = \mathrm{e}^{\varepsilon \ln x} = 1 + \varepsilon \ln x + \mathcal{O}(\varepsilon^2) \tag{B.30}$$

and we obtain for the renormalized result, i.e. subtracting the ε poles and afterwards performing $\varepsilon \to 0$:

$$1. \;+\; 3. = \frac{\Gamma(\frac{n}{2}-1)}{(4\pi)^{\frac{n}{2}} b^{n-2}} + \frac{\Gamma(1-\frac{n}{2})}{(4\pi)^{\frac{n}{2}} m^{2-n}} \tag{B.31}$$

$$= -\frac{1}{2\pi}\left(\gamma_{\mathrm{E}} + \ln\frac{mb}{2}\right)\,. \tag{B.32}$$

so that

$$I(b) = \frac{1}{2\pi}\left(\gamma_{\mathrm{E}} + \ln\frac{mb}{2} + K_0(mb)\right)\,, \tag{B.33}$$

which leads us to the desired result when multiplying with the other factors of the kernel $\mathcal{C}$ (cf. def. (5.31)).

B.2.2 Boundary conditions

The Fourier transform gives some constraints on the limiting behaviour of the functions ψ and $\mathbf{f}$, since the functions have to fulfil

$$\lim_{b\to\infty} \psi(\mathbf{b}) = 0 \quad \text{and} \quad \lim_{b\to\infty} \mathbf{f}(\mathbf{b}) = 0\,. \tag{B.34}$$

For the limit $b \to 0$ we find $\mathcal{K}(b) \sim D(b) \sim b^2 \ln b$ so that we can neglect this term here, furthermore, only terms including derivatives are important, hence, we are left with (cf. eq. (B.20)):

$$\text{I.} \quad \Delta_{\mathbf{b}}\psi(\mathbf{b}) = \frac{\mathrm{i}}{\beta}\,\delta^2(\mathbf{b}) \tag{B.35a}$$

$$\text{II.} \quad \Delta_{\mathbf{b}}\mathbf{f}(\mathbf{b}) = \frac{2}{\beta}\nabla_{\mathbf{b}}\,\delta^2(\mathbf{b})\,. \tag{B.35b}$$

These are two Poisson equations of the form $\Delta_{\mathbf{b}}\phi(\mathbf{b}) = v(\mathbf{b})$ in two dimensions with fundamental solution

$$\phi(\mathbf{b}) = \frac{1}{2\pi}\ln|\mathbf{b}|\,. \tag{B.36}$$

The general solution is obtained by performing a convolution with the fundamental solution. Hence we obtain for the first Poisson equation (B.35a) with $\phi_1(\mathbf{b}) \equiv \psi(\mathbf{b})$ and

$v_1(\mathbf{b}) \equiv \frac{\mathrm{i}}{\beta}\,\delta^2(\mathbf{b})$:

$$\begin{aligned}(\phi_1 * v_1)(\mathbf{b}) &= \frac{\mathrm{i}}{2\pi\beta}\int \mathrm{d}^2t\,\ln|\mathbf{t}|\,\delta^2(\mathbf{b}-\mathbf{t}) \\ &= \frac{\mathrm{i}}{2\pi\beta}\ln b\,. \end{aligned} \tag{B.37}$$

For the second equation (B.35b) with $\phi_2 \equiv \mathbf{f}$ and $v_2 \equiv \frac{2}{\beta}\nabla_{\mathbf{b}}\,\delta^2(\mathbf{b})$ we have to perform a partial integration and a redefinition of the integration variable $\mathbf{w} \equiv \mathbf{b}-\mathbf{t}$ and thus we find

$$\begin{aligned}(\phi_2 * v_2)(\mathbf{b}) &= \frac{1}{\pi\beta}\int \mathrm{d}^2t\,\ln|\mathbf{t}|\,\nabla_{\mathbf{b}-\mathbf{t}}\,\delta^2(\mathbf{b}-\mathbf{t}) \\ &= -\frac{1}{\pi\beta}\nabla_{\mathbf{w}}\ln|\mathbf{b}-\mathbf{w}|\Big|_{\mathbf{w}=\mathbf{0}} \\ &= \frac{1}{\pi\beta}\frac{\mathbf{b}}{b^2}\,. \end{aligned} \tag{B.38}$$

Summarizing we obtain the limiting behaviour[1]

$$\psi(\mathbf{b}) = c_\psi \ln b + \mathcal{O}(b^0)\,, \qquad c_\psi = \frac{\mathrm{i}}{2\pi\beta} \tag{B.39a}$$

$$\mathbf{f}(\mathbf{b}) = c_f\frac{\mathbf{b}}{b^2} + \mathcal{O}(b)\,, \qquad c_f = \frac{1}{\pi\beta}\,. \tag{B.39b}$$

B.2.3 Recipe for numerical calculation

In the following the schematic overview of how to solve the ordinary differential equations (ODEs) (B.22) and (B.24) can be solved, following [108]. Since the algorithm holds for both, we only present the procedure in terms of ψ, again.

1. Split the function into a tree-level and a higher order part according to

$$\psi(b) = \psi_0(b) + \psi_1(b)\,, \tag{B.40}$$

   where $\psi_0(b)$ solves (B.22) by putting $D(b) = 0$. Thus $\psi_0(b)$ is proportional to Bessel functions as can be seen in the next section.

2. Write the general solution for $\psi_1(b)$ pursuant to

$$\psi_1(b) = c_1\psi_1^{(1)}(b) + c_2\psi_1^{(2)}(b) + \psi_1^{(\mathrm{p})}(b)\,, \tag{B.41}$$

   so that the latter one is the particular solution of the inhomogeneous equation and the linearly dependent functions $\psi_1^{(1,2)}(b)$ solve the homogeneous one.

3. Use the limiting behaviour (B.39) so that $c_1 = 0$ and with (B.34) compute

$$c_2 = -\lim_{b\to\infty}\frac{\psi_1^{(\mathrm{p})}(b)}{\psi_1^{(2)}(b)}\,. \tag{B.42}$$

[1] Here only the dependence on b is presented, for gaining dimensionless variables of the logarithm, certainly the Debye masshas to be added according to $\ln(bm_{\mathrm{D}})$, cf. B.33.

4. Choose values for $b \to 0$ and $b \to \infty$ and implement the following algorithm:
   a) Solve homogeneous equation for $\psi_1(b)$ with initial conditions (i. c.) $\psi_1(b_0) = 1$, $\psi_1'(b_0) = 0$ to obtain $\psi_1^{(2)}$.
   b) Solve inhomogeneous equation for $\psi_1(b)$ with i. c. $\psi_1(b_0) = \mathrm{i}$, $\psi_1'(b_0) = 0$ to obtain $\psi_1^{(\mathrm{p})}$.
5. Use eq. (B.42) for calculating c_2 so that the result is obtained by $\mathrm{Re}\,\psi_1(b \to 0) = \mathrm{Re}\,c_2$.

The same procedure solves the ODE for $h(b)$, only in step 5. one has to use the initial conditions $h_1(b_0) = 1$, $h_1'(b_0) = 0$ since then it is $\mathrm{Im}\,h_1(b \to 0) = \mathrm{Im}\,c_2$ (for a proof, see app. B.3.2).

B.2.4 Implementing the Ordinary Differential Equations (ODEs)

Now we have a closer look on the steps described in the previous section. We start with equation (B.22)

$$-\mathrm{i}\beta\left(\partial_b^2 + \frac{1}{b}\partial_b - M_{\mathrm{eff}}^2\right)\psi(b) - \mathcal{K}(b)\psi(b) = 0\,, \tag{B.43}$$

which we want to solve for $b > 0$.

1. We split the function into $\psi(b) = \psi_0(b) + \psi_1(b)$, where $\psi_0(b)$ solves (B.22) with $D(b) = 0$, i. e. $(\partial_b^2 + \frac{1}{b}\partial_b - M_{\mathrm{eff}}^2)\psi_0(b) = 0$. This tree-level solution in its general form looks like

$$\psi_0(b) = a_1 J_0\left(\mathrm{i}b\sqrt{M_{\mathrm{eff}}^2}\right) + a_2 Y_0\left(-\mathrm{i}b\sqrt{M_{\mathrm{eff}}^2}\right)\,, \qquad a_1,\, a_2 \in \mathbb{C}\,, \tag{B.44}$$

   with the Bessel functions $J_n(z)$ of the first and $Y_n(z)$ of the second kind. Due to the definition

$$M_{\mathrm{eff}}^2 = \frac{p_\parallel(p_\parallel - k_\parallel)M^2 - k_\parallel(p_\parallel - k_\parallel)m_l^2 + k_\parallel p_\parallel m_\phi^2}{k_\parallel^2}\,, \tag{B.45}$$

   M_{eff}^2 can become negative, so we need a case differentiation for $M_{\mathrm{eff}}^2 \geq 0$ and $M_{\mathrm{eff}}^2 < 0$:

   a) $M_{\mathrm{eff}}^2 \geq 0 \;\to\; \sqrt{M_{\mathrm{eff}}^2} \equiv M_{\mathrm{eff}}$: Using some features of the Bessel functions [136] for complex arguments, we can rewrite the Bessel functions in terms of the modified Bessel functions $I_0(x)$ and $K_0(x)$ of real arguments x. Furthermore, we have to investigate the behaviour for $b \to 0$, that is given by

$$K_0(b) \overset{b\to 0}{\sim} -\ln b \tag{B.46a}$$

$$I_0(b) \overset{b\to 0}{\sim} \frac{1}{\Gamma(1)} = 1\,. \tag{B.46b}$$

   This renders the behaviour of (B.39a) and comparison leads to the result

$$\psi_0(b) = \left(a_1^{(1)} - \frac{3}{4\beta}\right) I_0(M_{\mathrm{eff}}b) - \frac{\mathrm{i}}{2\pi\beta} K_0(M_{\mathrm{eff}}b)\,, \quad a_1^{(1)} \in \mathbb{C}\,. \tag{B.47}$$

b) $M_{\text{eff}}^2 < 0 \;\rightarrow\; \sqrt{M_{\text{eff}}^2} \equiv \mathrm{i}M_{\text{eff}}$: In this case, $Y_0(x)$ and $J_0(x)$ only depend on real values so that we can directly consider the behaviour of the two functions for $b \to 0$:

$$J_0(b) \overset{b\to 0}{\sim} \frac{(\frac{b}{2})^0}{\Gamma(1)} = 1\,, \tag{B.48a}$$

$$Y_0(b) \overset{b\to 0}{\sim} \frac{2}{\pi}\ln b\,, \tag{B.48b}$$

so that we reproduce (B.39a) again. Comparison then leads to

$$\psi_0(b) = a_1^{(2)} J_0(M_{\text{eff}} b) + \frac{\mathrm{i}}{4\pi} Y_0(M_{\text{eff}} b)\,, \quad a_1^{(2)} \in \mathbb{C}\,. \tag{B.49}$$

We also have to look at the behaviour of the functions of $b \to \infty$ to affirm the square-integrability (B.34) as well as a continuous transition. Thus we have to choose in the first case $a_1^{(1)} = \frac{3}{4\pi}$ and in the second $a_1^{(2)} = 0$. The solution of $\psi_0(b)$ then becomes purely imaginary and reads

$$\psi_0(b) = -\frac{\mathrm{i}}{2\pi\beta} K_0\left(\sqrt{M_{\text{eff}}^2}\, b\right)\,, \quad \text{for} \quad M_{\text{eff}}^2 \geq 0 \tag{B.50a}$$

$$\psi_0(b) = \quad \frac{\mathrm{i}}{4\beta} Y_0\left(\sqrt{|M_{\text{eff}}^2|}\, b\right)\,, \quad \text{for} \quad M_{\text{eff}}^2 < 0\,. \tag{B.50b}$$

2. – 4. Now we continue with the separation $\psi_1(b) = c_1\psi_1^{(1)}(b) + c_2\psi_1^{(2)}(b) + \psi_1^{(\text{p})}(b)$. For $b \to 0$, we already found $D(b) \sim b^2 \ln b$ and this was the limiting behaviour of $\psi_0(b)$ (cf. 1.), so that $\psi_1(b)$ becomes regular for $b \to 0$. With a subtle choice of the initial conditions and the use of the limits for $b \to \infty$, we can achieve

$$\psi_1^{(1)}(b) \overset{b\to 0}{\sim} c_\psi \ln b \quad (\sim K_0(b)) \quad \Rightarrow \quad c_1 = 0 \tag{B.51a}$$

$$\psi_1^{(2)}(b) \overset{b\to 0}{\sim} \text{regular} \quad (\sim I_0(b)) \quad \Rightarrow \quad c_2 = -\lim_{b\to\infty} \frac{\psi_1^{(\text{p})}(b)}{\psi_1^{(2)}(b)}\,. \tag{B.51b}$$

For the program we found the values $b_0 = 10^{-5}/T$ and $b_\infty = 30/T$ to deliver stable results. Then solving the homogeneous ODE for $\psi_1(b)$ with i. c. $\psi_1(b_0) = 1$, $\psi_1'(b_0) = 0$ leads to $\psi_1^{(2)}(b)$, since $c_1 \equiv 0$. The solution of the inhomogeneous ODE for $\psi_1(b)$ with i. c. $\psi_1(b_0) = \mathrm{i}$, $\psi_1'(b_0) = 0$ then gives $\psi_1^{(\text{p})}(b)$.

a) Solve homogeneous equation for $\psi_1(b)$:

$$-\mathrm{i}\beta\left(\partial_b^2 + \frac{1}{b}\partial_b - M_{\text{eff}}^2\right)\psi_1^{(2)}(b) - \mathcal{K}(b)\psi_1^{(2)}(b) = 0 \tag{B.52}$$

For all solutions are complex-valued we define from now on $\psi_j^{(k)} \equiv \psi_{j\text{r}}^{(k)} + \mathrm{i}\,\psi_{j\text{i}}^{(k)}$. The functions $\mathcal{K}(b) \sim K_0(b)$, $\beta(k_\parallel, p_\parallel), M_{\text{eff}}^2(M, k_\parallel, p_\parallel)$ are all real functions. Thus we obtain two real-valued ODEs:

$$\left(\partial_b^2 + \frac{1}{b}\partial_b - M_{\text{eff}}^2\right)\psi_{1\text{r}}^{(2)}(b) + \frac{\mathcal{K}(b)}{\beta}\psi_{1\text{i}}^{(2)}(b) = 0 \tag{B.53a}$$

$$\left(\partial_b^2 + \frac{1}{b}\partial_b - M_{\text{eff}}^2\right)\psi_{1\text{i}}^{(2)}(b) - \frac{\mathcal{K}(b)}{\beta}\psi_{1\text{r}}^{(2)}(b) = 0\,. \tag{B.53b}$$

b) Solve inhomogeneous equation for $\psi_1(b)$:

$$-\mathrm{i}\beta\left(\partial_b^2+\frac{1}{b}\partial_b-M_{\mathrm{eff}}^2\right)\left(\psi_0(b)+\psi_1^{(\mathrm{p})}(b)\right)-\mathcal{K}(b)\left(\psi_0(b)+\psi_1^{(\mathrm{p})}(b)\right)=0\,. \tag{B.54}$$

Remembering that $\psi_0(b)$ is the tree-level solution $(\partial_b^2+\frac{1}{b}\partial_b-M_{\mathrm{eff}}^2)\psi_0(b)=0$ we again find two real-valued ODEs

$$\left(\partial_b^2+\frac{1}{b}\partial_b-M_{\mathrm{eff}}^2\right)\psi_{1\mathrm{r}}^{(p)}(b)+\frac{\mathcal{K}(b)}{\beta}\left(\psi_{0\mathrm{i}}(b)+\psi_{1\mathrm{i}}^{(2)}(b)\right)=0 \tag{B.55a}$$

$$\left(\partial_b^2+\frac{1}{b}\partial_b-M_{\mathrm{eff}}^2\right)\psi_{1\mathrm{i}}^{(p)}(b)-\frac{\mathcal{K}(b)}{\beta}\left(\psi_{0\mathrm{r}}(b)+\psi_{1\mathrm{r}}^{(2)}(b)\right)=0\,, \tag{B.55b}$$

with the values for $\psi_{0\mathrm{i/r}}(b)$ from eqs. (B.50).

As already mentioned, the same procedure holds also for deriving the ODEs for $h(b)$. The results are slightly different, especially one obtains for the general solution of the tree-level part:

$$h_0(b)=-\frac{a_1}{b}J_1\left(\mathrm{i}\sqrt{M_{\mathrm{eff}}^2}b\right)+\frac{a_2}{b}Y_1\left(-\mathrm{i}\sqrt{M_{\mathrm{eff}}^2}b\right)\,,\qquad a_1,\ a_2\in\mathbb{C}\,, \tag{B.56}$$

so that after using the properties of the Bessel functions and integrating the limiting conditions we find a pure real solution

$$h_0(b)=\frac{M_{\mathrm{eff}}}{\pi\beta b}K_1\left(\sqrt{M_{\mathrm{eff}}^2}b\right)\,,\quad \text{for}\quad M_{\mathrm{eff}}^2\geq 0 \tag{B.57a}$$

$$h_0(b)=-\frac{M_{\mathrm{eff}}}{2\beta b}Y_1\left(\sqrt{|M_{\mathrm{eff}}^2|}b\right)\,,\quad \text{for}\quad M_{\mathrm{eff}}^2<0\,. \tag{B.57b}$$

Equations (B.55) then are valid for $h(b)$ if in the second term $\frac{1}{b}\partial_b$ is replaced by $\frac{3}{b}\partial_b$. The values for $h_{0\mathrm{r}}(b)$ have to be taken from eqs. (B.57), note that the imaginary part vanishes $h_{0\mathrm{i}}(b)=0$.

B.2.5 ODE solver and Monte Carlo integration

As we have seen in the last section, we have to solve now 4 ordinary differential equations of second order (B.53) and (B.55), where two of them are coupled, respectively. Therefore it is suggestive to transform a second order ODE into two coupled ODEs of first order according to

$$\frac{\mathrm{d}^2y}{\mathrm{d}x^2}+q(x)\frac{\mathrm{d}y}{\mathrm{d}x}=r(x)\quad\rightarrow\quad\begin{array}{c}\frac{\mathrm{d}y}{\mathrm{d}x}=z(x)\\ \frac{\mathrm{d}z}{\mathrm{d}x}=r(x)-q(x)z(x)\,.\end{array} \tag{B.58}$$

Thus we have to solve the following 8 ODEs for $\psi(b)$, while 4 of them are coupled now:

$$\partial_b \psi^{(2)}_{1\mathrm{r/i}} \equiv z^{(2)}_{\mathrm{r/i}} \tag{B.59a}$$

$$\partial_b\, z^{(2)}_{\mathrm{r/i}} = -\frac{1}{b} z^{(2)}_{\mathrm{r/i}} + M^2_{\mathrm{eff}} \psi^{(2)}_{1\mathrm{r/i}} \mp \frac{\mathcal{K}(b)}{\beta} \psi^{(2)}_{1\mathrm{i/r}} \tag{B.59b}$$

and

$$\partial_b \psi^{(p)}_{1\mathrm{r/i}} \equiv z^{(p)}_{\mathrm{r/i}} \tag{B.59c}$$

$$\partial_b\, z^{(p)}_{\mathrm{r/i}} = -\frac{1}{b} z^{(p)}_{\mathrm{r/i}} + M^2_{\mathrm{eff}} \psi^{(p)}_{1\mathrm{r/i}} \mp \frac{\mathcal{K}(b)}{\beta} \left(\psi_{0\mathrm{i/r}} + \psi^{(p)}_{1\mathrm{i/r}} \right) . \tag{B.59d}$$

For $h(b)$ we obtain similar equations, one only has to replace the terms $\frac{1}{b}$ by $\frac{3}{b}$ and use the corresponding solutions of $h_{0\mathrm{i/r}}$ instead of $\psi_{0\mathrm{i/r}}$.

Furthermore, we deal with an initial value problem as mentioned also in the last section. For these kind of problems the *Numerical Recipes* [137] allocate several types of methods for dealing with it that are *Runge-Kutta methods*, *Richardson extrapolation including Bulirsch-Stoer method* and *multistep methods*. The method of our choice is the Bulirsch-Stoer one [138], since this one is supposed to be a very good way of obtaining high accuracy solutions by using minimal computational effort. Runge-Kutta methods for example have a lack of computational efficiency for our problem, while the multistep methods need very smooth functions for getting better results than Bulirsch-Stoer. The latter one is technically based on a modified midpoint method, with the numbers of substeps n is varied in a special sequence.

The ODE routine is implemented in a `C++` program [139]. We have to solve all ODEs at once since the result $c_2 = c_2(M, k_\parallel, p_\parallel)$ is needed for each step of an integration over $k_\parallel$ and $p_\parallel$. Therefore we are interested in the limit

$$c_2 = -\lim_{b\to\infty} \frac{\psi^{(\mathrm{p})}_1(b)}{\psi^{(2)}_1(b)} \tag{B.60}$$

and thus have to find a value b_∞, where the result reaches a plateau and does not change the result any further. A good choice appears to be $b_\infty = 30/T$ and so one can derive the value

$$\mathrm{Re}\, c_2 = -\frac{\psi^{(\mathrm{p})}_{1\mathrm{r}}(b_\infty)\psi^{(2)}_{1\mathrm{r}}(b_\infty) + \psi^{(\mathrm{p})}_{1\mathrm{i}}(b_\infty)\psi^{(2)}_{1\mathrm{i}}(b_\infty)}{(\psi^{(2)}_{1\mathrm{r}}(b_\infty))^2 + (\psi^{(2)}_{1\mathrm{i}}(b_\infty))^2} . \tag{B.61}$$

For the multi-dimensional integrations we apply the CUBA-library [140, 141]. It provides 4 multi-dimensional integration algorithms *Vegas*, *Suave*, *Divonne* and *Cuhre*. We will concentrate on Vegas since it was mainly used, while we cross-checked some results with Divonne, also. The Vegas routine is a Monte Carlo algorithm. It uses importance sampling and a variance-reduction technique and is well implementable in a `C++` environment.

Normally Monte Carlo algorithms integrate over the unit cube $[0,1]^n$. That is why we have to rearrange the integration variables. For the tree-level result (6.2) we need

finite limits $\int_a^b \mathrm{d}x f(x)$. The intrinsic transformation then becomes

$$\int_0^1 \mathrm{d}y f(a+(b-a)y)(b-a)\,, \tag{B.62}$$

so that the Monte Carlo algorithm can be used. For infinite boundaries as will be needed for the full calculation one can use the transformations

$$y = \frac{1}{\pi}\arctan x + \frac{1}{2}\,, \qquad \text{for} \qquad (-\infty,\infty) \;\to\; [0,1]\,, \tag{B.63a}$$

$$y = \frac{2}{\pi}\arctan x\,, \qquad \text{for} \qquad [0,\infty) \;\to\; [0,1]\,. \tag{B.63b}$$

B.3 Proofs

B.3.1 Partial fractioning

In equation (5.19) we used partial fractioning. The proof for this is easily derived by starting with

$$D_l(p) - D_\phi(p-k) \equiv \epsilon(k,\mathbf{p})\, D_l(p)\, D_\phi(p-k)\,. \tag{B.64}$$

Considering the definitions for the two propagators

$$D_l^{-1}(p) = -\left(vp - \frac{\mathbf{p}_\perp + m_l^2}{2p_\parallel}\right) \quad , \quad D_\phi^{-1}(p-k) = -\left(v(p-k) - \frac{(\mathbf{p}_\perp - \mathbf{k}_\perp)^2 + m_\phi^2}{2(p_\parallel - k_\parallel)}\right)\,,$$

we directly can read off the difference

$$\begin{aligned} D_l(p) - D_\phi(p-k) &= \frac{-v(p-k) + \frac{(\mathbf{p}_\perp-\mathbf{k}_\perp)^2+m_\phi^2}{2(p_\parallel-k_\parallel)} + vp - \frac{\mathbf{p}_\perp+m_l^2}{2p_\parallel}}{\left(vp - \frac{\mathbf{p}_\perp+m_l^2}{2p_\parallel}\right)\left(v(p-k) - \frac{(\mathbf{p}_\perp-\mathbf{k}_\perp)^2+m_\phi^2}{2(p_\parallel-k_\parallel)}\right)} \\ &= \frac{vk + \frac{(\mathbf{p}_\perp-\mathbf{k}_\perp)^2+m_\phi^2}{2(p_\parallel-k_\parallel)} - \frac{\mathbf{p}_\perp+m_l^2}{2p_\parallel}}{\left(vp - \frac{\mathbf{p}_\perp+m_l^2}{2p_\parallel}\right)\left(v(p-k) - \frac{(\mathbf{p}_\perp-\mathbf{k}_\perp)^2+m_\phi^2}{2(p_\parallel-k_\parallel)}\right)} = \frac{\epsilon}{(D_l\cdot D_\phi)^{-1}}\,, \end{aligned}$$

with

$$\epsilon(k,\mathbf{p}) \equiv v\cdot k + \frac{(\mathbf{p}_\perp - \mathbf{k}_\perp)^2 + m_\phi^2}{2(p_\parallel - k_\parallel)} - \frac{\mathbf{p}_\perp^2 + m_l^2}{2p_\parallel}\,,$$

what needed to be shown.

B.3.2 The perpendicular momentum integration

Now we would like to proof the equations (B.17):

$$\int \frac{\mathrm{d}^2 p_\perp}{(2\pi)^2}\,\mathrm{Re}\,[\mathbf{p}_\perp\cdot\mathbf{f}(\mathbf{p}_\perp)] = \lim_{b\to 0}\mathrm{Im}\,\nabla\cdot\mathbf{f}(\mathbf{b}) = \lim_{b\to 0}\mathrm{Im}\,h(b)\,,$$

$$\int \frac{\mathrm{d}^2 p_\perp}{(2\pi)^2}\,\mathrm{Re}\,\psi(\mathbf{p}_\perp) = \lim_{b\to 0}\mathrm{Re}\,\psi(\mathbf{b})\,,$$

where we added the last identity in the first equation. Since the second one is easier to derive, we start there by using the definition of the δ-function

$$\delta^2(\mathbf{b}) = \int \frac{\mathrm{d}^2 p_\perp}{(2\pi)^2} \mathrm{e}^{\pm \mathrm{i}\mathbf{p}_\perp \mathbf{b}} \tag{B.65}$$

and the rotational invariance of $\psi(\mathbf{b}) = \psi(b)$. So we find already

$$\int \frac{\mathrm{d}^2 p_\perp}{(2\pi)^2} \operatorname{Re}\psi(\mathbf{p}_\perp) = \operatorname{Re}\int \mathrm{d}^2 b\, \delta^2(\mathbf{b})\psi(\mathbf{b}) = \lim_{b\to 0} \operatorname{Re}\psi(b) = \operatorname{Re} c_2\,. \tag{B.66}$$

The second equation needs some more effort. For the real-part it is

$$\operatorname{Re}\left[\mathbf{p}_\perp \cdot \mathbf{f}(\mathbf{p}_\perp)\right] = p_1 \operatorname{Re} f_1(\mathbf{p}_\perp) + p_2 \operatorname{Re} f_2(\mathbf{p}_\perp)\,. \tag{B.67}$$

We can further plug in the Fourier transform of $\mathbf{f}(\mathbf{p}_\perp)$ and replace $p_1 \to \mathrm{i}\frac{\mathrm{d}}{\mathrm{d}b_i}$ to obtain

$$\begin{aligned}
\int \frac{\mathrm{d}^2 p_\perp}{(2\pi)^2} \operatorname{Re}\left[\mathbf{p}_\perp \cdot \mathbf{f}(\mathbf{p}_\perp)\right] &= \int \frac{\mathrm{d}^2 p_\perp}{(2\pi)^2} \operatorname{Re}\int \mathrm{d}^2 b\, \mathrm{i}\left(f_1(\mathbf{b})\frac{\mathrm{d}}{\mathrm{d}b_1} + f_2(\mathbf{b})\frac{\mathrm{d}}{\mathrm{d}b_2}\right)\mathrm{e}^{-\mathrm{i}\mathbf{p}_\perp\mathbf{b}} \\
&= -\operatorname{Re}\int \mathrm{d}^2 b\, \mathrm{i}\,\delta^2(\mathbf{b})\left(\frac{\mathrm{d}f_1(\mathbf{b})}{\mathrm{d}b_1} + \frac{\mathrm{d}f_2(\mathbf{b})}{\mathrm{d}b_2}\right) \\
&= \lim_{b\to 0} \operatorname{Im}\nabla\cdot\mathbf{f}(\mathbf{b})\,.
\end{aligned} \tag{B.68}$$

In the second step a partial integration was performed and the definition of the δ-function was used. In the third step we adopted the δ-function and rewrote the derivative. Note that $\operatorname{Re}(\mathrm{i}a) = -\operatorname{Im} a$. This proves the first part of (B.17a). For the second part, we apply $\mathbf{f}(\mathbf{b}) = h(b)\mathbf{b}$, so that for the derivative we find

$$\frac{\partial f_i(\mathbf{p}_\perp)}{\partial b_j} = \delta_{ij}\, h(b) + \frac{b_i b_j}{b} h'(b), \quad \text{since} \quad h(b) \equiv h(\sqrt{b_1^2 + b_2^2})\,, \tag{B.69}$$

and so in total we get

$$\int \frac{\mathrm{d}^2 p_\perp}{(2\pi)^2} \operatorname{Re}\left[\mathbf{p}_\perp \cdot \mathbf{f}(\mathbf{p}_\perp)\right] = \lim_{b\to 0} \operatorname{Im}\left(2h(b) + bh'(b)\right) \tag{B.70}$$

$$= \lim_{b\to 0} \operatorname{Im} 2h(b) = 2\operatorname{Im} c_2\,. \tag{B.71}$$

The last term in (B.70) vanishes due to the limiting behaviour of eq. (B.39b). Therefore in this limit the derivative of $\operatorname{Im} h(b)$ has to become zero while terms proportional to $\operatorname{Re} h(b)$ diverge according to b^{-2}.

B.3.3 Retarded self-energy

As stated in sec. 7.2 we now proof that the imaginary part of the retarded self-energy equals

$$\operatorname{Im}\Sigma^{\mathrm{R,ret}}(p) = \int \frac{\mathrm{d}^3 k}{(2\pi)^3} \frac{\mathcal{F}(p_\parallel, k_\parallel)}{k_\parallel - p_\parallel} \begin{pmatrix} \frac{\operatorname{Re}\mathbf{k}_\perp \mathbf{f}}{8k_\parallel^2} & -\frac{k_1}{2k_\parallel}\operatorname{Re}\psi \\ -\frac{\operatorname{Re} f_1}{4k_\parallel} & \operatorname{Re}\psi \end{pmatrix}\,.$$

Therefore we start from the definition of the retarded self-energy eq. (7.12). Calculating the vector product and using the expansion of the Weyl spinor (B.2) and only the imaginary part then leads to

$$\operatorname{Im}\Sigma^{\mathrm{R,ret}}(p) = \int \frac{\mathrm{d}^3k}{(2\pi)^3}\frac{\mathcal{F}(p_\parallel,k_\parallel)}{k_\parallel - p_\parallel}\begin{pmatrix} \frac{\operatorname{Re}\mathbf{k}_\perp\mathbf{f} - k_1\operatorname{Im}f_2 + k_2\operatorname{Im}f_1}{8k_\parallel^2} & -\frac{k_1\operatorname{Re}\psi + k_2\operatorname{Im}\psi}{2k_\parallel} \\ -\frac{\operatorname{Re}f_1 - \operatorname{Im}f_2}{4k_\parallel} & \operatorname{Re}\psi \end{pmatrix} . \tag{B.72}$$

Due to rotational invariance of the function $\mathbf{f}(\mathbf{b}) = h(b)\mathbf{b}$, and thus as can be proven using the Fourier transform it is also $\mathbf{f}(\mathbf{k}_\perp) = h(k_\perp)\mathbf{k}_\perp$. Hence the second and third main diagonal term in the upper left entry vanishes: $-k_1\operatorname{Im}f_2 + k_2\operatorname{Im}f_1 = 0$.

Two terms of the secondary diagonal also vanish. To show this, we have to calculate the integrals

$$\int \frac{\mathrm{d}^2k_\perp}{(2\pi)^3}\operatorname{Im}f_2 = 0\,, \quad \text{and} \quad \int \frac{\mathrm{d}^2k_\perp}{(2\pi)^3}\,k_2\operatorname{Im}\psi = 0\,. \tag{B.73}$$

For both, we again use the procedure presented in the last section B.3.2. Hence we find

$$\int \frac{\mathrm{d}^2k_\perp}{(2\pi)^3}\operatorname{Im}f_2 = \lim_{b\to 0} b_2\operatorname{Im}h(b)\,, \tag{B.74a}$$

$$\int \frac{\mathrm{d}^2k_\perp}{(2\pi)^3}\,k_2\operatorname{Im}\psi = \lim_{b\to 0}\frac{b_2}{b}\operatorname{Re}\psi'(b)\,. \tag{B.74b}$$

From the limiting behaviour (B.39), we can read off

$$\lim_{b\to 0} b_i\operatorname{Im}h(b) = 0 \quad \Rightarrow \quad \lim_{b\to 0}\operatorname{Im}h(b) = \text{const.}\,, \tag{B.75a}$$

$$\lim_{b\to 0}\operatorname{Re}\psi(b) = \text{const.} \quad \Rightarrow \quad \lim_{b\to 0}\operatorname{Re}\psi'(b) = 0\,. \tag{B.75b}$$

This is also consistent with the features used for the numerical treatment, cf. eqs. (B.66) and (B.71). Thus we directly see that both integrals (B.74) vanish and we have proven the result for the retarded self-energy.

Bibliography

[1] **NASA/WMAP Science Team**, January 2013. `http://map.gsfc.nasa.gov/media/060915/index.html`.

[2] D. J. Schwarz and M. Stuke, "Lepton asymmetry and the cosmic qcd transition," *JCAP* **0911** 025. [arXiv:hep-ph/0906.3434].

[3] A. Hohenegger, A. Kartavtsev, and M. Lindner, "Deriving Boltzmann Equations from Kadanoff-Baym Equations in Curved Space-Time," *Phys.Rev.* **D78** (2008) 085027, `0807.4551`. [arXiv:hep-ph/0807.4551].

[4] M. Garny, A. Hohenegger, A. Kartavtsev, and M. Lindner, "Systematic approach to leptogenesis in nonequilibrium qft: Vertex contribution to the cp-violating parameter," *Phys.Rev.* **D80** 125027. [arXiv:hep-ph/0909.1559].

[5] M. Garny, A. Hohenegger, A. Kartavtsev, and M. Lindner, "Systematic approach to leptogenesis in nonequilibrium qft: Self-energy contribution to the cp-violating parameter," *Phys.Rev.* **D81** 085027. [arXiv:hep-ph/0911.4122].

[6] M. Garny, A. Hohenegger, and A. Kartavtsev, "Medium corrections to the cp-violating parameter in leptogenesis," *Phys.Rev.* **D81** 085028. [arXiv:hep-ph/1002.0331].

[7] M. Beneke, B. Garbrecht, M. Herranen, and P. Schwaller, "Finite number density corrections to leptogenesis," *Nucl.Phys.* **B838** (2010) 1–27. [arXiv:hep-ph/1002.1326].

[8] B. Garbrecht, "Leptogenesis: The other cuts," *Nucl.Phys.* **B847** 350–366. [arXiv:hep-ph/1011.3122].

[9] M. Beneke, B. Garbrecht, C. Fidler, M. Herranen, and P. Schwaller, "Flavoured leptogenesis in the ctp formalism," *Nucl.Phys.* **B843** 177–212. [arXiv:hep-ph/1007.4783].

[10] C. P. Kiessig, M. Plumacher, and M. H. Thoma, "Decay of a yukawa fermion at finite temperature and applications to leptogenesis," *Phys.Rev.* **D82** 036007. [arXiv:hep-ph/1003.3016].

[11] G. F. Giudice, A. Notari, M. Raidal, A. Riotto, and A. Strumia, "Towards a complete theory of thermal leptogenesis in the sm and mssm," *Nucl.Phys.* **B685** 89–149. [arXiv:hep-ph/0310123].

[12] J.-S. Gagnon and M. Shaposhnikov, "Baryon asymmetry of the universe without boltzmann or kadanoff-baym equations," *Phys.Rev.* **D83** 065021. [arXiv:hep-ph/1012.1126].

[13] A. Salvio, P. Lodone, and A. Strumia, "Towards leptogenesis at nlo: the right-handed neutrino interaction rate," *JHEP* **1108** 116. [arXiv:hep-ph/1106.2814].

[14] J. Racker, M. Pena, and N. Rius, "Leptogenesis with small violation of B-L," *JCAP* **1207** (2012) 030. [arXiv:hep-ph/1205.1948].

[15] A. Anisimov, W. Buchmuller, M. Drewes, and S. Mendizabal, "Nonequilibrium dynamics of scalar fields in a thermal bath," *Annals Phys.* **324** (2009) 1234–1260. [arXiv:hep-th/0812.1934].

[16] A. Anisimov, W. Buchmuller, M. Drewes, and S. Mendizabal, "Quantum leptogenesis i," *Annals Phys.* **326** (2011) 1998–2038. [arXiv:hep-ph/1012.5821].

[17] A. Anisimov, D. Besak, and D. Bodeker, "Thermal production of relativistic majorana neutrinos: Strong enhancement by multiple soft scattering," *JCAP* **1103** (2011) 042. [arXiv:hep-ph/1012.3784].

[18] D. Besak and D. Bodeker, "Thermal production of ultrarelativistic right-handed neutrinos: Complete leading-order results,". [arXiv:hep-ph/1202.1288].

[19] V. Kuzmin, V. Rubakov, and M. Shaposhnikov, "On the Anomalous Electroweak Baryon Number Nonconservation in the Early Universe," *Phys.Lett.* **B155** (1985) 36.

[20] E. W. Kolb and M. S. Turner, *The Early Universe.* Addison-Wesley, New York, 1990. Volume 69 of Frontiers in Physics: Lecture note series.

[21] W. Buchmuller and S. Fredenhagen, "Quantum mechanics of baryogenesis," *Phys.Lett.* **B483** 217–224. [arXiv:hep-ph/0004145].

[22] W. Buchmuller, "Baryogenesis: 40 Years Later," `0710.5857`. [arXiv:hep-ph/0710.5857].

[23] M. Trodden, "Baryogenesis and leptogenesis," *eConf* **C040802** (2004) L018. [arXiv:hep-ph/0411301].

[24] **WMAP** Collaboration, E. Komatsu *et al.*, "Seven-Year Wilkinson Microwave Anisotropy Probe (WMAP) Observations: Cosmological Interpretation," *Astrophys.J.Suppl.* **192** (2011) 18. [arXiv:astro-ph/1001.4538].

[25] K. Nakamura *et al.*, "Review of particle physics," *Journal of Physics G37, 075021* (2010) . Particle Data Group: http://pdg.lbl.gov.

[26] A. H. Guth, "Inflation,". [arXiv:astro-ph/0404546].

[27] J. M. Cline, "Der Ursprung der Materie," *Spektrum der Wissenschaft* **November 2004** (2004) 32–41.

[28] A. D. Sakharov, "Violation of CP Invariance, c Asymmetry, and Baryon Asymmetry of the Universe," *Pisma Zh.Eksp.Teor.Fiz.* **5** (1967) 32–35.

[29] J. Zinn-Justin, *Quantum Field Theory and Critical Phenomena.* Oxford University Press, Oxford, 4. ed., 2002. International Series of Monographs on Physics.

[30] M. E. Peskin and D. V. Schroeder, *An Introduction to Quantum Field Theory.* Addison-Wesley, Reading, USA, 1995.

[31] T. P. Cheng and L. F. Li, *Gauge theory of elementary particle physics.* Oxford University Press, Oxford, 1991.

[32] G. 't Hooft, "Symmetry Breaking Through Bell-Jackiw Anomalies," *Phys.Rev.Lett.* **37** (1976) 8–11.

[33] G. 't Hooft, "Computation of the Quantum Effects Due to a Four-Dimensional Pseudoparticle," *Phys.Rev.* **D14** (1976) 3432–3450.

[34] N. S. Manton, "Topology in the Weinberg-Salam Theory," *Phys.Rev.* **D28** (1983) 2019.

[35] F. R. Klinkhamer and N. S. Manton, "A Saddle Point Solution in the Weinberg-Salam Theory," *Phys.Rev.* **D30** (1984) 2212.

[36] S. L. Adler, "Axial vector vertex in spinor electrodynamics," *Phys.Rev.* **177** (1969) 2426–2438.

[37] J. Bell and R. Jackiw, "A PCAC puzzle: $\pi^0 \to \gamma\gamma$ in the sigma model," *Nuovo Cim.* **A60** (1969) 47–61.

[38] O. Philipsen, "Sphaleron transitions in the symmetric phase of the standard model," *Phys.Lett.* **B304** (1993) 134–140.

[39] O. Philipsen, "The Sphaleron rate in the 'symmetric' electroweak phase," *Phys.Lett.* **B358** (1995) 210–216. [arXiv:hep-ph/9506478].

[40] D. Bodeker, "On the effective dynamics of soft nonAbelian gauge fields at finite temperature," *Phys.Lett.* **B426** 351–360. [arXiv:hep-ph/9801430].

[41] P. B. Arnold, D. T. Son, and L. G. Yaffe, "Effective dynamics of hot, soft nonAbelian gauge fields. Color conductivity and log(1/alpha) effects," *Phys.Rev.* **D59** 105020. [arXiv:hep-ph/9810216].

[42] G. D. Moore, C. Hu, and B. Muller, "Chern-Simons number diffusion with hard thermal loops," *Phys.Rev.* **D58** (1998) 045001, `arXiv:hep-ph/9710436 [hep-ph]`.

[43] **NA48** Collaboration, V. Fanti *et al.*, "A New measurement of direct CP violation in two pion decays of the neutral kaon," *Phys.Lett.* **B465** 335–348. [arXiv:hep-ex/9909022].

[44] P. Huet and E. Sather, "Electroweak baryogenesis and standard model CP violation," *Phys.Rev.* **D51** (1995) 379–394, `arXiv:hep-ph/9404302`. [arXiv:hep-ph/9204302].

[45] W. Buchmuller and O. Philipsen, "Phase structure and phase transition of the SU(2) Higgs model in three-dimensions," *Nucl.Phys.* **B443** (1995) 47–69. [arXiv:hep-ph/9411334].

[46] K. Kajantie, M. Laine, K. Rummukainen, and M. E. Shaposhnikov, "The Electroweak phase transition: A Nonperturbative analysis," *Nucl.Phys.* **B466** (1996) 189–258, `hep-lat/9510020`. [arXiv:hep-lat/9510020].

[47] F. Csikor, Z. Fodor, and J. Heitger, "Where does the hot electroweak phase transition end?," *Nucl.Phys.Proc.Suppl.* **73** (1999) 659–661, `hep-ph/9809293`. [arXiv:hep-ph/9809293].

[48] **ATLAS** Collaboration, "Latest Results from ATLAS Higgs Search,". `http://www.atlas.ch/news/2012/latest-results-from-higgs-search.html`.

[49] **CMS** Collaboration, "Observation of a New Particle with a Mass of 125 GeV,". `http://cms.web.cern.ch/news/observation-new-particle-mass-125-gev`.

[50] A. D. Dolgov, "NonGUT baryogenesis," *Phys.Rept.* **222** (1992) 309–386.

[51] P. Langacker, "Grand Unified Theories and Proton Decay," *Phys.Rept.* **72** (1981) 185.

[52] V. A. Kuzmin, V. A. Rubakov, and M. E. Shaposhnikov, "Anomalous Electroweak Baryon Number Nonconservation and GUT Mechanism for Baryogenesis," *Phys.Lett.* **B191** (1987) 171.

[53] M. Shaposhnikov, "Possible Appearance of the Baryon Asymmetry of the Universe in an Electroweak Theory," *JETP Lett.* **44** (1986) 465–468.

[54] M. Shaposhnikov, "Baryon Asymmetry of the Universe in Standard Electroweak Theory," *Nucl.Phys.* **B287** (1987) 757–775.

[55] D. E. Morrissey and M. J. Ramsey-Musolf, "Electroweak baryogenesis,". [arXiv:hep-ph/1206.2942].

[56] S. Dimopoulos and H. Georgi, "Softly Broken Supersymmetry and SU(5)," *Nucl.Phys.* **B193** (1981) 150.

[57] I. Affleck and M. Dine, "A New Mechanism for Baryogenesis," *Nucl.Phys.* **B249** (1985) 361.

[58] M. Fukugita, and T. Yanagida, "Baryogenesis without grand unification," *Phys.Lett.* **B174** (1986) 45.

[59] R. N. Mohapatra and J. C. Pati, "Left-Right Gauge Symmetry and an Isoconjugate Model of CP Violation," *Phys.Rev.* **D11** (1975) 566–571.

[60] R. N. Mohapatra and G. Senjanovic, "Exact Left-Right Symmetry and Spontaneous Violation of Parity," *Phys.Rev.* **D12** (1975) 1502.

[61] M. Gell-Mann, P. Ramond, and R. Slanski, *Supergravity*. P. Van Nieuwenhuizen and D. Z. Freedman, North Holland, 1979.

[62] W. Buchmuller and M. Plumacher, "Baryon asymmetry and neutrino mixing," *Phys.Lett.* **B389** 73–77. [arXiv:hep-ph/9608308].

[63] W. Buchmuller, P. Di Bari, and M. Plumacher, "The neutrino mass window for baryogenesis," *Nucl.Phys.* **B665** 445–468. [arXiv:hep-ph/0302092].

[64] P. Di Bari, "An introduction to leptogenesis and neutrino properties,". [arXiv:hep-ph/1206.3168].

[65] S. Blanchet and P. Di Bari, "The minimal scenario of leptogenesis," *New J.Phys.* **14** (2012) 125012, 1211.0512. [arXiv:hep-ph/1211.0512].

[66] C. S. Fong, E. Nardi, and A. Riotto, "Leptogenesis in the Universe," *Adv.High Energy Phys.* **2012** (2012) 158303, 1301.3062. [arXiv:hep-ph/1301.3062].

[67] J. Gluza and M. Zralek, "Feynman rules for majorana neutrino interactions," *Phys.Rev.* **D45** (1992) 1693–1700.

[68] L. Covi, E. Roulet, and F. Vissani, "CP violating decays in leptogenesis scenarios," *Phys.Lett.* **B384** (1996) 169–174. [arXiv:hep-ph/9605319].

[69] R. E. Cutkosky, "Singularities and discontinuities of Feynman amplitudes," *J.Math.Phys.* **1** (1960) 429–433.

[70] C. P. Kiessig and M. Plumacher, "Hard-thermal-loop corrections in leptogenesis i: Cp-asymmetries,". [arXiv:hep-ph/1111.1231].

[71] C. P. Kiessig and M. Plumacher, "Hard-thermal-loop corrections in leptogenesis ii: Solving the boltzmann equations,". [arXiv:hep-ph/1111.1235].

[72] L. Covi, N. Rius, E. Roulet, and F. Vissani, "Finite temperature effects on CP violating asymmetries," *Phys.Rev.* **D57** (1998) 93–99. [arXiv:hep-ph/9704366].

[73] C. P. Kiessig and M. Plumacher, "Thermal masses in leptogenesis," *AIP Conf.Proc.* **1200** 999–1002. [arXiv:hep-ph/0910.4872].

[74] A. Halprin, P. Minkowski, H. Primakoff, and S. P. Rosen, "Double-beta Decay and a Massive Majorana Neutrino," *Phys.Rev.* **D13** (1976) 2567.

[75] A. Giuliani and A. Poves, "Neutrinoless Double-Beta Decay," *Adv.High Energy Phys.* **2012** (2012) 857016.

[76] A. Strumia, "Baryogenesis via leptogenesis,". [arXiv:hep-ph/0608347].

[77] W. Buchmuller, P. Di Bari, and M. Plumacher, "Cosmic microwave background, matter - antimatter asymmetry and neutrino masses," *Nucl.Phys.* **B643** 367–390. [arXiv:hep-ph/0205349].

[78] W. Buchmuller, P. Di Bari, and M. Plumacher, "Leptogenesis for pedestrians," *Annals Phys.* **315** 305–351. [arXiv:hep-ph/0401240].

[79] S. Davidson and A. Ibarra, "A Lower bound on the right-handed neutrino mass from leptogenesis," *Phys.Lett.* **B535** (2002) 25–32, `arXiv:hep-ph/0202239`. [arXiv:hep-ph/0202239].

[80] M. Plumacher, "Baryogenesis and lepton number violation," *Z.Phys.* **C74** (1997) 549–559. [arXiv:hep-ph/9604229].

[81] M. A. Luty, "Baryogenesis via leptogenesis," *Phys.Rev.* **D45** (1992) 455–465.

[82] J. A. Harvey, E. W. Kolb, D. B. Reiss, and S. Wolfram, "Cosmological baryon number generation in grand unified models," *Phys.Rev.Lett.* **47** (1981) 391–394.

[83] S. Y. Khlebnikov and M. E. Shaposhnikov, "The Statistical Theory of Anomalous Fermion Number Nonconservation," *Nucl.Phys.* **B308** (1988) 885–912.

[84] H. A. Weldon, "Covariant Calculations at Finite Temperature: The Relativistic Plasma," *Phys.Rev.* **D26** (1982) 1394.

[85] J. F. Donoghue, B. R. Holstein, and R. W. Robinett, "Quantum electrodynamics at finite temperature," *Annals Phys.* **164** (1985) 233.

[86] M. Le Bellac, *Thermal Field Theory*. Cambridge University Press, Cambridge, 2004. Cambridge Monographs on Mathematical Physics.

[87] J. I. Kapusta and C. Gale, *Finite-Temperature Field Theory: Principles and Applications*. Cambridge University Press, Cambridge, 2. ed., 2006. Cambridge Monographs on Mathematical Physics.

[88] M. Laine, "Basics of thermal field theory," 2010. Lectures. University of Bielefeld. `www.physik.uni-bielefeld.de/~laine/thermal/contents.pdf`.

[89] P. Danielewicz, "Quantum theory of nonequilibrium processes. 1.," *Annals Phys.* **152** (1984) 239–304.

[90] P. Danielewicz, "Quantum theory of nonequilibrium processes. ii. application to nuclear collisions," *Annals Phys.* **152** (1984) 305–326.

[91] J. Berges, "Introduction to nonequilibrium quantum field theory," *AIP Conf.Proc.* **739** 3–62. [arXiv:hep-ph/0409233].

[92] S. Juchem, W. Cassing, and C. Greiner, "Nonequilibrium quantum field dynamics and off-shell transport for phi**4 theory in (2+1)-dimensions," *Nucl.Phys.* **A743** (2004) 92–126, `nucl-th/0401046`. [arXiv:nucl-th/0401046].

[93] G. Baym, J.-P. Blaizot, and B. Svetitsky, "Emergence of new quasiparticles in quantum electrodynamics at finite temperature," *Phys.Rev.* **D46** (1992) 4043–4051.

[94] C. P. Herzog and D. T. Son, "Schwinger-keldysh propagators from ads/cft correspondence," *JHEP* **0303** (2003) 046. [arXiv:hep-th/0212072].

[95] C. Greiner and S. Leupold, "Stochastic interpretation of Kadanoff-Baym equations and their relation to Langevin processes," *Annals Phys.* **270** (1998) 328–390, `hep-ph/9802312`. [arXiv:hep-ph/9802312].

[96] C. Greiner and S. Leupold, "Interpretation and resolution of pinch singularities in nonequilibrium quantum field theory," *Eur.Phys.J.* **C8** (1999) 517–522, `hep-ph/9804239`. [arXiv:hep-ph/9804239].

[97] Y. Fujimoto and R. Grigjanis, "Higher order calculation in thermo field theory," *Z.Phys.* **C28** (1985) 395.

[98] S. Mendizabal, "Quantum mechanics of leptogenesis," 2010. Dissertation. Deutsches Elektronen-Synchrotron, Hamburg. (DESY-THESIS-2010-029).

[99] D. Boyanovsky, K. Davey, and C. M. Ho, "Particle abundance in a thermal plasma: Quantum kinetics vs. boltzmann equation," *Phys.Rev.* **D71** 023523. [arXiv:hep-ph/0411042].

[100] A. Anisimov, W. Buchmuller, M. Drewes, and S. Mendizabal, "Leptogenesis from quantum interference in a thermal bath," *Phys.Rev.Lett. 104:121102* (2010) . [arXiv:hep-ph/1001.3856].

[101] A. De Simone and A. Riotto, "Quantum boltzmann equations and leptogenesis," *JCAP* **0708** 002. [arXiv:hep-ph/0703175].

[102] M. M. Muller, "Comparing boltzmann vs. kadanoff-baym," *J.Phys.Conf.Ser.* **35** (2006) 390–397.

[103] R. D. Pisarski, "Computing finite temperature loops with ease," *Nucl.Phys.* **B309** (1988) 476.

[104] E. Braaten and R. D. Pisarski, "Soft amplitudes in hot gauge theories: A general analysis," *Nucl.Phys.* **B337** (1990) 569.

[105] E. Braaten and R. D. Pisarski, "Deducing Hard Thermal Loops from Ward Identities," *Nucl.Phys.* **B339** (1990) 310–324.

[106] U. Kraemmer, A. K. Rebhan, and H. Schulz, "Resummations in hot scalar electrodynamics," *Annals Phys.* **238** 286–331. [arXiv:hep-ph/9403301].

[107] D. Besak, "Thermal particle production in the early universe," 2010. Dissertation. Fakultät für Physik, Universität Bielefeld.

[108] D. Besak and D. Bodeker, "Hard thermal loops for soft or collinear external momenta," *JHEP* **1005** (2010) 007. [arXiv:hep-ph/1002.0022].

[109] L. D. Landau and I. Pomeranchuk, "Limits of applicability of the theory of bremsstrahlung electrons and pair production at high-energies," *Dokl.Akad.Nauk Ser.Fiz.* **92** (1953) 535–536.

[110] A. B. Migdal, "Bremsstrahlung and pair production in condensed media at high-energies," *Phys.Rev.* **103** (1956) 1811–1820.

[111] D. Bieletzki, K. Lessmeier, O. Philipsen, and Y. Schroder, "Resummation scheme for 3d Yang-Mills and the two-loop magnetic mass for hot gauge theories," *JHEP* **1205** (2012) 058, 1203.6538. [arXiv:hep-ph/1203.6538].

[112] O. Philipsen, "The QCD equation of state from the lattice," 1207.5999. [arXiv:hep-lat/1207.5999].

[113] P. B. Arnold, G. D. Moore, and L. G. Yaffe, "Photon emission from ultrarelativistic plasmas," *JHEP* **0111** (2001) 057. [arXiv:hep-ph/0109064].

[114] H. A. Weldon, "Simple rules for discontinuities in finite temperature field theory," *Phys.Rev.* **D28** (1983) 2007.

[115] D. Boyanovsky and H. J. de Vega, "Photon production from a thermalized quark gluon plasma: Quantum kinetics and nonperturbative aspects," *Nucl.Phys.* **A747** (2005) 564–608, hep-ph/0311156. [arXiv:hep-ph/0377756].

[116] F. Michler, B. Schenke, and C. Greiner, "Finite lifetime effects on the photon production from a quark-gluon plasma," arXiv:0906.1734. [arXiv:hep-ph/0906.1734].

[117] P. Aurenche, F. Gelis, and H. Zaraket, "A simple sum rule for the thermal gluon spectral function and applications," *JHEP* **0205** (2002) 043. [arXiv:hep-ph/0204146].

[118] P. Aurenche, F. Gelis, G. D. Moore, and H. Zaraket, "Landau-pomeranchuk-migdal resummation for dilepton production," *JHEP* **0212** (2002) 006. [arXiv:hep-ph/0211036].

[119] P. B. Arnold, G. D. Moore, and L. G. Yaffe, "Photon emission from quark gluon plasma: Complete leading order results," *JHEP* **0112** (2001) 009. [arXiv:hep-ph/0111107].

[120] P. B. Arnold, G. D. Moore, and L. G. Yaffe, "Photon and gluon emission in relativistic plasmas," *JHEP* **0206** (2002) 030, hep-ph/0204343. [arXiv:hep-ph/0204343].

[121] M. E. Carrington, "The Effective potential at finite temperature in the Standard Model," *Phys.Rev.* **D45** (1992) 2933–2944.

[122] P. B. Arnold, G. D. Moore, and L. G. Yaffe, "Transport coefficients in high temperature gauge theories. 1. Leading log results," *JHEP* **0011** (2000) 001, hep-ph/0010177. [arXiv:hep-ph/0010177].

[123] B. Schrempp and M. Wimmer, "Top quark and higgs boson masses: Interplay between infrared and ultraviolet physics," *Prog.Part.Nucl.Phys.* **37** (1996) 1–90. [arXiv:hep-ph/9606386].

[124] H. Arason, D. J. Castano, B. Keszthelyi, S. Mikaelian, E. Piard, *et al.*, "Renormalization group study of the standard model and its extensions. 1. the standard model," *Phys.Rev.* **D46** (1992) 3945–3965.

[125] P. Nogueira, "Automatic Feynman graph generation," *J.Comput.Phys.* **105** (1993) 279–289.

[126] A. Pilaftsis and T. E. J. Underwood, "Resonant leptogenesis," *Nucl.Phys.* **B692** 303–345. [arXiv:hep-ph/0309342].

[127] S. Iso, N. Okada, and Y. Orikasa, "Resonant leptogenesis in the minimal b-l extended standard model at tev," *Phys.Rev.* **D83** 093011. [arXiv:hep-th/1011.4769].

[128] M. Garny, A. Kartavtsev, and A. Hohenegger, "Leptogenesis from first principles in the resonant regime,". [arXiv:hep-ph/1112.6428].

[129] W. Buchmuller, K. Schmitz, and G. Vertongen, "Matter and dark matter from false vacuum decay," *Phys.Lett.* **B693** 421–425. [arXiv:hep-ph/1008.2355].

[130] W. Buchmuller, "Leptogenesis and gravitino dark matter," *AIP Conf.Proc.* **903** 56–64. [arXiv:hep-ph/0611368].

[131] D. G. E. Walker, "Dark baryogenesis,". [arXiv:hep-ph/1202.2348].

[132] W. Buchmuller, V. Domcke, and K. Schmitz, "WIMP Dark Matter from Gravitino Decays and Leptogenesis," *Phys.Lett.* **B713** (2012) 63–67, 1203.0285. [arXiv:hep-ph/1203.0285].

[133] M. Kaku, *Quantum field theory: A Modern introduction.* Oxford University Press, Oxford, 1993.

[134] J. Collins, *Renormalization.* Cambridge University Press, Cambridge, 1985.

[135] J. Hütig, "Der quantenchromodynamische Feldstärkekorrelator in Kontinuums- und Gitterstörungstheorie," 2009. Diplomarbeit. Institut für Theoretische Physik, Westfälische Wilhelms-Universität Münster.

[136] M. Abramowitz and A. Stegun, I. *Handbook of Mathematical Funktions with Formulas, Graphs, and Mathematical Tables.* Dover Publications, New York, 9. ed., 1972.

[137] W. H. Press, S. A. Teukolsky, W. T. Vetterling, and B. P. Flannery, *Numerical Recipes: The Art of Scientific Computing.* Cambridge University Press, Cambridge, 3. ed., 2007.

[138] J. Stoer and R. Bulirsch, *Introduction to Numerical Analysis.* Springer, New York, 3. ed., 2002.

[139] J. Wolf, *C++ von A bis Z.* Galileo Press, Bonn, 2. ed., 2010.

[140] T. Hahn, "Cuba: A library for multidimensional numerical integration," *Comput.Phys.Commun.* **168** (2005) 78–95. [arXiv:hep-ph/0404043].

[141] T. Hahn, "The cuba library ," *Nucl.Instrum.Meth.* **A559** (2006) 273–277. [arXiv:hep-ph/0509016].